ASD-TDR-62-156

NONLINEAR AND THERMAL EFFECTS ON ELASTIC VIBRATIONS

TECHNICAL DOCUMENTARY REPORT NO. ASD-TDR-62-156

June 1962

Flight Dynamics Laboratory
Aeronautical Systems Division
Air Force Systems Command
Wright-Patterson Air Force Base, Ohio

Project No. 1370, Task No. 137006

(Prepared under Contract No. AF 33(616)-7898 by The Boeing Company, Seattle, Washington; Raymond C. Weikel, Robert E. Jones, James A. Seiler, Harold C. Martin, and Bruce E. Greene, Authors)

NOTICES

When Government drawings, specifications, or other data are used for any purpose other than in connection with a definitely related Government procurement operation, the United States Government thereby incurs no responsibility nor any obligation whatsoever; and the fact that the Government may have formulated, furnished, or in any way supplied the said drawings, specifications, or other data, is not to be regarded by implication or otherwise as in any manner licensing the holder or any other person or corporation, or conveying any rights or permission to manufacture, use, or sell any patented invention that may in any way be related thereto.

Qualified requesters may obtain copies of this report from the Armed Services Technical Information Agency, (ASTIA), Arlington Hall Station, Arlington 12, Virginia.

This report has been released to the Office of Technical Services, U.S. Department of Commerce, Washington 25, D.C., for sale to the general public.

Copies of this report should not be returned to the Aeronautical Systems Division unless return is required by security considerations, contractual obligations, or notice on a specific document.

FOREWORD

The research work in this report was performed by The Boeing Company, Aero-Space Division, Seattle, Washington, for the Flight Dynamics Laboratory, Directorate of Aeromechanics, Deputy Commander/Technology, Aeronautical Systems Division, Wright-Patterson Air Force Base, under AF Contract Nr. AF33 (616)-7898. This research is part of a continuing effort to advance the aeroelastic state-of-the-art knowledge for flight vehicles which is part of the Air Force Systems Command's Applied Research Program 750A, the Mechanics of Flight. The Project Nr. is 1370, "Dynamics Problems in Flight Vehicles", and the Task Nr. is 137006, "Thermal Effects on Structural Dynamic Characteristics". Donald J. Ketter, 1st Lt., USAF, and Thor M. Snaring, 1st Lt., USAF, of the Flight Dynamics Laboratory were the Project Engineers. The research was conducted from January 1961 to December 1961 by the Structural Analysis Unit of the Structures Research and Development Section. This is the final report on the contract.

Peter E. Grafton, Supervisor, Structural Analysis Unit, The Boeing Company, was Project Supervisor for the Contractor.

Raymond C. Weikel, Research Specialist, Structural Analysis Unit, The Boeing Company, was the Technical Leader for the Contractor.

The principal engineers for the Contractor were: Robert E. Jones, Research Specialist, and Bruce E. Green, Research Engineer, each from the Structural Analysis Unit, The Boeing Company; and Harold C. Martin, Research Specialist and Professor of Aeronautical Engineering, College of Engineering, University of Washington.

2-17M, 300, 8-31-62

James A. Seiler, Supervisor, Program Development Group, Applied Mathematics Section, The Boeing Company, was the chief consultant on the development of the digital procedures.

The authors wish to express their appreciation to M. J. Turner, Section Chief, Structures Research and Development Section, for his suggestions and criticisms; to Peter E. Grafton for his guidance and criticisms; to Louis Kiersky, Research Engineer, Applied Mathematics Section, for contributing to the development of the digital programs; to W. H. Sutherland, Associate Research Engineer, Structural Analysis Unit, for derivations basic to the stiffness method and for numerical analyses and summaries; and to R. R. Valla, Engineering Designer, Structural Analysis Unit, for his contributions to the design of the model and to the data summaries.

ABSTRACT

This report presents a theory and the digital procedures for predicting the effects of nonlinear structural behavior on the stresses, deformations, and small amplitude oscillations of a structure subjected simultaneously to loading and heating.

The method is used to analyze a thin wing to determine the frequencies and mode shapes of the first six natural vibration modes of the wing subjected to simultaneous heating and loading.

PUBLICATION REVIEW

This report has been reviewed and is approved.

FOR THE COMMANDER:

William C. Nielsen

WILLIAM C. NIELSEN
Colonel, USAF
Chief, Flight Dynamics Laboratory

TABLE OF CONTENTS

LIST OF ILLUSTRATIONS

LIST OF ILLUSTRATIONS (Cont'd)

LIST OF TABLES

LIST OF SYMBOLS

u, v, w	=	Cartesian displacements
X, Y, Z	=	Cartesian forces (lbs.)
ϵ_{ij}	=	strain components; ϵ = emissivity factor
ω	=	rotation of volume element
ψ	=	rotation of line element
E_x, E_y	=	extensional strains
ϕ	=	shear strain
σ	=	stress component, Steffen-Boltzmann constant
M	=	moment (in beam), also mass
θ	=	rotation of beam
L	=	length of beam or bar
λ, μ, ν	=	direction cosines
Δ	=	small finite increment
k, k_{ij}	=	stiffness coefficients
E	=	Young's modulus
G	=	shear modulus; [G] = geometry matrix
F	=	nodal forces, free energy
A	=	area; also designation of point [A] = [B] = transformation matrix
B, C, D	=	designation of points
I	=	moment of inertia (of beam); also unit matrix
T	=	temperature
t	=	thickness
d	=	shear web half-width
U	=	strain energy
[ ]	=	rectangular matrix
{ }	=	column matrix
[ ]	=	row matrix; $\{\overset{\Lambda}{V}\}$ = vector in central coordinate system
α	=	coefficient of thermal expansion

LIST OF SYMBOLS (Cont'd)

h	=	heat transfer coefficient
F_A	=	geometric view factor
F_ϵ	=	emissivity factor
x'	=	% of distance from leading edge to trailing edge at the center line of the wing
$\{\Delta L\}$	=	column of incremental loads

SUBSCRIPTS

AW	=	adiabatic wall
c	=	cold side
H	=	hot side

SECTION 1.0

INTRODUCTION

1.1 Statement of Problem

The class of structures under consideration includes all those having one or more dimensions small as compared to the others; such a class would include cables, slender beams, membranes, and thin plates and shells, as well as all structures consisting of assemblages of these basic structural elements. Specifically, the structure considered in this research is a thin wing built up from an assemblage of ribs and spars and covered with plates as shown in Figures 11, 12, and 13, pages 45, 46, and 47, respectively.

When such structures are subjected to certain types of loading and/or temperature gradients, they may exhibit finite bending and twisting deformation behavior; also, under such circumstances, the vibrational characteristics of these structures may be altered from those characteristics exhibited at room temperature with infinitesimal bending and twisting. The ultimate problem to be solved is to determine the quantitative effects of finite bending and twisting and residual stresses on the vibrational characteristics of thin wings. In its most general form, this problem is nonlinear to a high degree and virtually defies a closed solution. However, it is possible to study the nature of small (linear) oscillations of a structure about an equilibrium configuration characterized by geometric nonlinearities and/or residual stresses.

The specific problem of this research program may be essentially divided into two areas:

Manuscript released by the authors January 1962 for publication as an ASD Technical Documentary Report.

(1) Determine the equilibrium configuration of a thin wing forced into nonlinear behavior by applying loads, heat, or other influences.

(2) Calculate the linear behavior of the deformed structure undergoing infinitesimal deflections about its equilibrium configuration; evaluate the apparent stiffness effects due to the presence of large internal stresses and geometric nonlinearities.

1.2 Objectives of Program

The objectives of this research program may be summarized by the following items:

(1) Develop the theory and computational procedures for predicting the structural vibrational characteristics of thin, built-up, low aspect ratio lifting surfaces undergoing finite bending and twisting in the presence of large temperature gradients.

(2) Demonstrate the practicability of the theory and procedures developed in item (1) by applying them to a representative structural model; specifically, calculate the first six natural frequencies and the corresponding mode shapes of this model subjected simultaneously to elevated temperature gradients and external loads.

(3) Compare the predictions of the nonlinear theory with those of the linear theory.

(4) Compare the calculated data with experimentally determined results; therefore, the representative structural model to be used in program analysis will be designed such that it will adequately exhibit the desired behavior when it is subjected to practical thermal and shake tests in a laboratory.

1.3 Method of Approach

The necessary theory, equations, and digital procedures are developed from the basic equations and digital procedures of the direct stiffness

method described in Reference 2. When the stiffness matrix is computed in terms of the final equilibrium configuration, however far it departs from the original shape, it is an exact expression for determining the infinitesimal loads associated with an arbitrary set of infinitesimal displacements from the final shape, if the structure is elastic (Reference 5). A stiffness matrix so derived can be used to predict the small incremental loads arising from small increments of deflections from a nonlinear equilibrium shape. This fact is used to develop a step-by-step procedure for predicting a finite state of deformation by accumulating the deformations occurring in a sequence of small changes in the load and temperature. The stiffness matrix computed at any step may be used to compute the small amplitude vibration modes and frequencies relative to that state of deformation.

These procedures are derived and discussed in this report.

1.4 Scope of Work

The basic ideas developed in this report are applicable to any nonlinear problem of heated elastic structures. The specific procedures developed in this work are applicable only to the class of structures defined in Section 1.1.

The important vibration characteristics studied include the determination of the first six frequencies and the corresponding mode shapes.

Consideration is limited to the small oscillations about an equilibrium configuration containing geometric nonlinearities.

SECTION 2.0

THEORY

2.1 General Discussion of Nonlinear Elasticity

Nonlinearity is introduced into the theory of structures in three ways: (1) through the strain-displacement equations, (2) through the equilibrium equations, and (3) through the stress-strain relations. The first two sources are termed geometrical nonlinearities, while the third is due to material behavior and is, therefore, classed as a physical nonlinearity.

Four general types of problems arise as a result of the considerations listed above. These are:

(1) Problems having both geometric and physical nonlinearities,
(2) Problems which are physically linear and geometrically nonlinear,
(3) Problems which are geometrically linear and physically nonlinear,
(4) Problems which are both geometrically and physically linear.

This report is concerned with problems which are physically linear and geometrically nonlinear. Structures of this class behave elastically, but, nevertheless, are nonlinear; hence, they present a need for the nonlinear theory of elasticity.

Novozhilov (Reference 1) lists the following problems as basically belonging to the geometrically nonlinear theory of elasticity:

(1) The stability of elastic equilibrium,
(2) The deformation of bodies having initial stresses,
(3) The large deflections of extremely thin rods (cables),
(4) The problem of torsion and bending being complicated by the presence of axial or membrane forces,
(5) The bending of plates and shells having deflections on the order of magnitude of the thickness.

The following discussion briefly describes the problems which are physically linear and geometrically nonlinear. As stated above, geometrical nonlinearities affect the elasticity problem through the strain displacement equations and the equilibrium equations; the effects are discussed in that order.

Figure 1 shows an infinitesimal element of material which undergoes translation, rotation, and deformation (the two-dimensional case is considered for simplicity). Displacements of points in the x- and y-directions, respectively, are denoted by u and v. Rotations of line elements about the z-axis (projecting out of the paper) are denoted by ψ_z. The shear strain ϕ_{xy} is the decrease in the right angle between two perpendicular lines initially along the x and y axes. Note that ψ_z varies throughout the element due to shear strain; the association in the figure between ψ_z and line AB-$\bar{A}\bar{B}$ serves only to illustrate the definition. The extensional strains undergone by a material fiber originally parallel to the x- or y-axis are denoted by E_x or E_y, respectively.

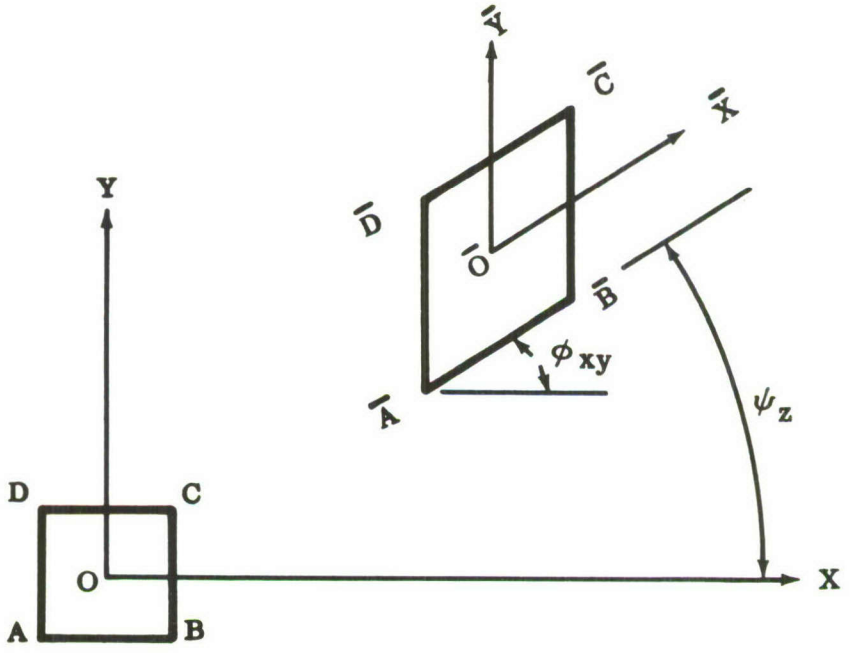

FIGURE 1: FINITE STRAIN OF VOLUME ELEMENT

Figure 2 shows the motion of a line element (dx), which during the motion, extends to length $(1+E_x)dx$ and rotates an amount ψ_z about the z-axis; no generality is lost if its left end is held fixed. The displacements of the right end of the element are $\frac{\partial u}{\partial x}dx$ and $\frac{\partial v}{\partial x}dx$ (Figure 2). It is clear that $\frac{\partial u}{\partial x}$ and $\frac{\partial v}{\partial x}$ (and hence u, v) are influenced by both the rotation (ψ_z) and the stretching (E_x) of the element.

For example, it is seen that:

$$(\frac{\partial u}{\partial x})\, dx = (1 + E_x) \cos \psi_z \, dx - dx \qquad (1)$$

$$(\frac{\partial v}{\partial x})\, dx = (1 + E_x) \sin \psi_z \, dx \qquad (2)$$

Note that E_x and ψ_z occur in product combination, and that not ψ_z itself, but $\sin \psi_z$ and $\cos \psi_z$ appear in the equations. Figure 1 makes it clear that the shear strains (ϕ_{xy}) are similarly involved in trigonometric functions in the description of the displacements. The nonlinear character of the equations is apparent.

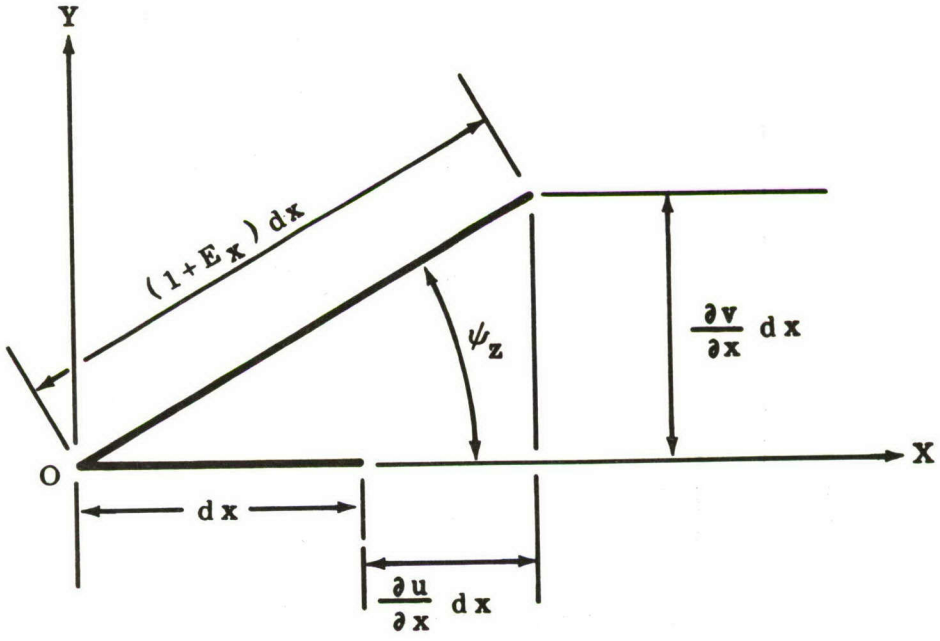

FIGURE 2: FINITE STRAIN AND ROTATION OF LINE ELEMENT

The mathematical description of the strain is most conveniently expressed in terms of the square of the length of a line element. Referring to Figure 2 and denoting by $(ds_f)^2$ the final and $(ds_i)^2$ the initial squared element length, it is seen that:

$$(ds_f)^2 = (dx + \frac{\partial u}{\partial x} dx)^2 + (\frac{\partial v}{\partial x} dx)^2 \tag{3}$$

$$(ds_i)^2 = dx^2 \tag{4}$$

$$(ds_f)^2 - (ds_i)^2 = (dx)^2 \left[2 \frac{\partial u}{\partial x} + (\frac{\partial u}{\partial x})^2 + (\frac{\partial v}{\partial x})^2 \right] \tag{5}$$

Considering now a state of plane deformation as illustrated by Figure 1, for an arbitrary line element ds we have:

$$(ds_f)^2 - (ds_i)^2 = 2 \left[\epsilon_{xx} dx^2 + \epsilon_{yy} dy^2 + \epsilon_{xy} dx\, dy \right] \tag{6}$$

in which ϵ_{xx}, ϵ_{yy}, ϵ_{xy} are the components of the strain tensor in rectangular cartesian coordinates and are given by:

$$\epsilon_{xx} = \frac{\partial u}{\partial x} + \frac{1}{2} \left[(\frac{\partial u}{\partial x})^2 + (\frac{\partial v}{\partial x})^2 \right] \tag{7}$$

$$\epsilon_{yy} = \frac{\partial v}{\partial y} + \frac{1}{2} \left[(\frac{\partial u}{\partial y})^2 + (\frac{\partial v}{\partial y})^2 \right] \tag{8}$$

$$\epsilon_{xy} = \frac{\partial u}{\partial y} + \frac{\partial v}{\partial x} + \frac{\partial u}{\partial x} \frac{\partial u}{\partial y} + \frac{\partial v}{\partial x} \frac{\partial v}{\partial y} \tag{9}$$

The preceding quantities are not actually physical strains. The following are:

$$E_x = \sqrt{1 + 2 \epsilon_{xx}} - 1 \tag{10}$$

$$E_y = \sqrt{1 + 2 \epsilon_{yy}} - 1 \tag{11}$$

$$\sin \phi_{xy} = \frac{\epsilon_{xy}}{(1 + E_x)(1 + E_y)} \tag{12}$$

The nonlinear dependence of E_x, E_y, ϕ_{xy} on the displacement is apparent, though its specific dependence on large rotations and strains is somewhat masked by the complexity of the equations.

A deformation corresponding to that in Figure 1 causes changes in the volume and area of the faces of material elements. The area effect is given by:

$$\frac{A_f}{A_i} = (1 + E_x)(1 + E_y) \cos \phi_{xy} \tag{13}$$

The rotation of a material element is defined as follows: $\tan \psi_z$ is averaged for all line elements passing through the center of the element; the result is:

$$\left[\text{Tan } \psi_z\right]_{\substack{\text{avg.} \\ \text{value}}} = \frac{\omega_z}{\sqrt{(1 + \frac{\partial u}{\partial x})(1 + \frac{\partial v}{\partial y}) - \frac{1}{4}(\frac{\partial u}{\partial y} + \frac{\partial v}{\partial x})^2}} \tag{14}$$

in which ω_z is the quantity defined by:

$$\omega_z = \frac{1}{2}\left\{\frac{\partial v}{\partial x} - \frac{\partial u}{\partial y}\right\} \tag{15}$$

It is seen from linear theory that ω_z is the average of the rotations of the dx and dy line elements which pass through the center of the element.

Next, consider small strains, by which is meant that the strains (E_x, E_y, ϕ_{xy}) can be neglected compared to unity. The simplifications resulting from this limitation are due to the facts that line elements extend only slightly while they rotate and that rotations of the line elements of a material element differ from the average rotation of the element by small quantities. This condition places a negligible practical limitation on the applicability of the theory for most structures, since only a few

materials, such as rubber, have elastic strains large enough to invalidate the assumption. For example, it is seen that if $E_x \ll 1$, then $E_x \approx \epsilon_{xx}$. We have:

$$\begin{aligned} E_x &\approx \epsilon_{xx} \\ E_y &\approx \epsilon_{yy} \\ \phi_{xy} &\approx \epsilon_{xy} \end{aligned} \tag{16}$$

The volume and areas of the faces of a material element are unchanged by a deformation in which the strains can be neglected compared to unity.

Finally, consider small rotation, by which is meant that ψ_z^2 can be neglected compared to unity. An immediate consequence of this restriction is:

$$\begin{aligned} \sin \psi_z &\approx \tan \psi_z \approx \psi_z \\ \cos \psi_z &\approx 1 \end{aligned} \tag{17}$$

Because of these trigonometric function approximations, the strain displacement equations are simplified. The rotations of line elements in a volume element can now be reduced to the form:

$$\psi_z \approx \omega_z \tag{18}$$

and the strains can be reduced to the simple and meaningful forms:

$$\begin{aligned} E_x \approx \epsilon_{xx} &\approx \frac{\partial u}{\partial x} + \frac{1}{2}\omega_z^2 \\ E_y \approx \epsilon_{yy} &\approx \frac{\partial v}{\partial y} + \frac{1}{2}\omega_z^2 \\ \phi_{xy} \approx \epsilon_{xy} &\approx \frac{\partial u}{\partial y} + \frac{\partial v}{\partial x} \end{aligned} \tag{19}$$

The precise influence of the rotation is clear in the above equations.

The classical theory of infinitesimal deformations is obtained by dropping all the nonlinear terms in the preceding equations. Though such a procedure may appear permissible for the strain-displacement equations because of the smallness of the strains and rotations, it nevertheless may be invalid for the equilibrium equations. This latter point will be clarified later. A discussion of the effects of geometrical nonlinearities on the equilibrium equations follows.

The usual stress-strain relation of the theory of elasticity is assumed to hold in the present discussion, since only geometrical nonlinearities are considered. It is seen from Figure 3 and from the stress-strain equations of elasticity that, for example, σ_{xx} is a stress which acts in the direction of the deformed x-axis on a deformed element face parallel to the deformed yz surface.

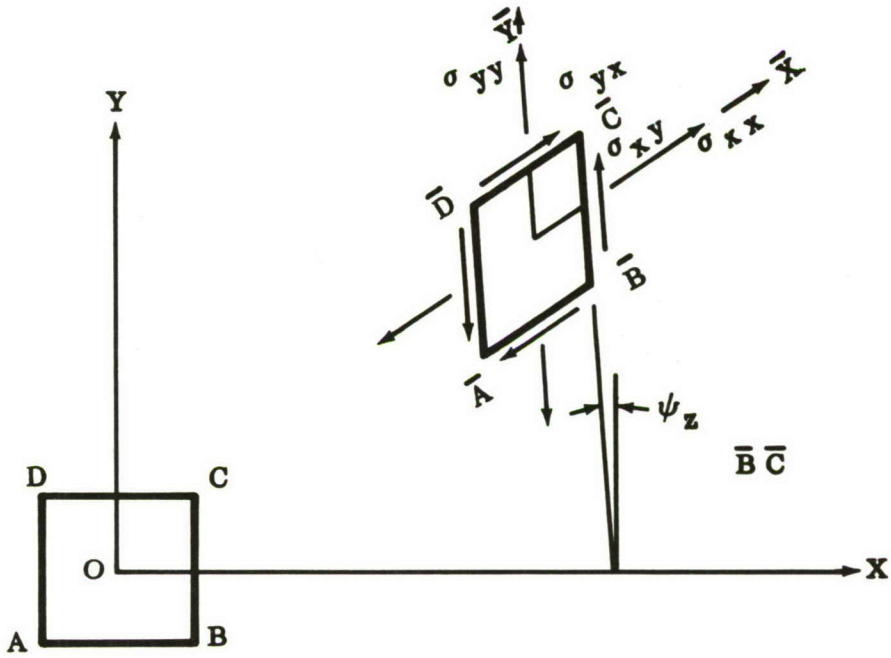

FIGURE 3: STRESSES ON DEFORMED ELEMENT

Similarly, σ_{xy} acts on the same face, but in the direction of the deformed y-axis. The stress vectors translate and rotate with the element itself. No generality is lost in considering the equilibrium of the element in Figure 3 by projecting forces onto the undeformed x and y axes. The resulting x- and y-force resultants depend on the rotation and the shear strains of the element, its stresses, the areas of its faces, and its volume. Since the equilibrium equations then depend on the deformation itself, they are highly nonlinear in character. The contrast with the classical elasticity theory is apparent.

The equations representing the described equilibrium are complicated, and little is accomplished by writing them here. Instead, to fix ideas, the x-resultant of the $\sigma_{x\bar{x}}$ stress on face BC will be discussed briefly. BC is rotated at an angle $\psi_{z\bar{B}\bar{C}}$ (which is different from the ψ_z values elsewhere in the element). The area of face BC, assuming that dz is the thickness of the element and that it does not change during the deformation, is $(1 + E_y)$ dydz. Therefore, due only to σ_{xx} there is an x-direction resultant of (σ_{xx}) $(1 + E_y)$ dy $(\cos \psi_{z\bar{B}\bar{C}})$ dx dz. The other faces and stresses are handled similarly. Because of the extensional and shear strains, the areas and rotation of the element faces are different for each face.

Consider again the small strains, defined as negligible compared to unity. The volume of the element and the areas of its faces then become unaffected by the deformation. In formulating the equilibrium equations the shear strains are present in combinations with unity and, thus, can be neglected. Therefore, the deformed element may be considered to be a cube which has translated and rotated relative to its original position. The equilibrium equations derived through the assumption of small strains are still very complicated. They are not written here because an examination of their form adds little insight into the nature of the problem.

The work of simplifying the equations for small angles of rotation is accomplished by the usual approximations: $\cos \psi_z \approx 1$; $\sin \psi_z \approx \psi_z$ $\tan \psi_z \approx \psi_z$. This approximation is based on neglecting ψ^2 compared to unity. The result for the plane problem, with zero body forces, is:

$$\frac{\partial}{\partial x}\left[\sigma_{xx} - \omega_z \sigma_{xy}\right] + \frac{\partial}{\partial y}\left[\sigma_{yx} - \omega_z \sigma_{yy}\right] = 0 \qquad (20)$$

$$\frac{\partial}{\partial x}\left[\omega_z \sigma_{xx} - \sigma_{xy}\right] + \frac{\partial}{\partial y}\left[\omega_z \sigma_{yx} - \sigma_{yy}\right] = 0 \qquad (21)$$

The influence of the small rotations is clear in these equations. For example, the term $\omega_z \sigma_{yy}$ in Equation 20 represents the x-direction force due to rotating σ_{yy} on the y-face of the element through angle ψ_z. Differentiation of this term with respect to y demonstrates the effect of element curvature; e.g., if σ_{yy} is constant in y, then:

$$\frac{\partial}{\partial y}\left[-\omega_z \sigma_{yy}\right] = -\sigma_{yy} \frac{\partial \omega_z}{\partial y} \qquad (22)$$

which represents the effect of element curvature, producing, in combination with σ_{yy}, an x-direction force.

The smallness of the rotations (and strains) is insufficient to justify omitting the nonlinear $(\sigma + \omega)$ terms in the equilibrium equations. What matters is the smallness of the $(\sigma + \omega)$ terms. For example, it may occur that even if ω is small, the value of σ is so large that in Equation 20 it is not neglectable when compared to the other terms. This is precisely the situation which occurs in the classical theory of buckling, in which curvatures (rotations) are retained in the equilibrium equations when they are multiplied by large stresses. To be consistent, a theory cannot retain the rotations in the equilibrium equation and ignore them in the strain-displacement equation. This inconsistency is

the reason for the linearity in the classical buckling theory and why this theory fails to describe adequately many nonlinear buckling phenomena (e.g., nonlinear buckling of shells).

The equilibrium equations (20 and 21) show that the presence of large self-equilibrating stresses from any source, such as manufacturing or heating, will influence the equilibrium of a structure as it undergoes further deformations. Therefore, residual stresses have a considerable effect on nonlinear structural behavior such as buckling.

The behavior involved when a structure already deflected into the nonlinear range is subjected to additional small deflections is the basis for analyzing small oscillations of highly stressed and deflected structures. Consider first the incremental strains produced by small incremental deflections. The strains are functions only of the displacements; hence, they can be written in the form of Taylor's series, expanding about the values of u and v at the start of the incremental deflection. For example,

$$\epsilon_{xx}(u_o + \delta u, v_o + \delta v) = \epsilon_{xx}(u_o, v_o) + \left.\frac{\partial \epsilon_{xx}}{\partial u}\right|_{\substack{u=u_o \\ v=v_o}} \delta u + \left.\frac{\partial \epsilon_{xx}}{\partial v}\right|_{\substack{u=u_o \\ v=v_o}} \delta v + \frac{1}{2}\left.\frac{\partial^2 \epsilon_{xx}}{\partial v^2}\right|_{\substack{u=u_o \\ v=v_o}} (\delta v)^2 + \frac{1}{2}\left.\frac{\partial^2 \epsilon_{xx}}{u^2}\right|_{\substack{u=u_o \\ v=v_o}} (\delta u)(\delta v) \qquad (23)$$

+ - - - - terms of higher order.

If attention is restricted to sufficiently small incremental deflections, only the constant and linear terms in Equation 23 need to be retained. The resulting incremental strain-displacement equation is that of the classical linear theory of elasticity applied to a structure in its deformed shape. The resulting incremental stresses follow directly from the classical linear theory of stress-strain relationships. The total stresses result from adding to these increments the values present at $u=u_o$ and $v=v_o$. During the incremental deflection, the equilibrium of the structure (Figure 3) indicates that there are contributions from both the changing stresses and changing rotations. For example, the term

$$\frac{\partial}{\partial y} \quad (\omega_z \ \sigma_{yy})$$

changes to:

$$\frac{\partial}{\partial y}\Big[(\omega_z)\ (\sigma_{yy}) + (\sigma_{yy})\ \delta\omega_z) + (\delta\sigma_{yy})\ (\omega_z) + (\delta\omega_z)\ (\delta\sigma_{yy})\Big] \tag{24}$$

By considering only increments small enough that the nonlinear term $(\delta\omega_z)\ (\delta\sigma_{zz})$ is negligible compared to $\sigma_{yy}\,\delta\omega_z + \delta\sigma_{yy}\,\omega_z$ and noting that the $\omega_z\ \sigma_{yy}$ term (upon writing all of the equation) vanishes because of the equilibrium at the start of the increment, there remains:

$$\frac{\partial}{\partial y}\Big[\sigma_{yy}\ \delta\omega_z + \omega_z\ \delta\sigma_{yy}\Big] \tag{25}$$

Therefore, the equilibrium equations contain the products of initial rotations times incremental stresses and initial stresses times incremental rotations, the unknown quantities being the incremental ones. Physically,

the terms are (1) the usual term of the classical linear theory applied to the deformed structure, plus (2) the initial stress acting through the incremental curvatures. Moreover, the mathematical description of the small increment is exactly that of the classical (linear) buckling theory. Such a theory is useful for many purposes, particularly for analyzing the small oscillations of a structure about a large deflection equilibrium position. The applications of this theory are developed in this report.

2.2 Discussion of Solution Approaches

The differential equations of the nonlinear theory of elasticity are nonlinear partial-differential equations and are difficult to solve. Only a few simple nonlinear elasticity problems have been solved; for example, extension of a cylinder, torsion of cylinder, flexure of a cuboid, inflation of a spherical shell, pure shearing deformation, etc. The approach used in solving the majority of these problems was to postulate a state of deformation and then to determine an equilibrium system of loads and stresses consistent with the deformations. Success usually was achieved only through postulating extremely simple deformations (e.g., postulating certain symmetries of deformation reduces the problem to a single independent variable so that only ordinary differential equations need be solved), incompressible material, etc. For more complicated problems, approximate solutions were obtained by expanding the solution (e.g., the displacements) in power series in a small parameter representing the magnitude of the overall deformation—the first term in the expansion being the classical linear solution; the second term a first correction, etc. For problems of complex built-up structures, the nonlinear theory has been of little value to the practical engineer. It is almost certain that consideration of complex structures through the medium of the governing nonlinear partial-differential equations will not provide useful results within the foreseeable future.

Because the differential-equation approach failed to give exact solutions to the problems of analyzing the arbitrarily complicated built-up structures, it was necessary to seek approximate methods of solution. These methods also begin by postulating a state of deformation. Generally, it is assumed that the space configuration of the deformed structure, which may actually have an infinite number of degrees of freedom, can be approximated by an equivalent idealized structure having a finite number of degrees of freedom.

There are three basic ideas around which approximate methods of structural analysis have been formulated: (1) a finite number of normal coordinates is postulated in solving the partial differential equations; (2) the space configuration of the deformed structure is described by a finite number of assumed mode shapes, e.g., the Rayleigh-Ritz method; and (3) the space configuration of the deformed structure is described by a finite number of concentrated generalized displacements of various parts of the structure (e.g., the lumped mass or rigid segment method of dividing the structure into a number of rigid segments with interconnecting weightless springs). The first two ideas consider a representation of the actual deformation shape as a superposition of explicitly defined continuous functions. The third idea (often referred to as the lumped parameter technique) approximates the deformed structure by an aggregate of simple structural elements interconnected in a simple manner at a finite number of points.

The lumped parameter method has been used quite successively to solve a number of practical aeroelastic problems (Reference 8). Because of the matrix equations present in this technique, it is relatively simple to establish standard routines for performing the arithmetical work on a high-speed digital computer.

Of the recent developments using the lumped parameter idea, the method of formulating the stiffness matrix directly from the stiffnesses of the subdivided structural elements of the structure (Reference 2) has been used to analyze arbitrarily complicated structures. Furthermore, since the stiffness matrix relating infinitesimal loads to infinitesimal deflections for a given deformed shape, may be written as:

$$K_{ij} = \frac{\partial^2 U}{\partial u_i \, \partial u_j}$$

(Where U = potential energy of strain; U being evaluated in terms of the deformed shape), the method has considerable potential for obtaining a step-by-step solution to nonlinear problems (References 3 and 4). Therefore, the lumped parameter method, phrased in the context of the "method of direct formulation of the stiffness matrix," was selected as the basis of the present research. The following sections describe and discuss the relevant theory.

2.3 Formulation of the Direct Stiffness Method of Solution

It is assumed that the idealization of a given structure can be related to a finite number of points or nodes appropriately selected on or within the structure in such a manner that: (1) the deformed shape of the entire structure will be adequately described in terms of the translations and rotations of each of the assumed nodes; (2) the stress pattern throughout the structure will be adequately expressed in terms of a statically equivalent system of concentrated internal forces acting at the respective node points selected for the structure; and (3) the external load system will be replaced by a statically equivalent set of concentrated loads applied to the respective node points.

If the given structure is a pin-jointed truss, the three preceding postulates are precise statements about the behavior and loading of the structure,

provided the pin joints of the bars are selected as the node points and the classical theory of trusses is accepted.

In a framework of beams (such as a Vierendeel truss), the rotations and translations of the ends of the respective beam elements will describe the entire deformation behavior of the structure, provided elementary beam theory is considered for each beam and the external loads consist of a set of concentrated loads applied at the beam ends. Under such circumstances the entire stress pattern may be determined. If the external loads are distributed along the beams between the joints, the end-point slopes and deflections of the beam elements are not sufficient to determine exactly the entire stress and deformation pattern of the structure. However, a given-distributed loading may be adequately replaced with a statically equivalent set of concentrated loads applied at the joints. In this manner, the stress condition may be adequately approximated from the end loads and end moments due to these concentrated loads. On the other hand, the idealization of a framework of beams may be made to include more joints than just the "natural" ends of the given beams. Additional nodes may be introduced on the beam axes between the end joints. In practice, the number of nodes may be increased until the behavior of the actual structure is adequately described by the behavior of the idealized structure.

Another composite structure is the reinforced membrane or stringer-skin construction commonly used in conventional airplane construction. The idealization of this structure for classical methods of analysis is a system of bars and shear plates connected together at points located at the stringer intersections.

Suppose that the material in a given structure is continuously and smoothly distributed throughout the structure (i.e., there are no ostensible

joints in the structure). In this case, there are infinite ways of idealizing the given structure in terms of a finite number of points. To illustrate the problem it is convenient to consider a flat thin membrane loaded only with inplane loads. Such a sheet could be subdivided into a series of triangles formed by straight lines joining an arbitratry set of points on the sheet—the approximate behavior of the sheet could be determined from the translations of the joints and the assumption that a state of uniform strain exists in each triangle. Also, such an assumption would indicate the approximate state of stress. The external loads could be replaced with a *set of statically equivalent concentrated loads* and the internal stresses could be replaced with a *set of statically equivalent internal forces.* In other words, the flat sheet could be idealized as a plane truss of flat triangular plates pin jointed at the apexes of the triangles with the loads applied at the joints. This is only one of the many ways of idealizing the membrane structure (see References 3 and 5).

Consider an idealized structure consisting of an aggregate of a finite number of joints interconnected by a system of bars, plates, and/or other types of structural subelements. In the stiffness method, the basic problem of determining what nodal forces are associated with a given set of arbitrary nodal displacements is solved first. Next, the problem is inverted to obtain a set of displacements arising from the application of a set of arbitrary loads. This is possible only by considering the support conditions (i.e., the displacements at the supports must be considered arbitrary, and the corresponding reactions at the supports must be determined along with the remaining displacements). (For an example, see Equation 28.)

It is believed that the conceptual basis for the stiffness method can be most easily understood by developing this technique for a typical beam

structure by utilizing the elementary beam theory common to all structural engineers. This structure is shown in Figure 4.

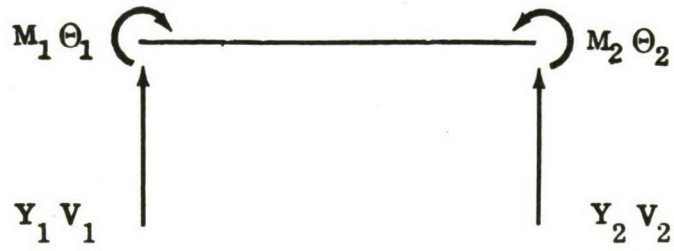

FIGURE 4: BEAM ELEMENT-LATERAL LOADS

The forces and deflection for the beam shown in Figure 4 are related by the following equation:

$$\begin{Bmatrix} M_1 \\ Y_1 \\ M_2 \\ Y_2 \end{Bmatrix} = \begin{bmatrix} k_{11} & k_{12} & k_{13} & k_{14} \\ k_{21} & k_{22} & k_{23} & k_{24} \\ k_{31} & k_{32} & k_{33} & k_{34} \\ k_{41} & k_{42} & k_{43} & k_{44} \end{bmatrix} \begin{Bmatrix} \Theta_1 \\ V_1 \\ \Theta_2 \\ V_2 \end{Bmatrix} \qquad (27)$$

For an arbitrary set of deflections, the forces are given by Equation 27. The specific forms for the k's can be calculated directly from beam theory. For example, $k_{11} = 4EI/L$ and $k_{13} = 2EI/L$, where L is the length of the beam and EI is the usual flexural stiffness.

In Equation 27, the k_{ij} elements form the stiffness matrix for the beam. This matrix is symmetrical ($k_{ij} = k_{ji}$); it is also singular (determinant equals zero). This condition is removed by providing supports or constraints which will prevent rigid-body motion. Supports or constraints are provided by prescribing the appropriate deflections in the column on the right side of the equation.

Suppose a cantilever beam is to be studied; this can be obtained by requiring $\Theta_2 = V_2 = 0$. Then M_2 and Y_2 become reactions, M_1 and Y_1 become applied loads, and Θ_1 and V_1 are unknown deflections. It is then useful to write Equation 27 in partitioned form:

$$\left\{\begin{array}{c} M_1 \\ Y_1 \\ \hline M_2 \\ Y_2 \end{array}\right\} \qquad \left[\begin{array}{c|c} k_{11} & k_{12} \\ \hline k_{21} & k_{22} \end{array}\right] \qquad \left\{\begin{array}{c} \theta_1 \\ V_1 \\ \hline 0 \\ \\ 0 \end{array}\right\} \tag{28}$$

Expanding Equation 28 leads to the two equations:

$$\left\{\begin{array}{c} M_1 \\ Y_1 \end{array}\right\} = \left[k_{11}\right]\left\{\begin{array}{c} \Theta_1 \\ V_1 \end{array}\right\} \quad \text{and} \quad \left\{\begin{array}{c} M_2 \\ Y_2 \end{array}\right\} = \left[k_{21}\right] \left\{\begin{array}{c} \Theta_1 \\ V_1 \end{array}\right\} \tag{29}$$

$$\tag{30}$$

Equation 29 relates all possible applied loads to all possible displacements for the chosen cantilever. As such, $\left[k_{11}\right]$ is the stiffness matrix for this problem. The inversion of Equation 29 yields deflections in terms of loading:

$$\left\{\begin{array}{c} \Theta_1 \\ V_1 \end{array}\right\} = \left[k_{11}\right]^{-1} \left\{\begin{array}{c} M_1 \\ Y_1 \end{array}\right\} \tag{31}$$

The inverse of the stiffness matrix is the flexibility matrix; that is, the matrix of deflection influence coefficients.

Substituting Equation 31 into Equation 30 yields the unknown reactions:

$$\begin{Bmatrix} M_2 \\ \\ Y_2 \end{Bmatrix} = \begin{bmatrix} k_{21} \end{bmatrix} \begin{bmatrix} k_{11} \end{bmatrix}^{-1} \begin{Bmatrix} M_1 \\ \\ Y_1 \end{Bmatrix} \tag{32}$$

This completes the solution.

An assemblage of beams (such as a continuous beam over multiple supports) can be treated similarly. It is necessary to assemble the separate beam-element stiffness matrixes into the composite stiffness matrix. This can be accomplished in various ways. For example, if n beam segments of the type illustrated in Figure 6 are combined into a continuous beam or other framework, the composite stiffness matrix can be assembled as:

$$\begin{bmatrix} K \end{bmatrix} = \begin{bmatrix} k_1 & & & \\ & k_2 & & \\ & & & \\ & & & k_n \end{bmatrix} \tag{33}$$

where each k_j is 4 by 4 as in Equation 27 and all other elements in Equation 33 are zero. The k_i's will overlap on common degrees of freedom.

The axial displacements u_1 and u_2 have been ignored in Figure 6 and in Equation 27. Such displacements do exist but they have no significance in the elementary theory of bending in beams. To ensure that no forces accompany such displacements, it is assumed that rollers are appropriately provided.

Using the direct stiffness method for the general structure necessitates the availability of a set of stiffness matrices associated with group of standard structural elements which may be used to formulate an idealization of the actual structure. The actual development of the elements of a stiffness matrix associated with a given structural element may be a lengthy algebraic process. The same is true of a stress matrix. It is sufficient to merely outline the procedure:

(1) Establish a set of nodal points for a given structural element and identify the degrees of freedom of deformation associated with each node. The number of nodes and degrees of freedom must be sufficient for the idealization to conform with the assumptions on Page 17.

(2) Define the idealized deformation of the structural element in terms of a linear combination of deformed shapes such that the number of shapes is the same as the number of degrees of freedom for the element. These deformation shapes are simply mathematical functions continuous within the boundaries of the structural element. For example, the deflected shape of a beam could be described by the general cubic as:

$$y = a + bx + cx^2 + dx^3$$

where the four constants are determined in terms of the four displacements (and rotations) v_1 , θ_1 , v_2 and θ_2 . It is desirable to have these shapes satisfy equilibrium throughout the element (e.g., y must satisfy $EI\frac{d^4y}{dx^4} = 0$ for the above shape, if EI is uniform.) However, this may not be possible without having an exact solution to the given problem, and then it is possible only to collocate the condition at a finite number of interior points or to resort to some process for minimizing the error.

(3) Compute the strain energy for the element in terms of the displacements of the nodes from the shape function and the material properties for the element.

(4) Compute the stiffness coefficients from the following equation:

$$K_{ij} = \frac{\partial^2 U}{\partial u_i \, \partial u_j}$$

The model wing structure analyzed in this report was idealized as an aggregate of triangular plates. The stiffness matrix for such an element was developed by assuming a shape based on linear displacements in the plane of the plate and cubic displacements normal to the plate. The actual stiffness and stress elements are described in Reference 7.

To summarize the basic procedure for the direct stiffness method is to compute the stiffness and stress matrices for the separate structural elements and then to merge the separate stiffness matrices into one gross matrix $\left[K\right]$ of stiffnesses for the composite structure. Once $\left[K\right]$ is known numerically, calculations follow the pattern described for the cantilever. To account for the full constraints, the rows and columns corresponding to these constraints are deleted from the stiffness matrix. The basic matrix equation for the general structure may be partitioned as follows:

$$\left\{\begin{array}{c} F \\ \hline R \end{array}\right\} = \left[\begin{array}{c|c} K_{11} & K_{12} \\ \hline K_{21} & K_{22} \end{array}\right] \left\{\begin{array}{c} u \\ \\ c \end{array}\right\} + \left[\begin{array}{c} A_1 \\ \hline A_2 \end{array}\right] \left\{T\right\} \qquad (34)$$

where: F = given arbitrary loads,

R = unknown reactions,

u = unknown displacements,

c = given arbitrary constraints (not necessarily zero).

These equations may be solved to give:

$$\left\{u\right\} = \left[K_{11}\right]^{-1}\left\{F\right\} - \left[K_{11}\right]^{-1}\left[K_{12}\right]\left\{c\right\} - \left[K_{11}\right]^{-1}\left[A_1\right]\left\{T\right\} \quad (35)$$

$$\left\{R\right\} = \left[K_{21}\right]\left[K_{11}\right]^{-1}\left\{F\right\} + \left(\left[K_{22}\right] - \left[K_{21}\right]\left[K_{11}\right]\left[K_{12}\right]\right)\left\{c\right\} + \left(\left[A_2\right] - \left[K_{21}\right]\left[K_{11}\right]^{-1}\left[A_1\right]\right)\left\{T\right\} \quad (36)$$

Having the matrix of the stress influence coefficients ($\left[S\right]$), the values of $\left\{u\right\}$ may be used to give the stresses:

$$\left\{\sigma\right\} = \left[S\right]\left\{u\right\}$$

$$= \left[S\right]\left[K_{11}\right]^{-1}\left\{F\right\} - \left[S\right]\left[K_{11}\right]^{-1}\left[K_{12}\right]\left\{c\right\} - \left[S\right]\left[K_{11}\right]^{-1}\left[A_1\right]\left\{T\right\} \quad (37)$$

The frequencies and mode shapes are then determined by a typical "lumped mass" procedure described in Sections 3-9 and 3-11 of Reference 12.

2.4 Nonlinear Problems and the Stiffness Matrix

The stiffness rate (i.e., the change of force per unit change of deformation) is related to the potential strain energy as follows:

$$\left[K_{ij}\right] = \left[\frac{\partial^2 U}{\partial u_i \, \partial u_j}\right] \quad (38)$$

(See Reference 5.) This expression is valid for any deformed shape, if the strain energy is expressed in terms of this shape and the structure is elastic. Explicitly, the stiffness matrix $\left[K\right]$ in Equation 38 relates the applied forces to the displacements:

$$\left\{\delta F\right\} = \left[K\right]\left\{\delta u\right\} \quad (39)$$

where δF and δu are infinitesimal forces and displacements, respectively.

In the classical linear theory of structures, the deformations, strains, and rotations are considered so small that the change in the matrix $\left[K \right]$ due to these effects is insignificant and can be ignored in the analysis of practical problems. The following expression relates the loads to the deflections:

$$\left\{ F \right\} = \left[K \right] \left\{ u \right\} \tag{40}$$

with $\left[K \right]$ being developed in terms of the initial shape.

Equation 39 could be used to develop a piecewise linear method of approximating a solution to the structures problems in which geometric nonlinearities are present, provided the advent of these nonlinearities is not too abrupt. In other words, if δF and δu are sufficiently small, the stiffness matrix $\left[K \right]$ will change little during the application of δF. This suggests that the value of $\left[K \right]$, given at the beginning of the application of the load can be used to predict δu for a given δF and for adding these δu's to the starting shape to get a new shape from which the new values of $\left[K \right]$ may be computed. The new matrix $\left[K \right]$ is used to predict another set of δu's from a second application of δF. The process is repeated until $\Sigma \delta F = F$, the total given load system. Each step is a linear step and the entire process is a piecewise linear process.

To understand the theoretical basis for developing such a linear method, it is helpful to consider the simplest structural element shown in Figure 5, which is a single bar from a pin-jointed truss. Furthermore, the exact relation of forces to displacements is easily derived.

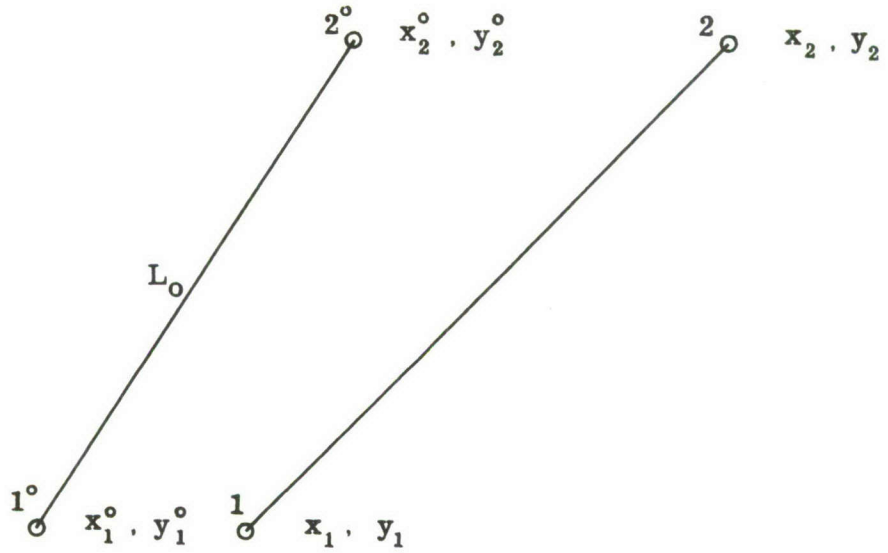

FIGURE 5: BAR OF SIMPLE TRUSS

In Figure 5 the coordinates (x_1^o, y_1^o) and (x_2^o, y_2^o) describe the bar position at the beginning of a load cycle, while (x_1, y_1) and (x_2, y_2) describe the bar position at the end of the load cycle. It is given that there exists an axial load (S_o) in the bar in the first position. The following terms are defined:

L_f = length of bar free of axial load and subject to room temperature,

L_o = length of bar at the beginning of the load cycle,

L = length of bar at the end of the load cycle,

S_o = axial load in bar at beginning of load cycle,

S = $(S_o + \Delta S)$ = axial load in bar at end of load cycle,

T_R = room temperature (°F.),

T_o = temperature (°F) at beginning of cycle,

T = temperature (°F) at end of cycle,

E = Young's modulus,

α = thermal coefficient of expansion,

A = cross-sectional area of bar.

It is postulated that the elongation of bar 1-2 (Figure 5) may be related to the axial load, temperature, and material properties as follows:

$$L - L_f = \frac{S\,L_f}{EA} + (T - T_R)\,\alpha\,L_f \tag{41}$$

from which it may be shown that the strain during the loading cycle is:

$$\epsilon = \frac{L-L_o}{L_f} = \frac{\Delta S}{EA} + \alpha\,\Delta T \tag{42}$$

Also, the incremental change in the axial load becomes:

$$\Delta S = \frac{EA}{L_f}\,(\Delta L - \alpha\,L_f\,\Delta T) \tag{43}$$

In the fundamental equations of thermoelasticity as given by Hemp in Reference 11, the "free energy" (F) is defined such that the partial derivatives of F with respect to temperature give the entropy and the partial derivatives of F with respect to the strains give the respective stresses. In this sense, the "free energy" for the thermoelastic problems is analogous to the strain energy for the uniform constant temperature problems (i.e., differentiation with respect to strain gives stresses).

Hemp's expression for the "free energy" in the bar shown in Figure 5 becomes:

$$F = \text{free energy/unit volume} = \frac{U}{AL_f} = \frac{1}{2}\,E\,\epsilon^2 + \frac{S_o}{A}\,\epsilon - E\epsilon\,\alpha\,(\Delta T) \tag{44}$$

The term $C_1(T)$ in Hemp's expression is disregarded because it does not contribute to the stresses on differentiation.

Then the strain energy for the bar becomes:

$$U = (S_o - EA\alpha\,\Delta T)\,(L-L_o) + \frac{1}{2}\,\frac{EA}{L_f}\,(L - L_o)^2 \tag{45}$$

The stiffness of the structure with respect to the displacements u_i and u_j may be written:

$$\left[K_{ij}\right] = \left[\frac{\partial^2 U}{\partial u_1 \, \partial u_j}\right] = (S_o - EA\,\alpha\,\Delta T)\left[\frac{\partial^2 L}{\partial u_i \, \partial u_j}\right] + \frac{EA}{L_f}\left(\left[\frac{\partial L}{\partial u_i} \quad \frac{\partial L}{\partial u_j}\right] + (L-L_o)\left[\frac{\partial^2 L}{\partial u_i \, \partial u_j}\right]\right) \tag{46}$$

If S_o is due only to thermal conditions, Equation 46 may be rewritten:

$$\left[K_{ij}\right] = \frac{EA}{L_f}\,(L - L_f - \alpha L_f T + \alpha L_f T_R)\left[\frac{\partial^2 L}{\partial u_i \, \partial u_j}\right] + \left[\frac{\partial L}{\partial u_i} \quad \frac{\partial L}{\partial u_j}\right] \tag{47}$$

To evaluate the derivatives in Equation 47, consider the bar to lie in the x-y plane (Figure 5) and let the final length of the bar be:

$$L^2 = (x_2 - x_1)^2 + (y_2 - y_1)^2$$

where x_1 and y_1 are joint coordinates for the deformed structure (i.e., $x_2 = x_2^o + u_2$, etc.). Then the derivatives in Equation 46 are evaluated as follows:

$$\frac{\partial L}{\partial u_1} = \left(\frac{X_2 - X_1}{L}\right)(-1) = -\lambda \quad , \quad \frac{\partial L}{\partial v_1} = \left(\frac{y_2 - y_1}{L}\right)(-1) = \mu \tag{48}$$

$$\frac{\partial^2 L}{\partial u_1^2} \quad \frac{L\,(-1) - (X_2 - X_1)\,\partial L/\partial u_1}{L^2} = - \frac{1}{L}(1 - \lambda^2) \tag{49}$$

where λ and μ are respective direction cosines. Assembling the results of all such derivations gives the following matrices:

$$\left[\frac{\partial L}{\partial u_i}\ \frac{\partial u}{\partial u_j}\right] = \begin{bmatrix} \lambda^2 & \lambda\mu & -\lambda^2 & -\lambda\mu \\ \lambda\mu & \mu^2 & -\lambda\mu & -\mu^2 \\ -\lambda^2 & -\lambda\mu & \lambda^2 & \lambda\mu \\ -\lambda\mu & -\mu^2 & \lambda\mu & \mu^2 \end{bmatrix} = \left[M^o\right] \tag{50}$$

$$\left[\frac{\partial^2 L}{\partial u_i\ \partial u_j}\right] = \frac{1}{L}\begin{bmatrix} (1-\lambda^2) & -\lambda\mu & -(1-\lambda^2) & \lambda\mu \\ -\lambda\mu & (1-\mu^2) & \lambda\mu & -(1-\mu^2) \\ -(1-\lambda^2) & \lambda\mu & (1-\lambda^2) & -\lambda\mu \\ & -(1-\mu^2) & -\lambda\mu & (1-\mu^2) \end{bmatrix} = \frac{1}{L}\left[M^1\right] \tag{51}$$

There are two important results from the preceding derivations: (1) the stiffness rates are significantly affected by the state of residual stress, e.g., the term $(S_o - EA\alpha\Delta T)\ \partial^2 L/\ \partial u_i\ \partial u_j$, even at the beginning of the loading cycle; and (2) at the beginning of loading, Equation 46 gives the same stiffness matrix as does the classical linear theory of trusses for the same shape. At the beginning of the loading period, Equation 46 becomes:

$$\left[K_{ij}\right] = \frac{EA}{L_f}\left[M^o\right] + \frac{S_o}{L_f}\left[M^1\right] = \left[K^o\right] + \left[K^1\right] \tag{52}$$

where $\left[K^o\right]$ is the so-called "elastic stiffness matrix" first derived in Reference 2. The quantity $\left[K^o\right]$ represents the essential stiffness resisting additional straining of the member. On the other hand, $\left[K^1\right]$ represents the "initial force stiffness matrix."

To establish some orders of magnitude for the approximations in the suggested piecewise linear technique, apply the preceding equations to the problem shown in Figure 6. Let $\tan\theta = u/L_f$. There is one degree

of freedom which is the displacement u_2. First, consider an exact solution to the problem. The load versus deflection relation may be written:

$$X = ku_2 + EA\ (\tan\theta - \sin\theta)$$
$$k = \text{rate of lateral spring—lb./in.} \tag{53}$$

The stiffness then becomes:

$$K = \frac{dX}{du_2} = k + EA\ \left(\frac{1}{\cos^2\theta} - \cos\theta\right)\frac{d\theta}{du_2}$$

$$\text{but } \tan\theta = \frac{u_2}{L_f} \text{ and } \frac{d\theta}{du_2} = \frac{1}{L_f}\cos^2\theta \tag{54}$$

$$\text{therefore, } K = k + \frac{EA}{L_f}(1-\cos^3\theta)$$

Secondly, consider the stiffness calculated from equations:

$$\left[M^o\right] = \frac{\partial L^2}{\partial u_2} = \lambda^2 = \cos^2\left(\frac{\pi}{2} + \theta\right) = \sin^2\theta \tag{55}$$

$$\left[M^1\right] = \frac{\partial^2 L}{\partial u_2^2} = \frac{1}{L}(1 - \lambda^2) = \frac{1}{L}\cos^2\theta \tag{56}$$

giving: (57)

$$K = k + \frac{S_o}{L}\cos^2\theta + \frac{EA}{L_f}\left(\sin^2\theta + \frac{L-L_o}{L}\cos^2\theta\right)$$

$$\text{However, } \frac{S_o}{L} = \frac{EA}{L_f}\left(\frac{1-\cos\theta_o}{\cos\theta_o}\right)\cos\theta \quad \text{and} \tag{58}$$

$$\frac{L-L_o}{L} = \frac{\cos\theta_o - \cos\theta}{\cos\theta_o}$$

Therefore, the stiffness becomes:

$$K = k + \frac{EA}{L_f} \quad (1-\cos^3\theta)$$

which is the same as Equation 54.

The problem in this case is to compute the deflection u for a given X using only stiffness Equation 54. The piecewise linear technique would be to apply a small load increment (δ F) and use Equation 54 with θ = O to give K_o = k and:

$$\delta X = k\delta u \qquad \text{or} \qquad \delta u_1 = \frac{1}{k}\,\delta X \tag{59}$$

Next, use $\theta_1 = \delta u/L_f$ and calculate $K_1 = k + \frac{EA}{L_f}\ (1 - \cos^3\theta_1)$

to get the next increment of deflection:

$$\delta u_2 = \frac{X}{k + \frac{EA}{L_f}\ (1-\cos^3\theta_1)} \qquad \text{etc.}$$

The results of such calculations are shown in Figure 6.

Next, use $\theta_2 = \frac{1}{L_f}\ (\delta u_1 + \delta u_2)$ and compute:

$$\delta u_3 = \frac{\delta X}{k + \frac{EA}{L_f}(-\cos^3\theta_2)}$$

By continuing this process, δu_4, δu_5, et al. may be computed and the total deflection obtained by summing the δu's.

The piecewise linear procedure was used in the preceding example to determine the deflection associated with the load applied first in $\frac{1}{4}$ increments and secondly with the load applied in $\frac{1}{10}$th increments. Such a process tacitly assumes convergence with an increased number of incremental loads used to build up the total required load. An improvement in

the approximate deflections (if any improvement exists) with an increase in the number of load increments may be graphically demonstrated by plotting deflection versus the reciprocal of the number of load increments. The results of such computations are shown in Figure 6.

Mathematically, the stiffness technique is a propagation problem in systems having a finite number of degrees of freedom, and may be stated as follows:

Given: $F_i(t)$ = set of arbitrary loads applied during the interval $0 \leq t \leq a$

$$\frac{\partial F_i}{\partial u_j} = K_{ij} \ (u_1(t), u_2(t), \ldots . u_n(t), t)$$

and $u_1(0), u_2(0), u_3(0), \ldots . u_n(0)$

Predict $u_1(t), u_2(t), u_3(t), \ldots u_n(t)$ for the given interval. Techniques of obtaining numerical solutions to propagation problems are described in Section 3-2 of Reference 8. However, the above problem differs from the problems discussed by S. H. Crandall in Reference 8 because the mode of F_i (t) is given; it is more common to find the mode of u(t) given. Nevertheless, the classical technique described by Crandall can be applied to the stiffness problem.

The numerical (piecewise linear) procedure described in the preceding example is based on a simple numerical integration procedure developed by Euler in 1768 (see Page 163 of Reference 8). The order of the truncation error in the recurrence formula is $0(h^2)$, where $h = \delta u$. Experience indicates that this method is sufficiently accurate for the majority of structural types because only the nonlinear effects associated with rotations are considered. (See Section 2.1.)

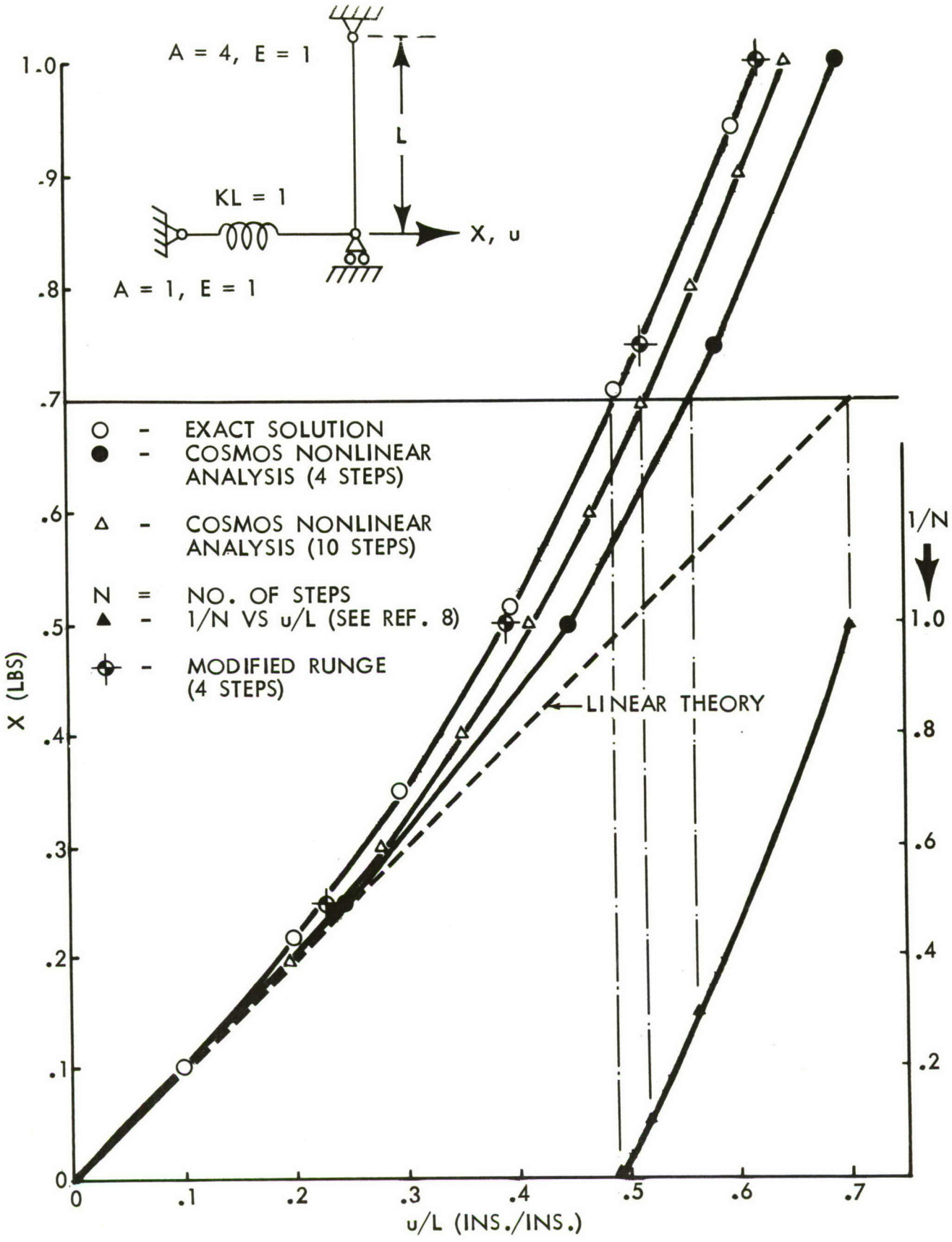

FIGURE 6: NONLINEAR LINKAGE

To ascertain the effects of using a recurrence formula with a higher-order truncation error, a modified Runge method may be applied to the stiffness problem. The truncation error is $0(h^3)$. Let points s and s+1 be two points or positions in the load versus deflection relation, with s being a given starting position and s+1 being the next position resulting from the application of a set of load increments. Then, for given values of F_s = load at s, u_s = deflection at s, K_s = stiffness at s, and ΔF = load increment, the problem is to compute F_{s+1} and u_{s+1}.

From the stiffness K_s an approximate value of the incremental increase in u may be computed:

$$\Delta^* u = K_s^{-1} \quad (\Delta F) \tag{63}$$

Having $\Delta^* u$, the stiffness at $(u + 1/2 \ \Delta^* u)$ and at $(u + \Delta^* u)$ may be computed as $K_{s+1/2}$ and K_{s+1}, respectively. Next, compute an increment of F as:

$$\Delta^* F = K_{s+1/2} \ \Delta^* u \tag{64}$$

This is the ordinary form of the Runge method with $\Delta^* u$ being given instead of ΔF. Substituting Equation 63 into 64 will lead to the expression:

$$\Delta^* F - \Delta F = (K_{s+1/2} K_s^{-1} - 1) \ (\Delta F) \tag{65}$$

If this expression is premultiplied by K_{s+1}^{-1}, the result is an estimate of $\Delta^* u - \Delta u$; i.e.,

$$\Delta^* u - \Delta u = K_{s+1}^{-1} \ (K_{s+1/2} K_s^{-1} - 1) \ (\Delta F) \tag{66}$$

from which the incremental change in u may be written in terms of a given incremental change in F as:

$$\Delta u = \left\{ K_s^{-1} - K_{s+1}^{-1} \ (K_{s+1/2} K_s^{-1} - 1) \right\} \quad (\Delta F) \tag{67}$$

A graphical picture of this process for one dimension is given in Figure 7. (See Figure 6 for application of this process to a numerical problem.) The first term of the above expression (Equation 7) is the same as the

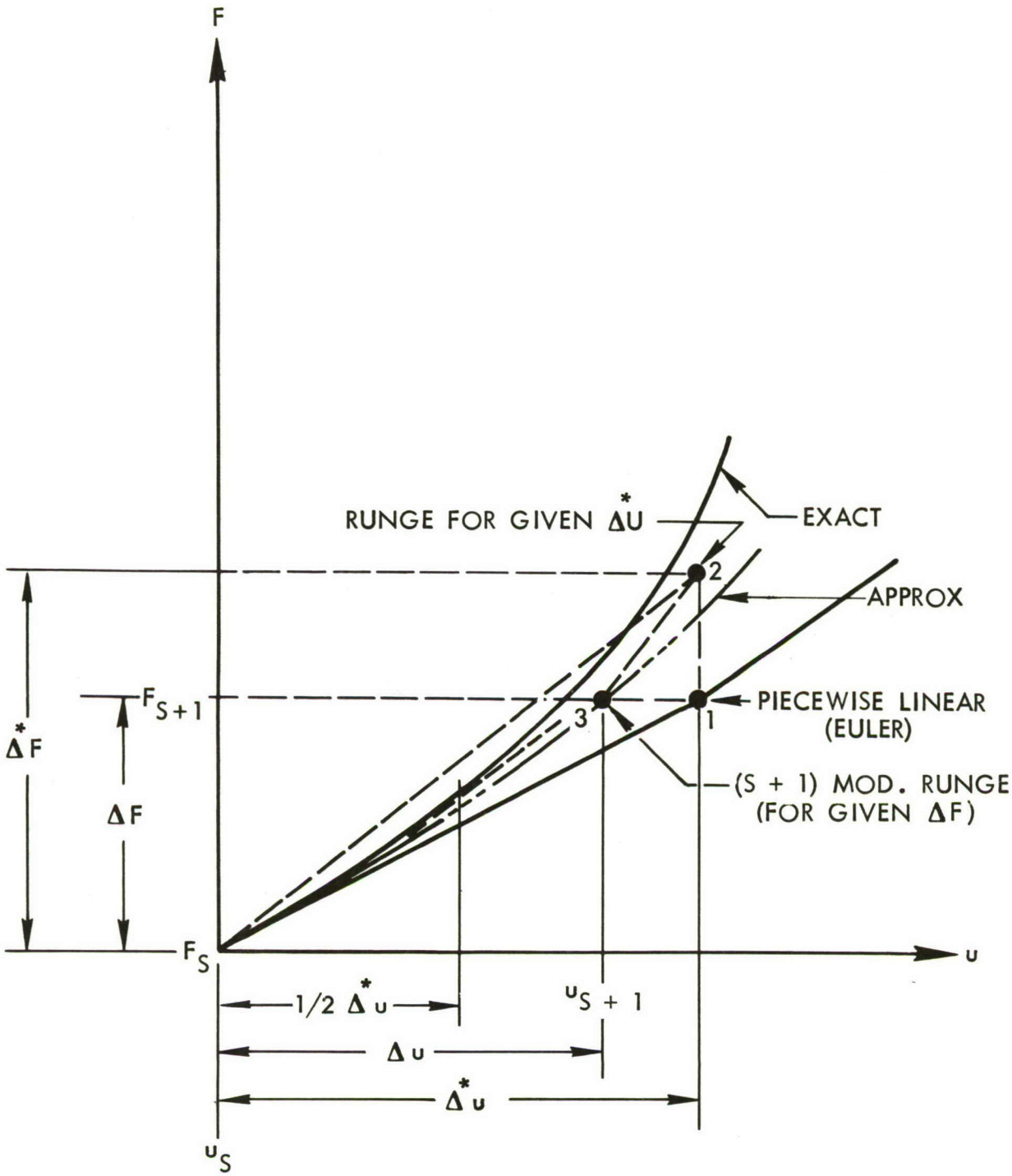

FIGURE 7: MODIFIED RUNGE METHOD

piecewise linear procedure. In a similar manner other methods of numerical integration may be applied to this problem.

In evaluating the expedient technique to be used, it is necessary to consider: (1) the nature of the theory of nonlinear elasticity as discussed in Section 2.1 of this document, and (2) the price of computing time for refinements.

In the preceding example, the range of $\frac{u}{L_f}$ for a practical problem is probably $0 \leq \frac{u}{L_f} \leq .2$ for which sufficiently accurate results can be obtained by the Euler method with an economical number of increments ($N \leq 10$).

If $k = 0$ in the above problem, a small increment of deflection is needed to determine the corresponding δF. Then the procedure of applying small F's may be used. However, this simple procedure cannot be applied to the problems of neutral equilibrium (e.g., buckling and snap through). Treatment of such complex problems is beyond the scope of this research.

Two other examples were tried using the Euler method:

(1) A beam having a uniform EI, uniformly loaded with a lateral load, and free to rotate at the ends, but otherwise constrained at the ends as shown in Figure 8—the present digital program was used to compute a five-step and a ten-step solution; both solutions are compared with an exact solution in Figure 8.

(2) A square plate subjected to a uniform-edge-compression load (P) and a normal load (Q) concentrated at the center (A) as shown in Figure 9—the normal deflection (δ) was computed for varying values of P, while Q was kept constant. The critical value of P (i.e., edge load to buckle plate when Q=0) is computed using the Southwell method by considering the critical value of P to be the slope of the line of (δ/P) versus δ as shown in Figure 9.

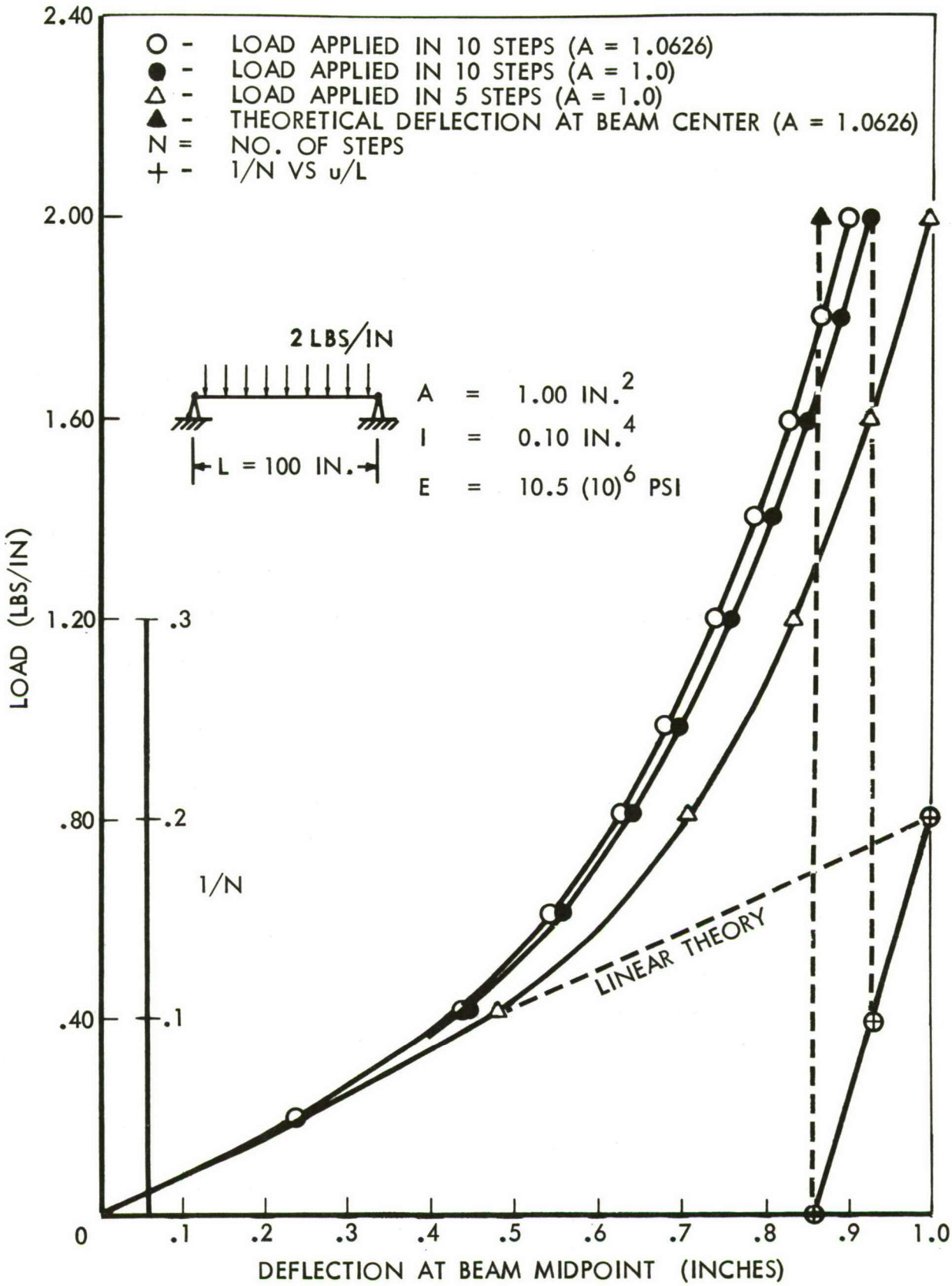

FIGURE 8: LOAD VERSUS DEFLECTION FOR BEAM-CATENARY

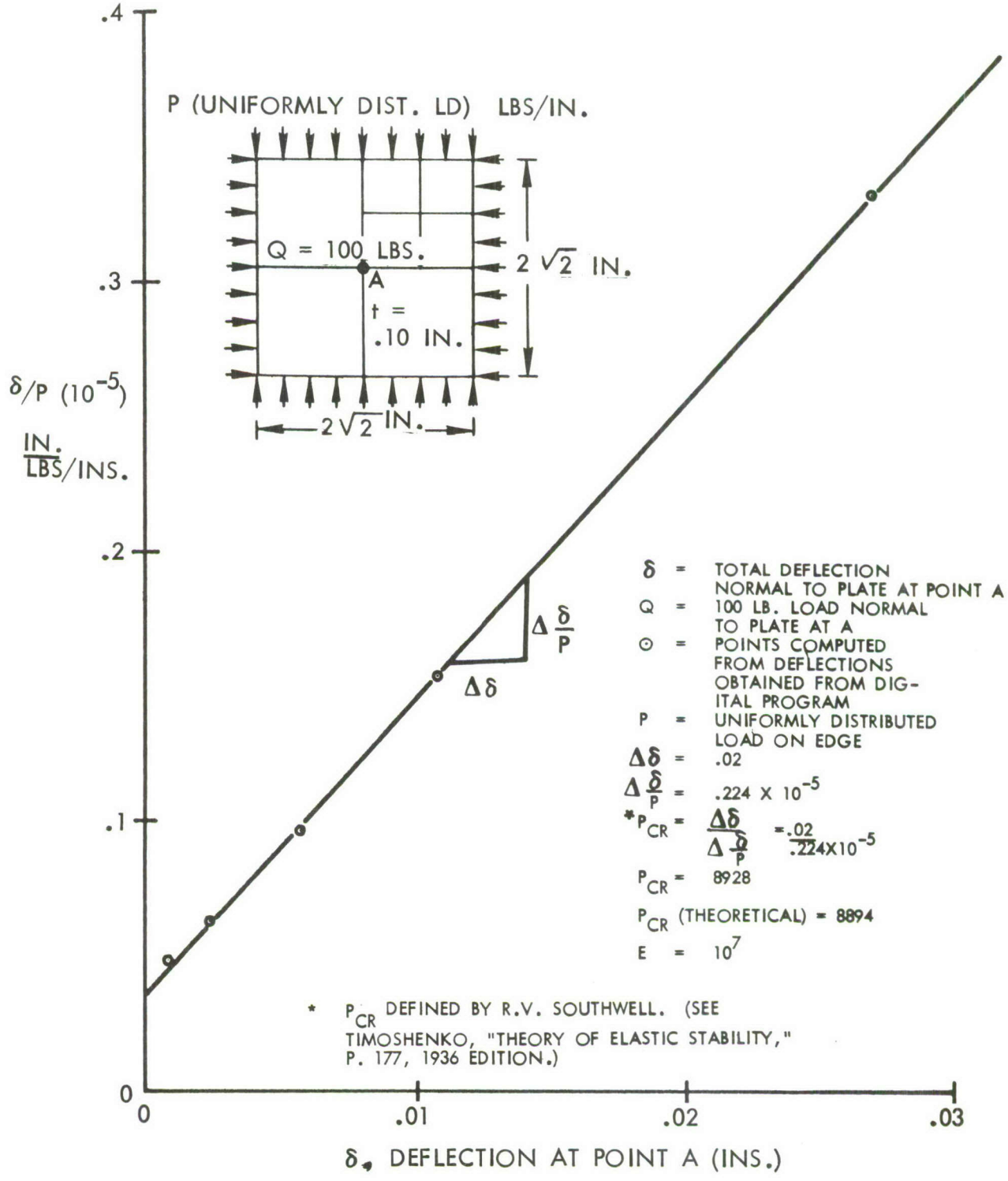

FIGURE 9: PLATE BUCKLING

If bending deformation and axial deformation were considered in the preceding example, the piecewise linear theory would postulate that the stiffness associated with the bending of the bar could be superimposed on the stiffness associated with axial behavior. This postulation is justified because the axial load is small compared to the critical load for the elemental length (i.e., $S \ll \frac{\pi^2 E I}{L_f}$).

If the local coordinates place the x axis normal to the beam axis, the total stiffness matrix is:

$$[K] = \left[\begin{array}{cc|cc} & & 0 & 0 \\ K_{AA} & & 0 & 0 \\ 2\times 2 & & 0 & 0 \\ \hline 0 & 0 & & \\ 0 & 0 & K_{BB} & \\ 0 & 0 & 4\times 4 & \\ 0 & 0 & & \end{array}\right] \qquad (68)$$

where $K_{AA} = K^o + K^1$ is given by Equation 52, Page 30, and K_{BB} is the bending stiffness given on Pages 20 and 21.

The stiffness matrices K^o and K^1 may be analogously developed for the triangular plate. The resultant K^o and K^1 matrices are given in Appendix A. To these matrices are added the stiffnesses for plate bending given in Reference 6.

Because of the bulk of the digital work required, it appears that the Euler method of integration coupled with the simple superposition of the normal-loading effects to those of the direct (axial) loading (i.e., piecewise linear) would give the most expedient technique for this research. The deflections computed in this manner were plotted versus the reciprocal of the number of steps ($\frac{1}{N}$) for simple examples in Figures 6 and 8. The accuracy for these plottings was considered an indication that the piecewise linear technique was sufficiently accurate for the present research.

2.5 Vibration Analysis

Of primary importance in this study is the vibration analysis of the heated structure, which determines the natural frequencies and principal modes about an equilibrium state.

The structural problem which arises is that of calculating the stiffness matrix; it is imperative that the correct stiffness be found. If the correct stiffness matrix is known, standard techniques for performing the vibration analysis may be employed.

As discussed in Reference 3, the nonlinear structural analysis outlined in this section will provide an approximation to the actual stiffness of the heated and loaded structure. Furthermore, the approximation improves as the number of linear steps increases. Ultimately, the intention is to show that results of adequate accuracy can be obtained with a reasonable number of linear steps. (See plot of $\frac{1}{N}$ versus deflection in Figures 6 and 8.)

2.6 Digital Programs for Linear Analysis

The basic digital programs for performing a linear structural analysis were available at the time this research was initiated. These programs are identified in Reference 6 as the COSMOS programs developed in the Applied Math Section, Aero-Space Division, The Boeing Company. A detailed description of these programs is given in Reference 6.

The digital programs may be roughly divided into the following areas:

(1) Assembly of identification, location, and properties of all the structural elements and their associated nodes.
(2) Computation of the stiffness elements and stress matrices for each structural element.

(3) Merging the stiffness matrices of the various structural elements into one gross stiffness matrix for the entire structure.

(4) Modification of the gross stiffness matrix to properly account for the boundary conditions. For example, supports may be accounted for by deleting the rows and columns corresponding to these supports, while partial constraints may be accounted for by adding supplementary springs. Arbitrary displacements require additional matrix manipulation.

(5) Inversion of the modified gross matrix.

(6) Computation of displacements corresponding to a given load condition.

(7) Computation of stresses corresponding to the displacements in (6).

The required input consists of the coordinates of the nodes, thicknesses of the plates, areas of the bars, the second moment of the bar areas, material properties of each element (E, G, α), and the temperature at each node.

2.7 Digital Programs for Nonlinear Analysis

The mechanics of the digital programs developed under this contract to perform a nonlinear analysis in accordance with the theory developed in this document are discussed in Appendix B. A flow diagram of the basic operations of the digital programs is shown in Figure 10.

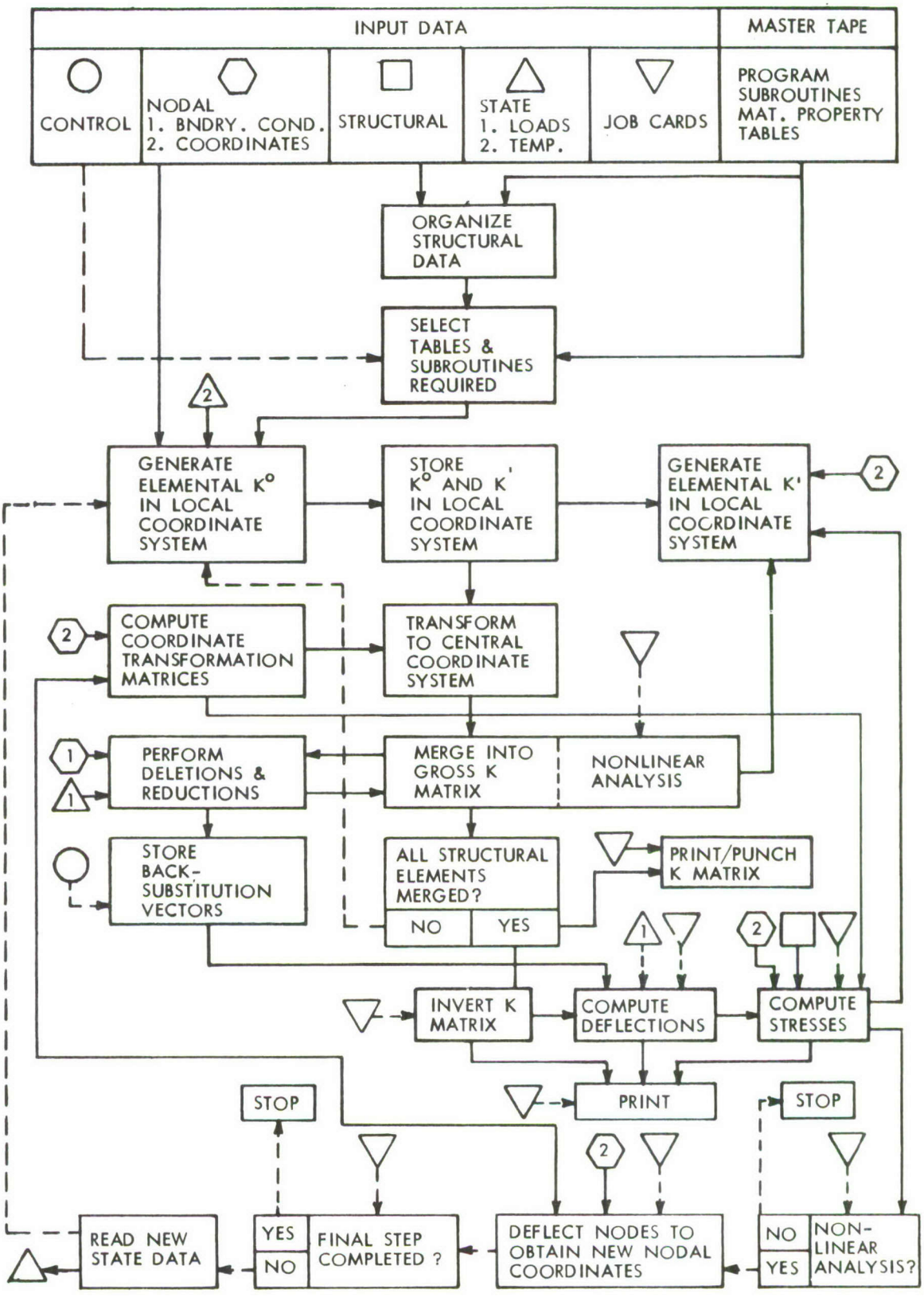

FIGURE 10: BASIC FLOW DIAGRAM OF DIGITAL PROGRAMS

SECTION 3.0

APPLICATION OF THEORY

3.1 Model Design

The basic phenomena described in the theoretical developments in this document are best exhibited by vehicles having relatively thin lifting surfaces abnormally distorted by thermal gradients and/or load conditions. A typical lifting surface of such a vehicle would have a low aspect ratio, a low thickness ratio, a highly swept leading edge, and possibly cropped tips.

The model configuration selected for analysis in this investigation is the cropped delta wing shown in Figures 11, 12, and 13. This wing was designed ostensibly to be fabricated and tested at some future date. It is supported at three points by bipod legs designed to act as flexure pivots to furnish two translational kinematic constraints at each support. The flexure pivots in the bipods are located for maximum rotational flexibility for a given strength. The skin gage and the skin panel sizes were selected such that theoretically the skin would not buckle under an estimated load of:

$$\sigma_x = 14.0 \text{ ksi}; \quad \sigma_y = 17.0 \text{ ksi}; \quad \tau_{xy} = 3.00 \text{ ksi}$$

The webs of the spars and ribs are corrugated to minimize thermal stresses. The spar caps are spot welded to the webs and riveted to the skin. Gages, dimensions, and construction details are shown in Figures 11, 12, and 13.

Since the nonlinear and thermal effects theory and procedures were developed for elastic structures, it is desired that the temperature profile selected for the investigation not seriously affect the elastic properties of the material. In order to use temperatures which are likely to bring about nonlinear behavior in the model, a maximum of twenty percent reduction in the material properties at 1000°F was accepted as a specification for the material to be used. On this basis, Inconel X was selected as the material.

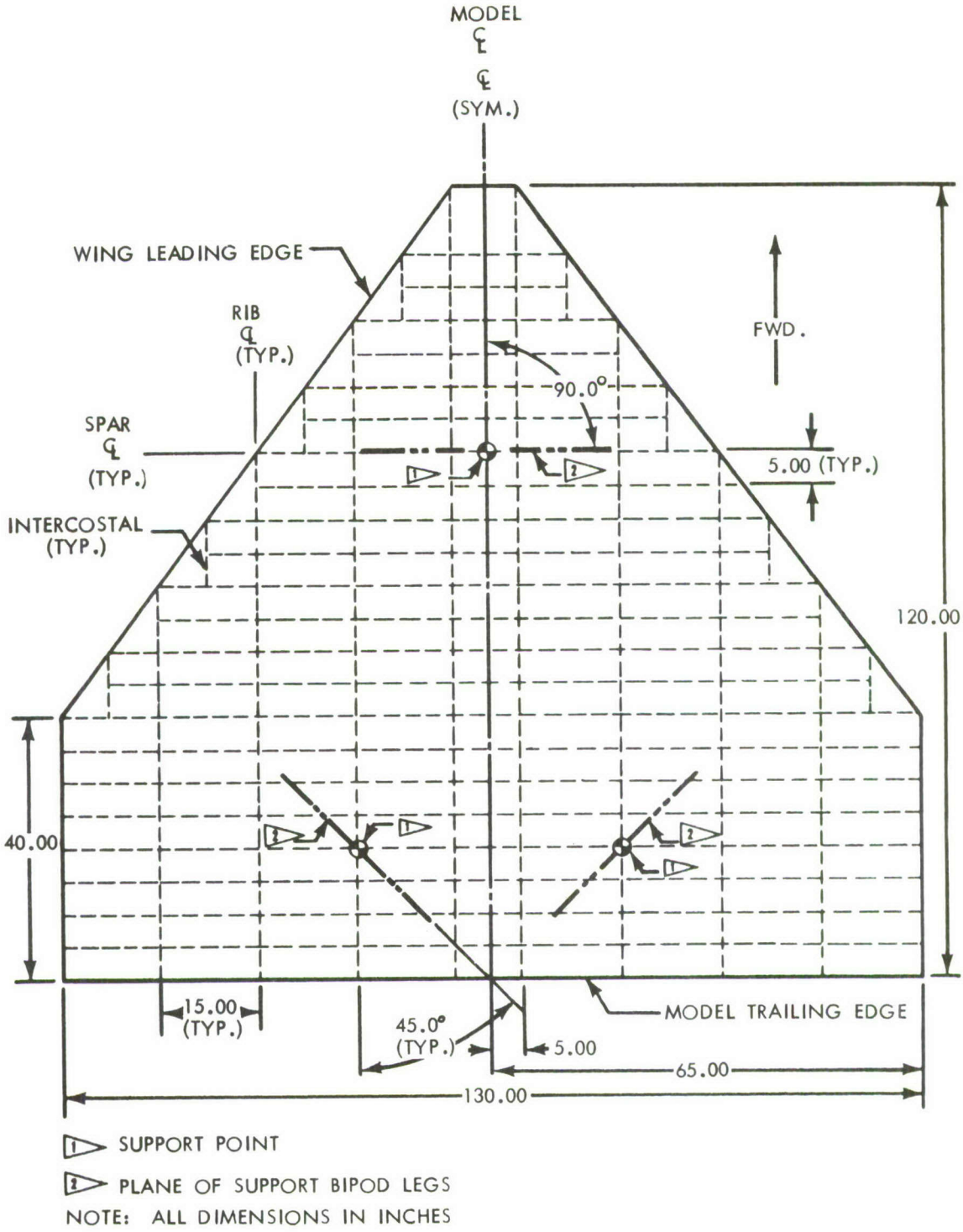

FIGURE 11: MODEL PLAN VIEW

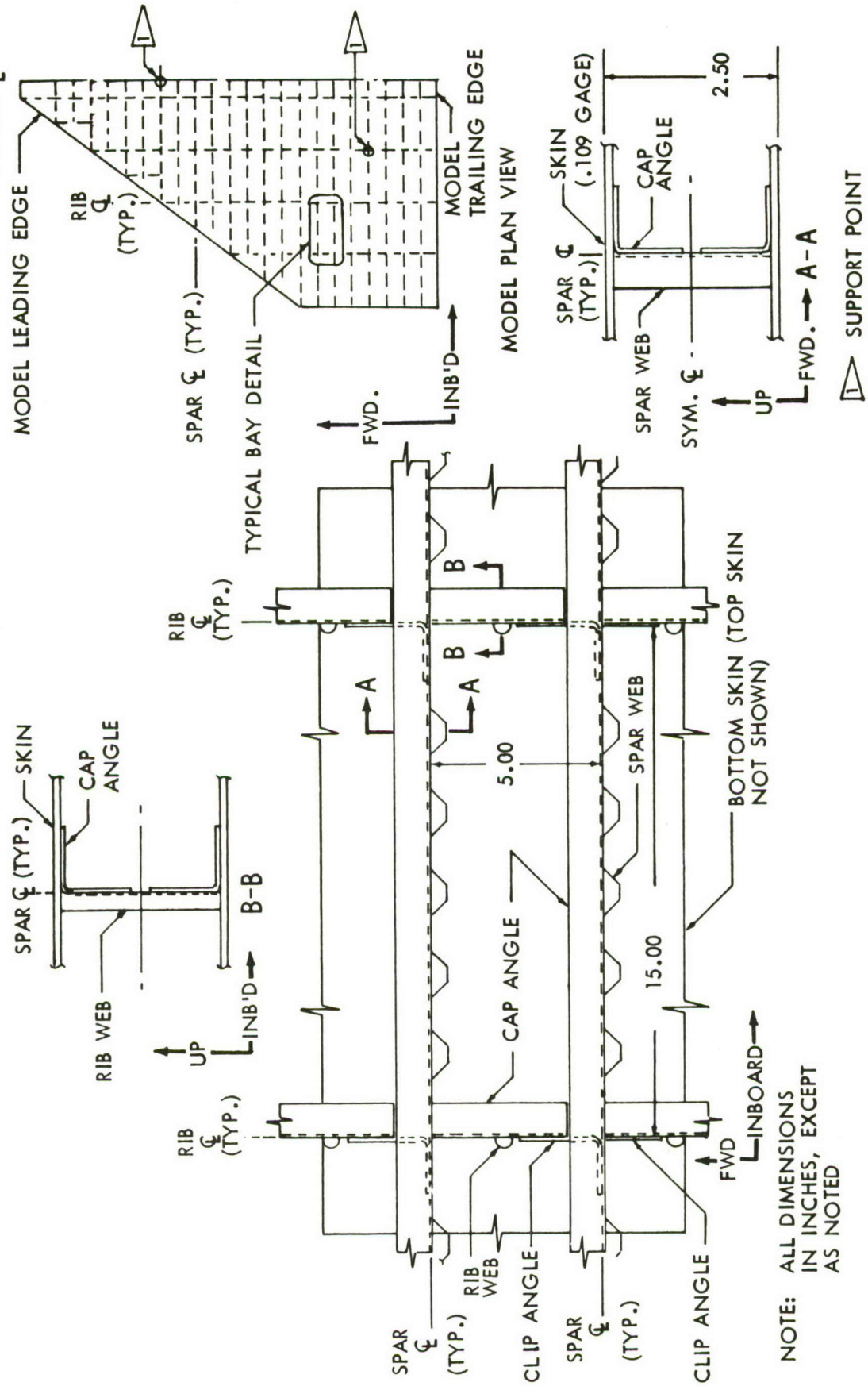

FIGURE 12: TYPICAL BAY DETAIL

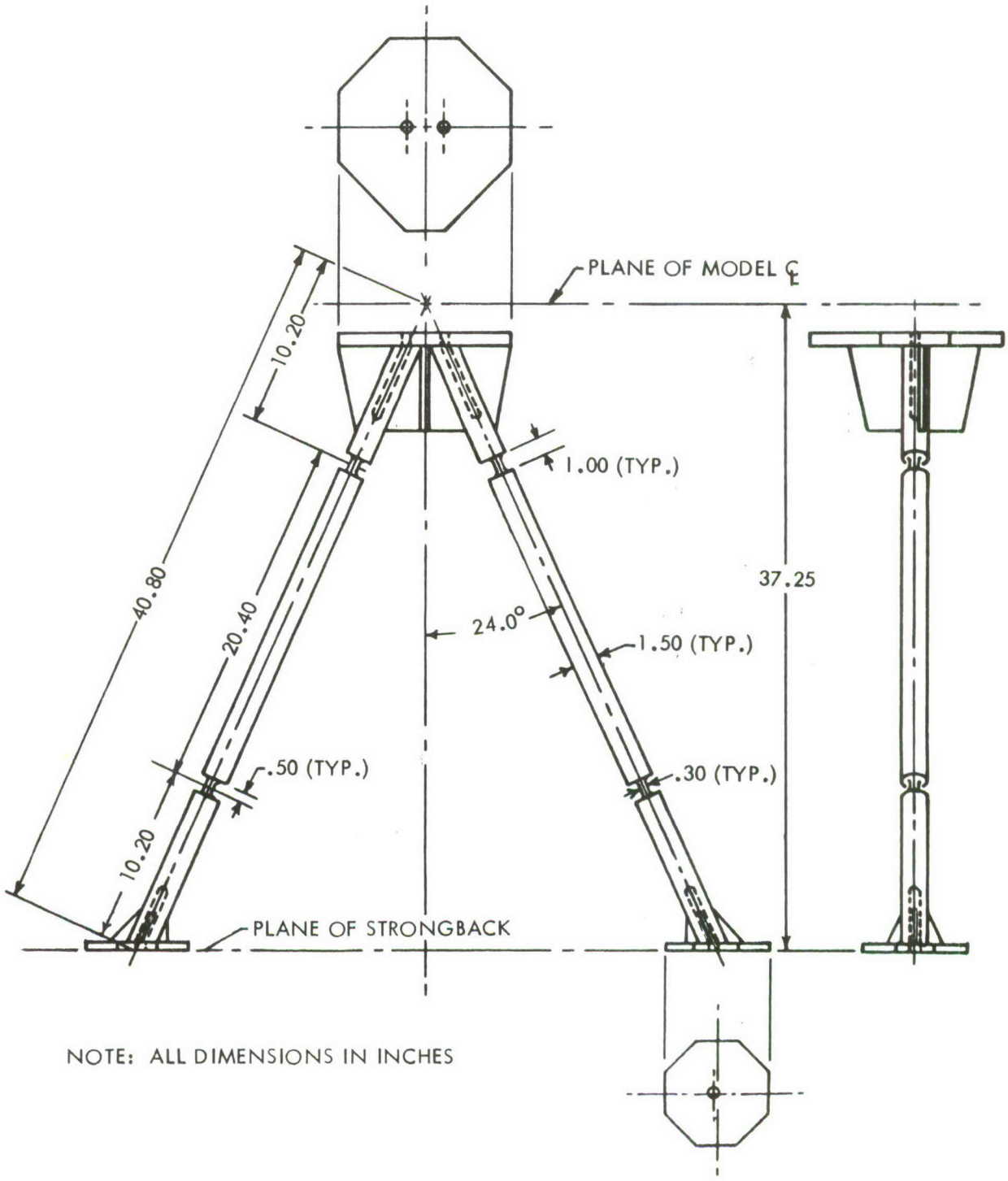

FIGURE 13 : TYPICAL BIPOD SUPPORT

3.2 Temperature Profiles

It is desired that the temperature profile be computed from a representative trajectory and that rather sharp thermal gradients be present. The requirements of future tests dictate the selection of a trajectory which achieves relatively low temperatures (1000°F maximum). A mild boost trajectory was selected. Using this trajectory, a temperature analysis was made with the following assumptions:

(1) A "quasi-steady-state," one-dimensional thermal analysis is used to compute the temperature.

(2) Using flat-plate theory, the aerodynamic heating is calculated for a flat prototype wing having a constant chord of 50 feet, with distance being measured in feet streamwise from the leading edge.

(3) Transition from laminar to turbulent flow occurs at a Reynolds number of 3×10^6, based on free-stream properties.

(4) Both sides of the wing reradiate to outer space ($T = -460°F$).

(5) No heat is conducted laterally in the wing; the heat flows only perpendicular to the surface of the wing.

(6) There is no appreciable temperature drop through the skin of the wing.

(7) The effects of heat conduction through the webs of the structure are negligible; heat transfer through the wing is accomplished by radiation only.

(8) The radiation from one skin to the other is equivalent to radiation between two infinite flat plates.

(9) Emissivity of the wing, $\epsilon = 0.6$.

Heat transfer coefficients and adiabatic wall temperatures were obtained from Reference 10. The hot-side and cold-side temperatures were then obtained from the following equations:

$$h_H (T_{AW_H} - T_H) = \sigma \epsilon_H T_H^4 + \sigma F_\epsilon F_A (T_H^4 - T_C^4) \qquad (69)$$

$$h_C (T_{AW_C} - T_C) = \sigma \epsilon_C T_C^4 - \sigma F_\epsilon F_A (T_H^4 - T_C^4) \qquad (70)$$

This gave the temperature profiles for the actual vehicle.

It is assumed that the temperature at a given percent of chord and a given percent of span on the model is the same as the temperature on the prototype wing at the same percentages of chord and span.

Since the temperature can be controlled on only one side of the model, the other side being exposed to the concrete floor and the ambient air, the upper skin was driven at the hot-side temperature and the other skin assumed whatever temperature resulted. This cold-side temperature was calculated using the previously computed hot-side temperature in the following equation:

$$\sigma F_\epsilon F_A (T_H^4 - T_C^4) = \sigma F_\epsilon F_A (T_C^4 - T_{floor}^4) \qquad (71)$$

The floor was assumed to remain at 70°F. The resulting temperatures are plotted on the model-temperature curves in Figure 14. The mean temperatures for the upper and lower surfaces of the model are shown in Figure 15. The resultant temperatures for the nodes are given in Tables 1 through 20 in Appendix C.

3.3 Structural Idealization of the Wing Model

The nodal breakdown consists of 62 nodes on each wing surface, or a total of 124 nodes, each with five degrees of freedom in the final K^o matrix except for constraints imposed at the support points and along the centerline as required by symmetry or antisymmetry (approximately 600 degrees of freedom). (See Figures 16 and 17.) The nodes are located in the centroidal plane of the skin. The panel arrangement consists of a basic 10- by 15-inch rectangular grid with rectangular spar and rib web panels along the grid lines. This requires lumping the spar webs which are spaced 5 inches apart in the actual model rather than 10 inches as assumed in the idealization.

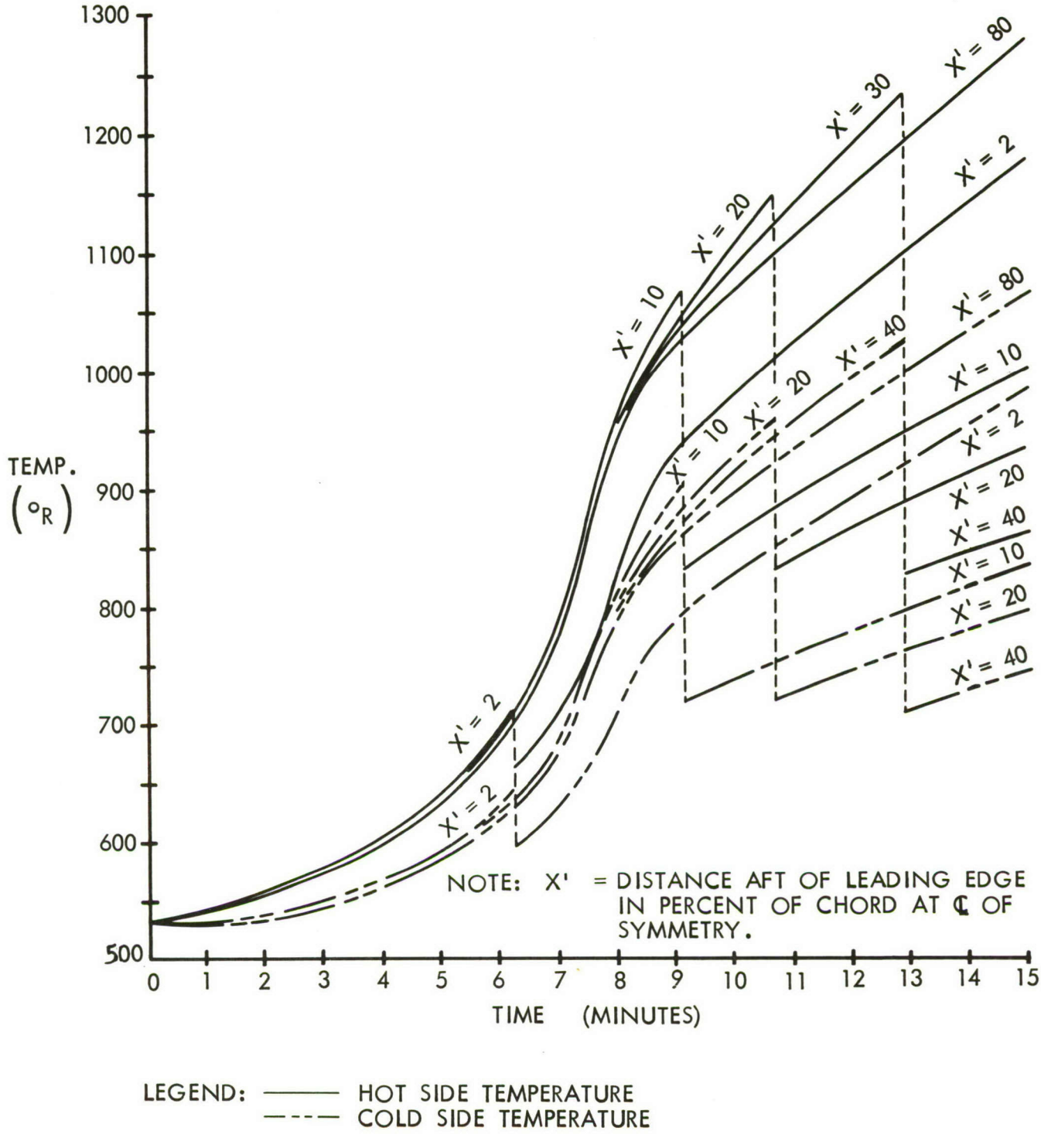

FIGURE 14: MODEL TEMPERATURES

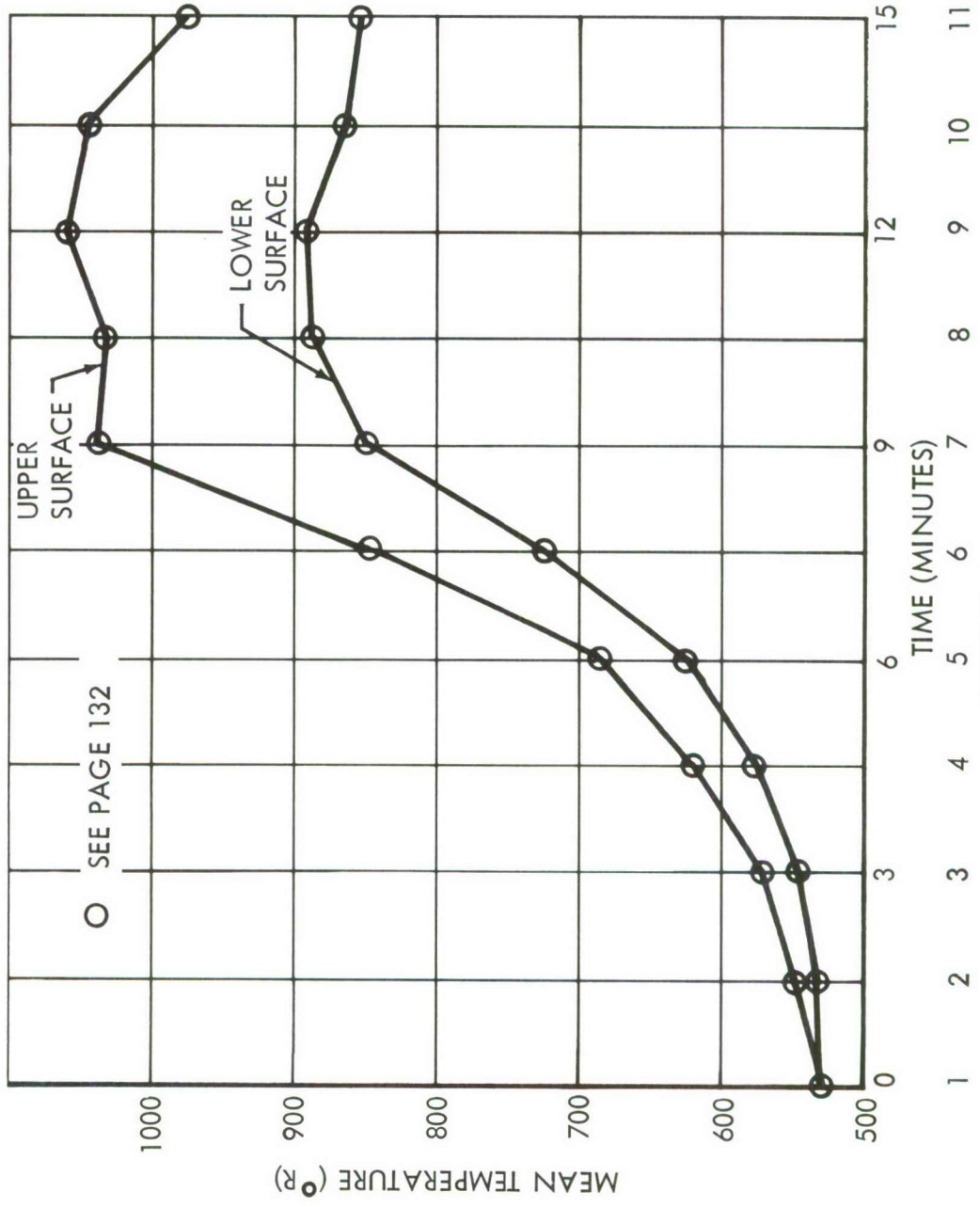

FIGURE 15 : MEAN TEMPERATURE VS TIME

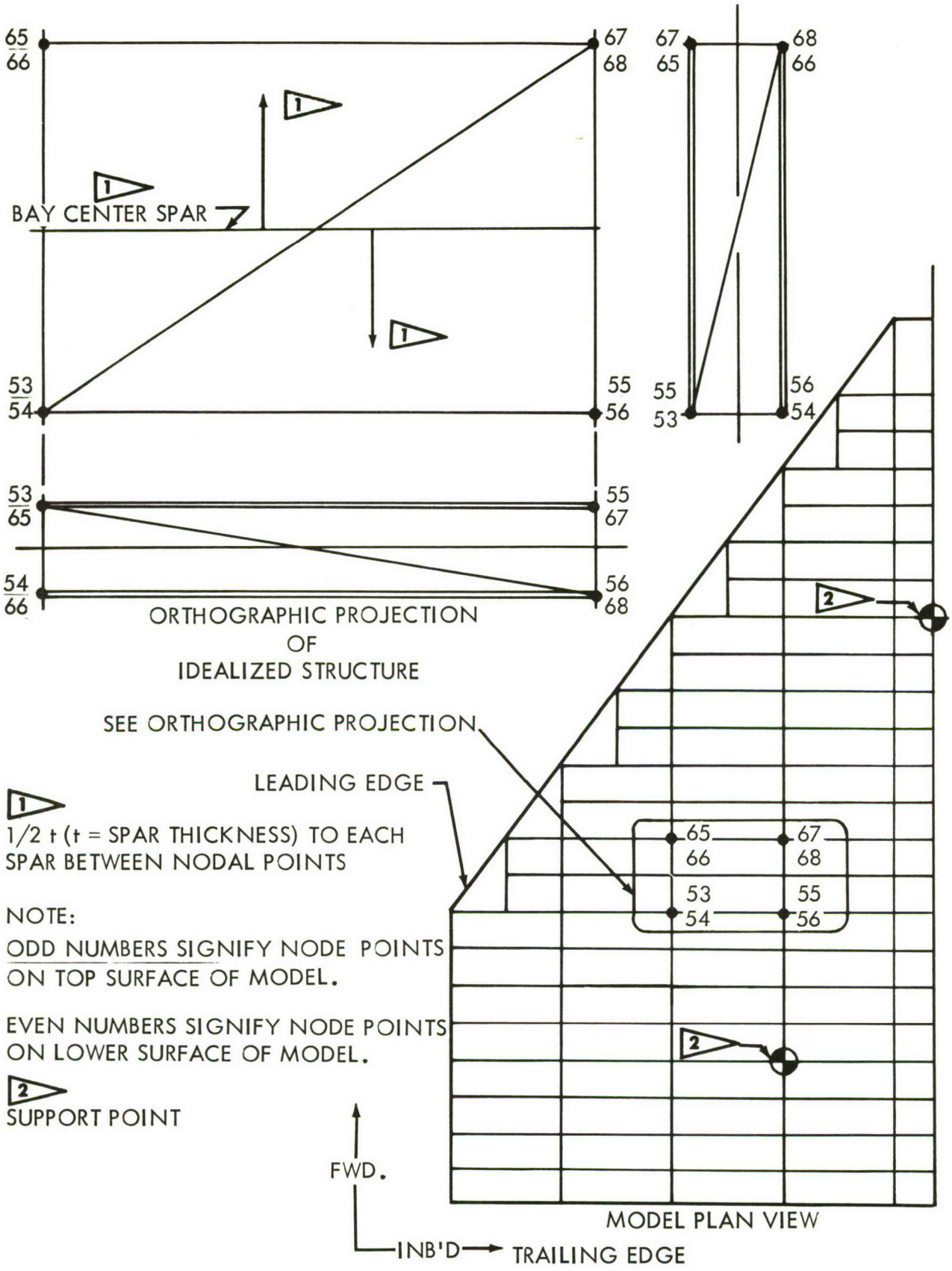

FIGURE 16: IDEALIZED STRUCTURE

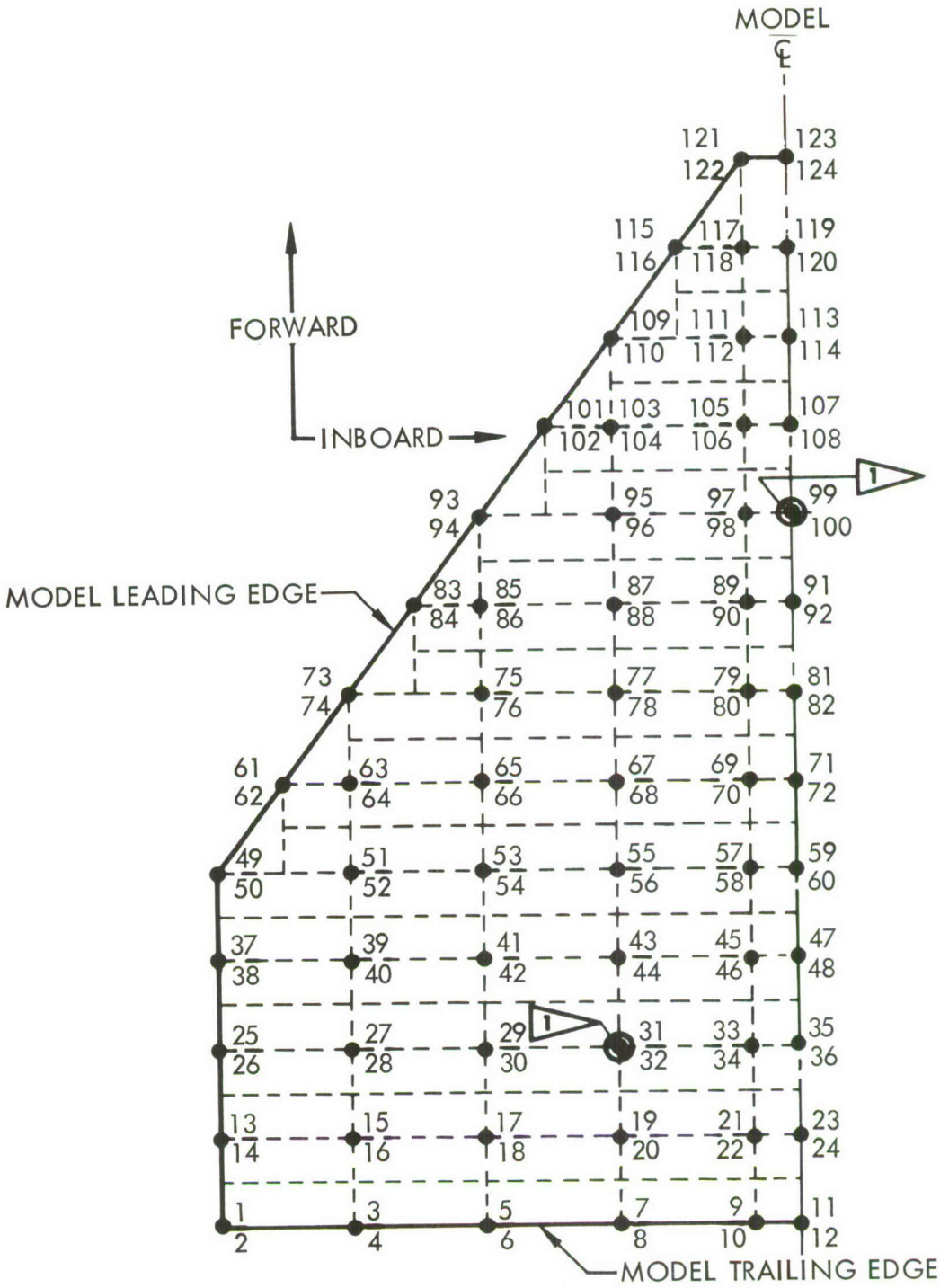

MODEL PLAN VIEW
(L.H. SIDE)

NOTE: ODD NUMBERS IDENTIFY NODES ON TOP SURFACE OF MODEL.

EVEN NUMBERS IDENTIFY NODES ON BOTTOM SURFACE OF MODEL

1 SUPPORT POINT

FIGURE 17: NODE LOCATION AND IDENTIFICATION

(1) Skin—Basic 10- by 15-inch rectangular panels will be broken down into isotropic triangular plates. Bending stiffness is included in the K^0 matrix, but only membrane effects will be considered in the K^1 matrix.

(2) Spar Flanges—To reduce the number of structural elements the effect of the spar flanges has been included by modifying the membrane skin thickness.

(3) Spar Webs—Basic 2- by 10-inch and 2- by 15-inch web panels will be broken down into two orthotropic triangular plates having membrane stiffness only. These plates will contribute to K^0 only. The orthotropic properties of the corrugated web are assumed to be as follows:

Effective thickness for stretching in plane of wing:

$$t_{eff} = 0$$

Effective thickness normal to plane of wing:

$$t_{eff} = t \text{ (where } t \text{ is gage of corrugated material)}$$

Effective thickness in shear:

$$t_{eff} = \frac{t}{2}\frac{\ell}{\ell'}$$ (where $\frac{\ell}{\ell'}$ is the ratio of the actual length to the developed length of the corrugated material.)

3.4 Deflection Analysis

The nonlinear digital program described in Appendix B was used to predict the deflections of the model subject to:

(1) Dead weight (.074 lbs/in^2) plus a live load of 2.00 lbs/in^2;

(2) Thermal environment described by the temperature increments given in Tables 1 through 13.

Contour graphs of these deflections are shown in Figures 20, 30, and 37.

In addition to deflections, the digital program predicted the stresses accrued during each step and the accumulated stresses. The stresses are

necessary for the computation of the K^1 matrix at the end of each step. Also, these stresses and deflections were qualitatively checked at the end of each step for obvious errors which might occur in a program of such magnitude.

3.5 Natural Frequencies and Mode Shapes

For a step-by-step solution of the equilibrium configuration, the gross stiffness matrix is extracted from the nonlinear program at the end of each step of the digital procedure.

The natural frequencies and the associated mode shapes were computed using an existing eigenvalue program from the stiffness matrix and the mass matrix.

Using a stiffness matrix computed for the deflected shapes, the first-six symmetrical modes were computed for (1) the cold unloaded structure, (2) the cold loaded structure, and (3) the structure sustaining the accumulated deformation and the temperature distribution for the ninth step. The first three antisymmetrical modes and frequencies were similarly computed for (1) the cold unloaded structure, and (2) the hot structure of the ninth step.

SECTION 4.0

CONCLUSIONS AND RECOMMENDATIONS

4.1 Numerical Results

All deflections and frequencies were computed for a constant E, assumed to be uniform throughout the wing. This conforms to the statement of work in Section 1.0. The E actually used for the digital analysis was the E corresponding to T = 700°F because, at the time of programming, it appeared that 700°F was a reasonable mean temperature. The digital program searches from a source of stored information for the E and α associated with a given material subject to a given temperature. According to the basic assumption, the final frequency data can be corrected by the factor $\sqrt{E/E_{700°}}$. Since each step is linear, such a correction factor could be applied to each step as shown in Table 21. No corrections were made for the small changes in the thermal coefficient of expansion.

The feasibility of modifying the programs to account for a simultaneous change in E, α, and T during each step is discussed in Section 4.3.

The deflections of the structure subjected to a uniform load of two pounds per square inch at room temperature (70°F) and the contours of these deflections are shown in Figure 20.

The first-six symmetrical mode shapes were computed for both the loaded and the unloaded cold (70°F) structures. However, the differences between the respective mode shapes (for loaded versus unloaded structures) were so insignificant that only the contours of the modes for the unloaded structure are presented (Figures 21 through 27). For a similar reason the antisymmetrical modes and frequencies were computed for only the unloaded structural conditions.

The first-six symmetrical modes of vibrations were computed for each of the deflected shapes in the ten increments of the temperature profile. The contours of those six mode shapes associated with the first step and the ninth step are presented in Figures 21 through 27 and 31 through 37, respectively. The ninth step was selected because the maximum mean temperature occurs during this period. During this period the structure is referred to as a hot structure.

The ratio of the frequency at each time interval to the frequency at room temperature (ω / ω_o) was computed for each of the first-four symmetrical modes. These ratios for constant E are presented in Figure 18, and these ratios corrected by the factor $\sqrt{E/E_{700°}}$ are presented in Figure 19. Preliminary computations indicated that the variation in the higher modes (5th and 6th) was insignificant. The frequencies given in Figures 20 through 49 have been corrected by the factor $\sqrt{E/E_{700°}}$.

4.2 Observations and Remarks

The total digital analysis of predicting the vibrational behavior of the structure for an entire spectrum of the given temperature profile required approximately 25 hours on the 704 digital computer. A linear analysis of the same problem would require approximately 2-1/2 hours. This time is strictly a function of the number of structural elements, nodes, and degrees of freedom (see Page 49 on idealization).

It was assumed that neither local buckling of the skin panels nor stability of the gross structure would create a problem in the digital analysis. Theoretically, the procedures developed under this research can predict the conditions of instability. The idealization of the subject model prevented the analysis from predicting skin buckling. The trend toward overall wing instability is indicated by (1) a serious decline in the value of the stiffness-matrix determinant, (2) a serious decline in the natural frequencies, and/or (3) the deflections approaching a branch line asymtotically.

Neither the stiffness-matrix determinant nor the deflections versus load were computed for the wing model. Only the time-interval frequencies were computed, and they indicated that the structure was quite stable under the given conditions.

The bipod supports were designed as flexure pivots (i.e., only the rigid-body motion of the wing was constrained with the external constraints being statically determined). However, the rotational spring rates of these pivots are not actually zero, but merely small enough to be neglected in this work. These spring rates could be considered by adding them to the rotational spring rates of the adjoining elements.

The effects of K^1 are relatively insignificant for this model and environment. The major effects of elevated temperature on the vibration characteristics of this model arise from the thermal deformation (warping) rather than thermal stress.

The preceding discussion applies to the model designed and analyzed in this effort. However, such discussion does not always apply (e.g., the significance of K^1 increases rapidly as incipient buckling is approached). The behavior of the given wing appeared to be far removed from a condition of buckling. It is believed that the wing would have to be considerably thinner before buckling of the gross structure would be exhibited. Direct tracing of the load-deflection curve in this regime cannot be done with the present program.

4.3 Recommendations for Future Research

Because the type of vehicle which will demand a nonlinear analysis will probably operate in an environment in which material properties will be significantly affected, it is recommended that the digital program be modified so that changes in the material properties of each structural

element can be considered in the stiffness computations and the merge programs. Such a program modification is feasible and probably could be implemented in a period of time comparable to that required to write the present control program. However, such a modification will increase the machine time required for each step and, hence, will decrease the reliability of the operation. This could result in modifications to the present control programs.

For wing structures similar to the one considered in this document, the effect of nonlinearity on vibration mode shape and frequency can often be determined with sufficient accuracy by calculating a revised stiffness matrix based on the stresses and deflections found by using the linear theory.

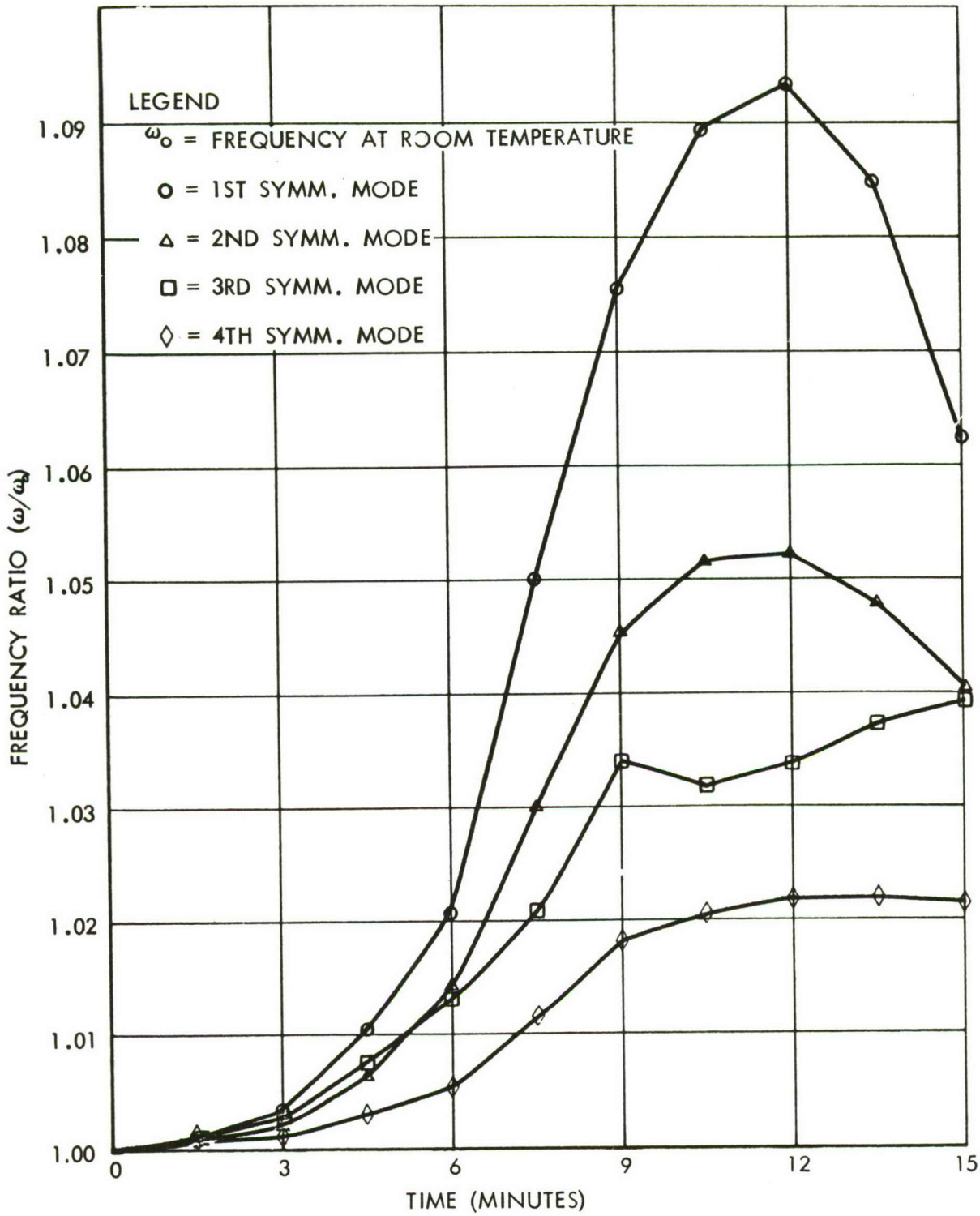

FIGURE 18: FREQUENCY RATIOS VS TIME: CONSTANT E

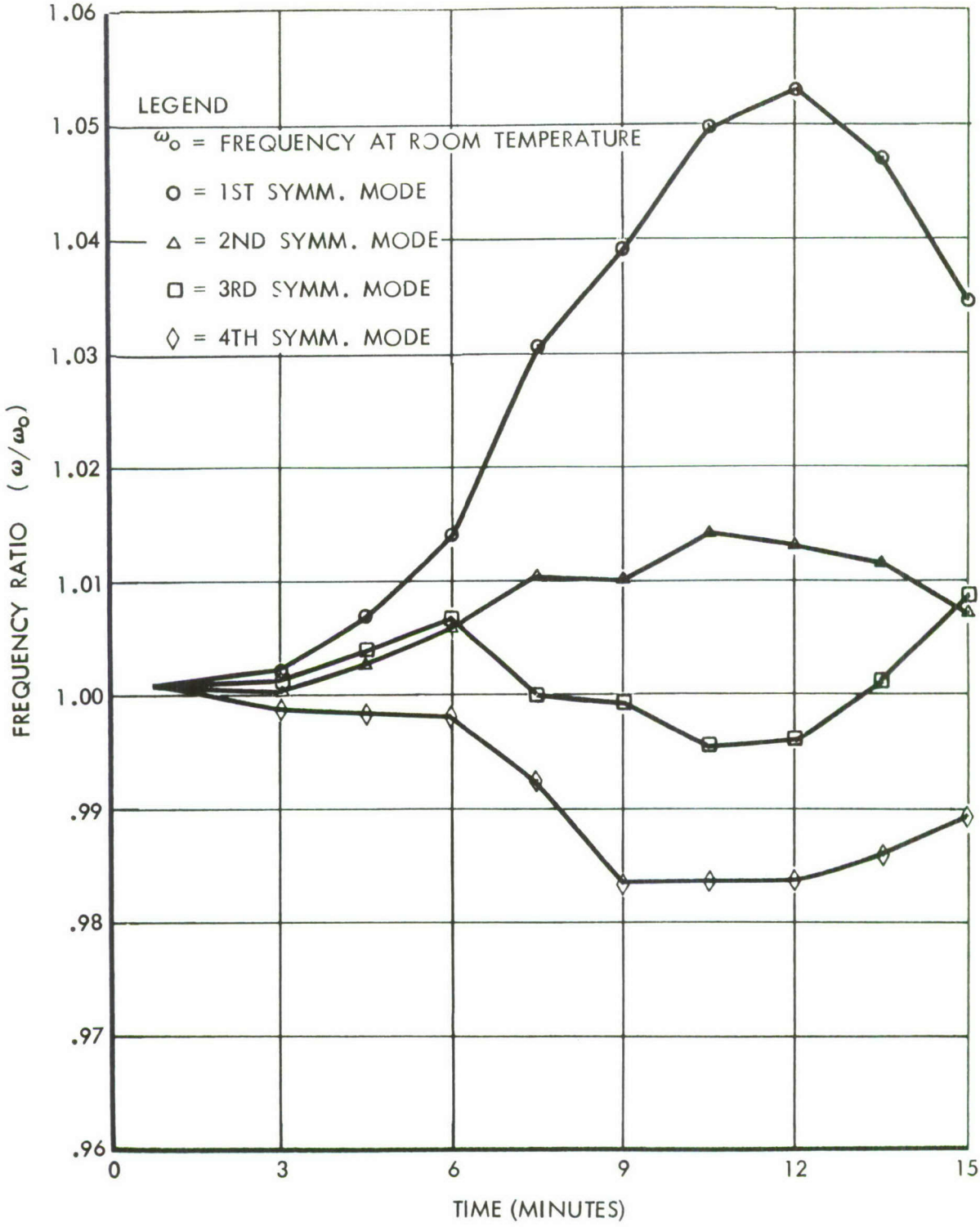

FIGURE 19: FREQUENCY RATIOS VS TIME CORRECTED FOR $\sqrt{E/E_{700°}}$

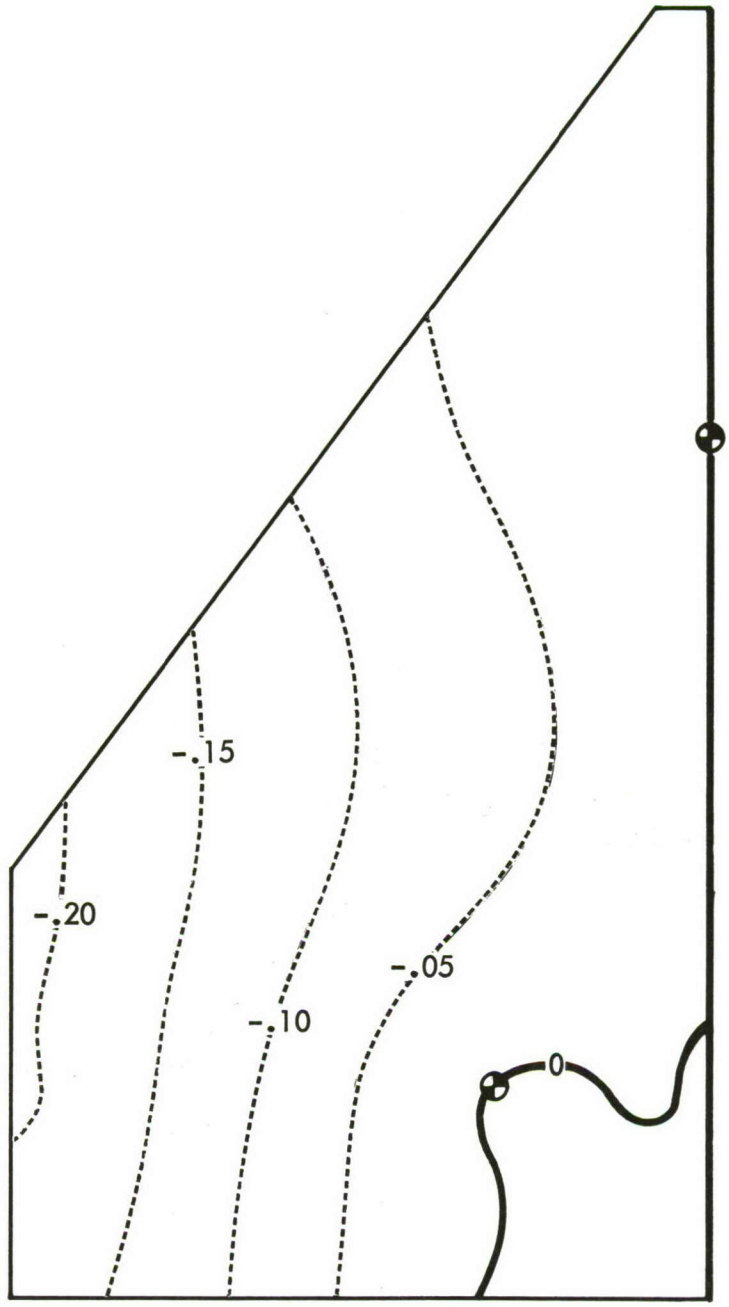

FIGURE 20: COLD LOADED STRUCTURE--DEFLECTIONS

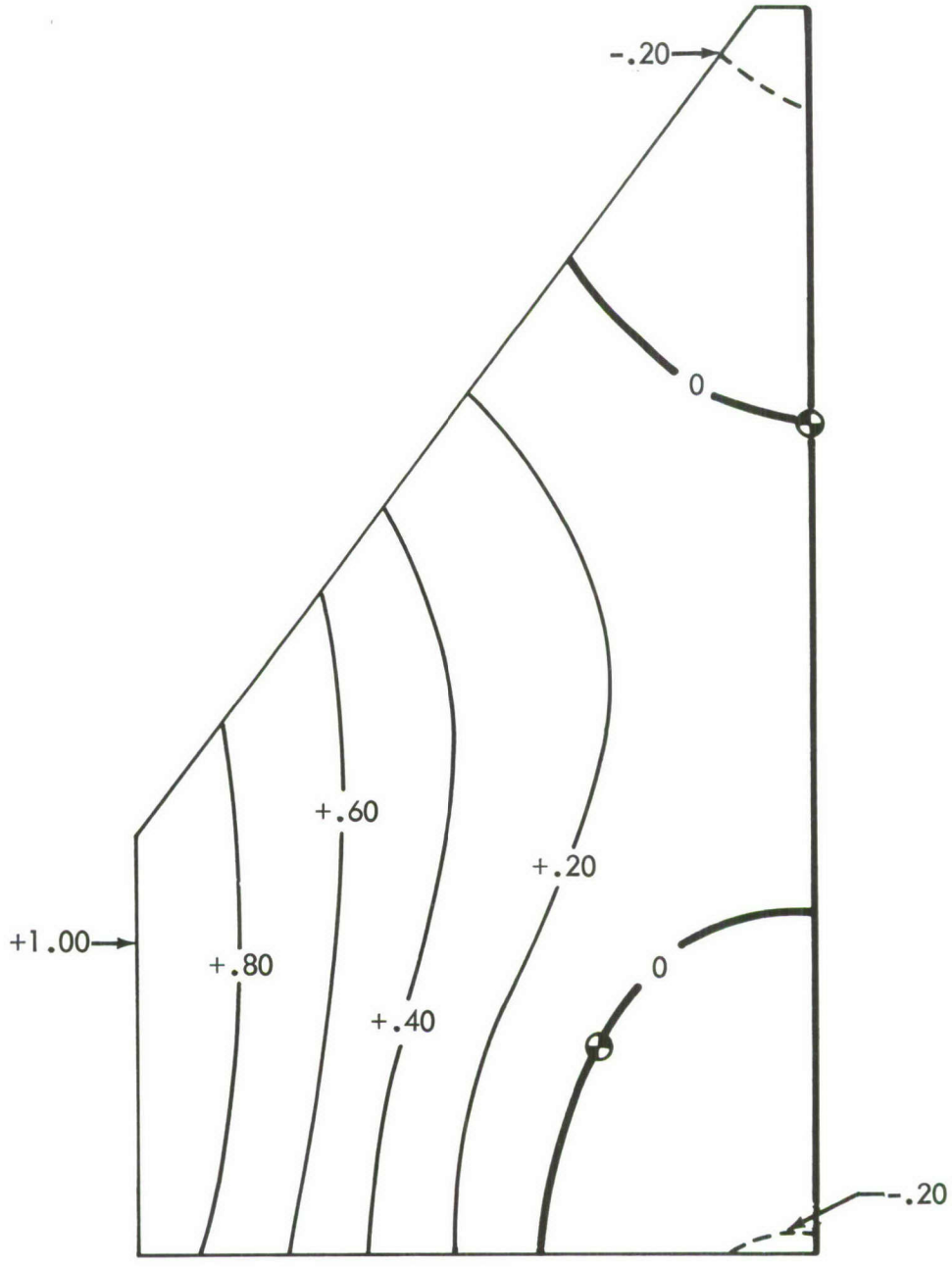

FIGURE 21: FIRST SYMMETRIC MODE--COLD UNLOADED STRUCTURE

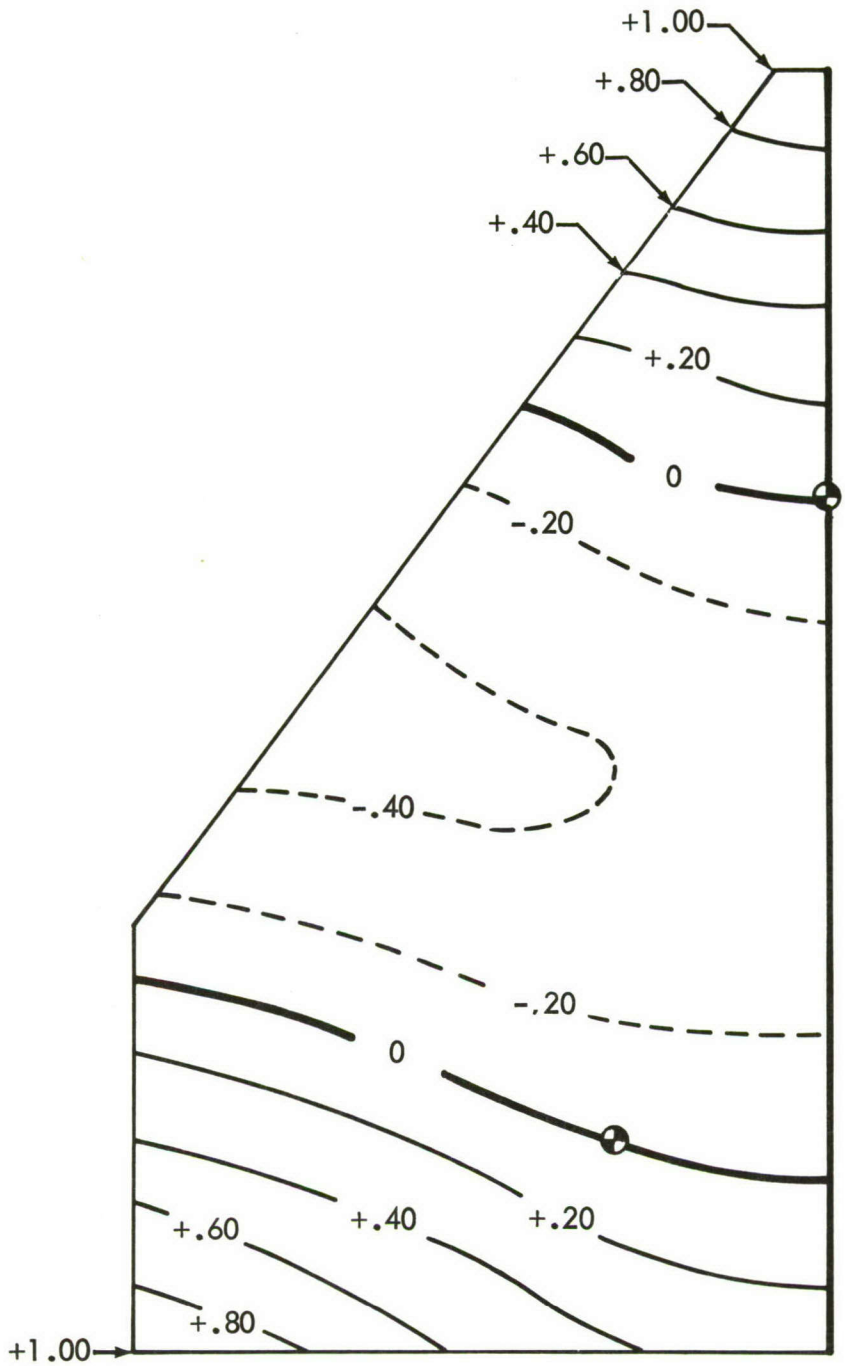

FREQUENCY 65.24 CPS

◓ SUPPORT POINT

FIGURE 22: SECOND SYMMETRIC MODE--COLD UNLOADED STRUCTURE

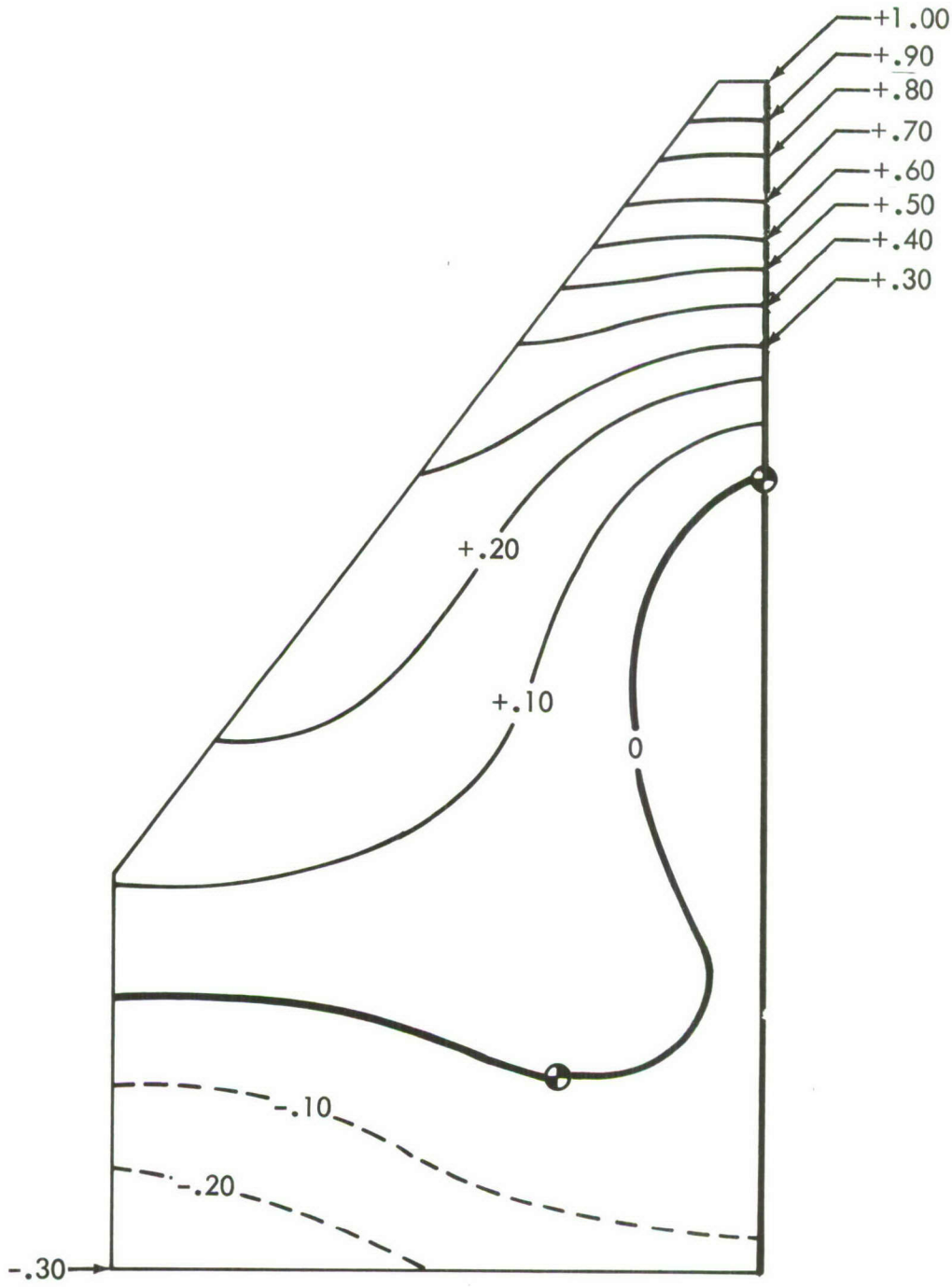

FIGURE 23: THIRD SYMMETRIC MODE--COLD UNLOADED STRUCTURE

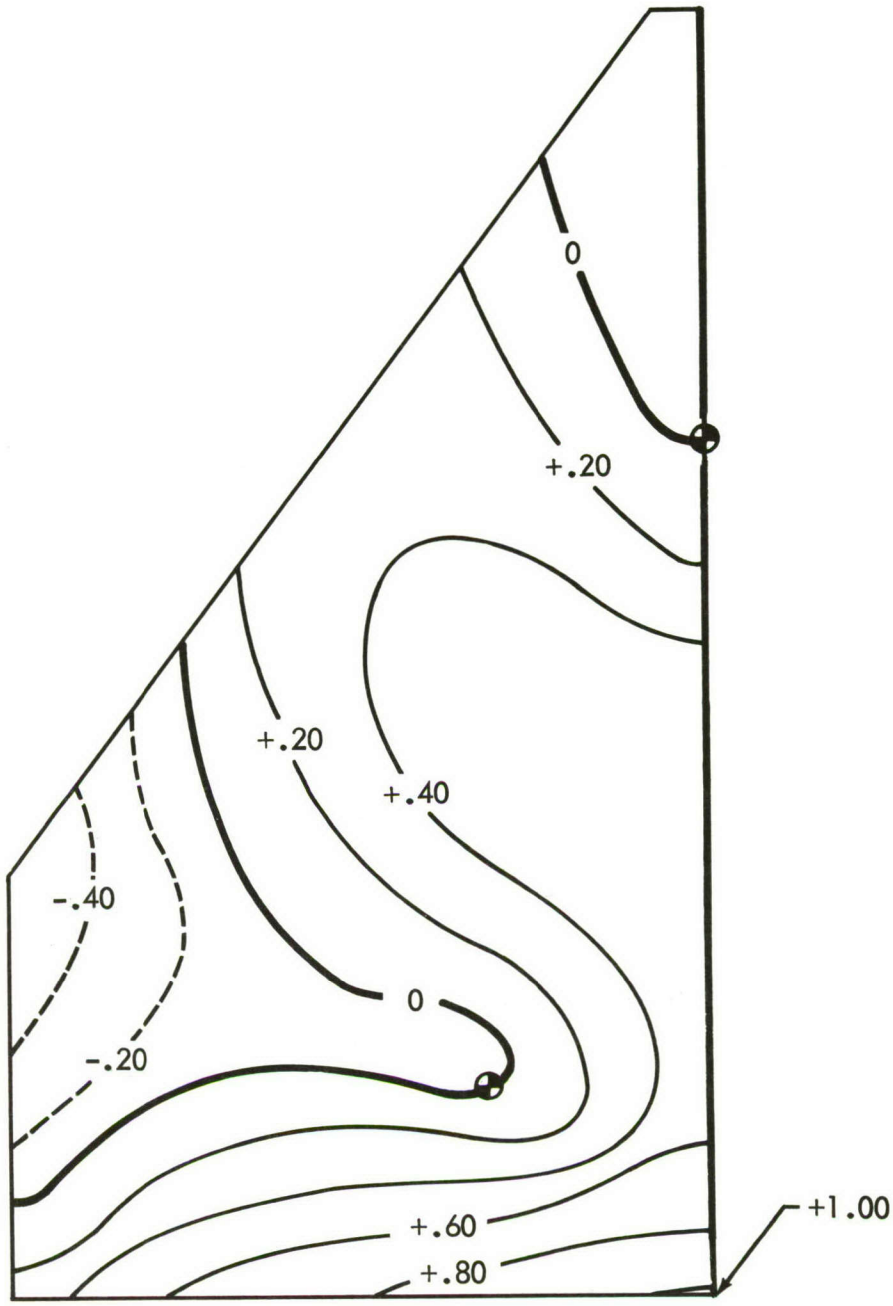

FREQUENCY 126.64 CPS

SUPPORT POINT

FIGURE 24: FOURTH SYMMETRIC MODE--COLD UNLOADED STRUCTURE

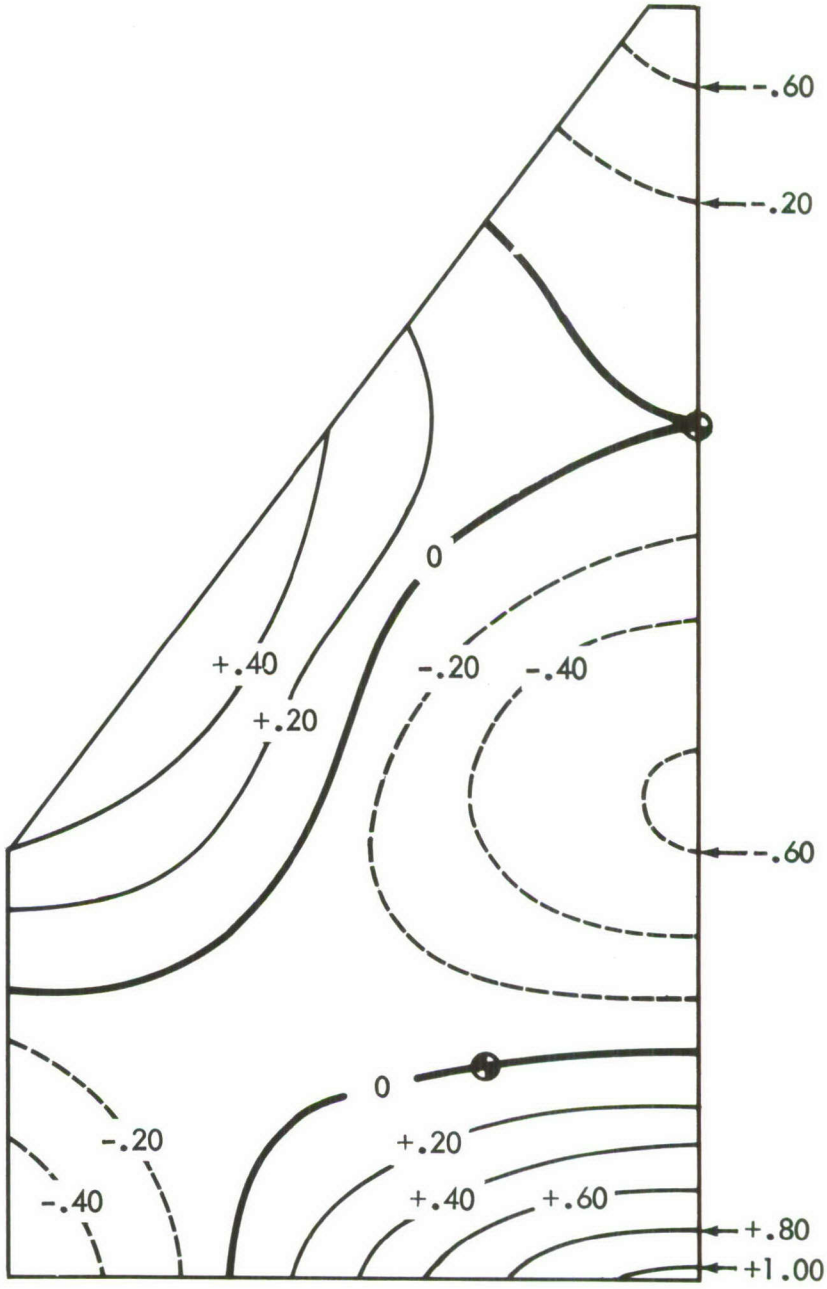

FREQUENCY 142.03 CPS

SUPPORT POINT

FIGURE 25: FIFTH SYMMETRIC MODE--COLD UNLOADED STRUCTURE

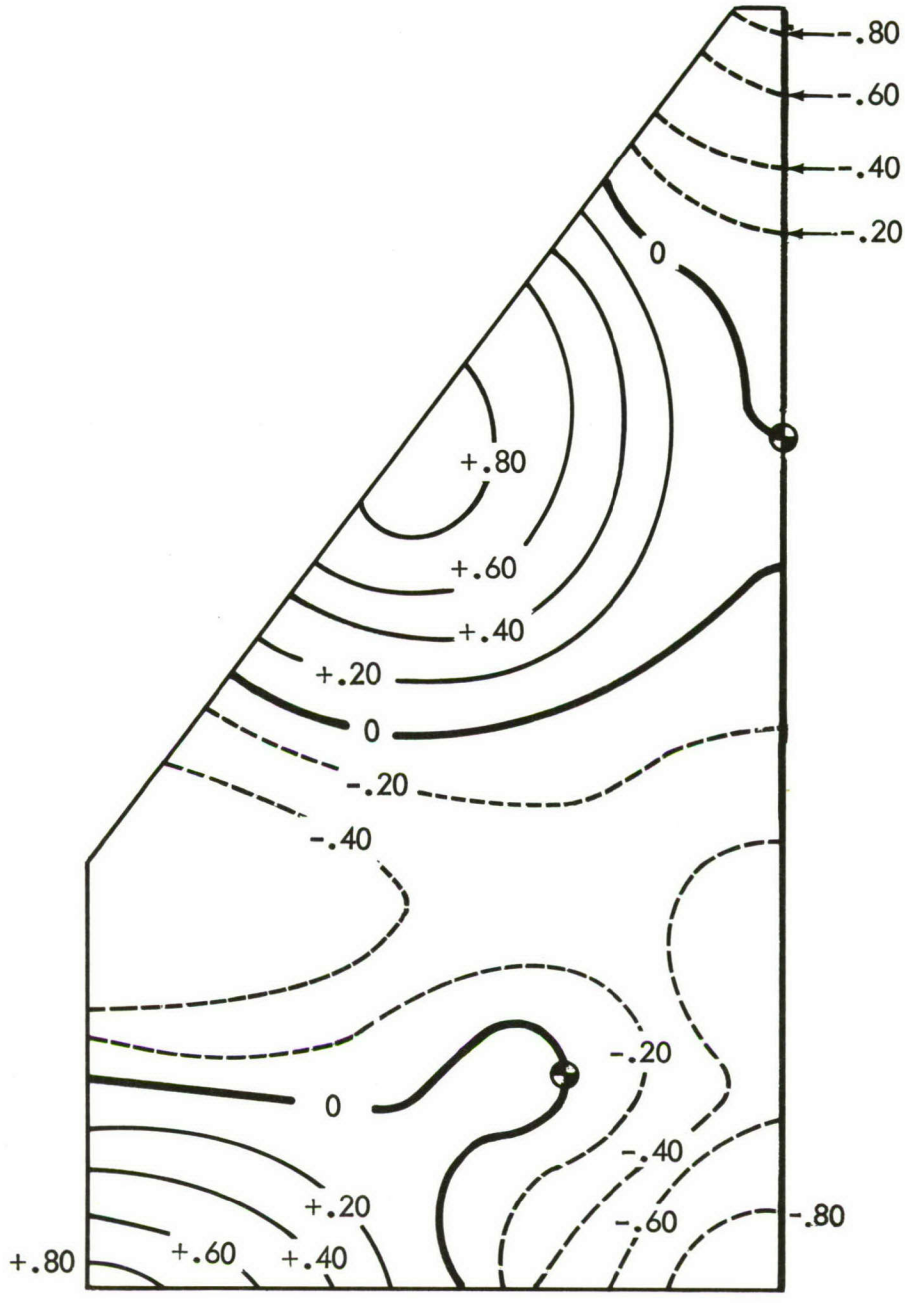

FREQUENCY 161.95 CPS

SUPPORT POINT

FIGURE 26: SIXTH SYMMETRIC MODE--COLD UNLOADED STRUCTURE

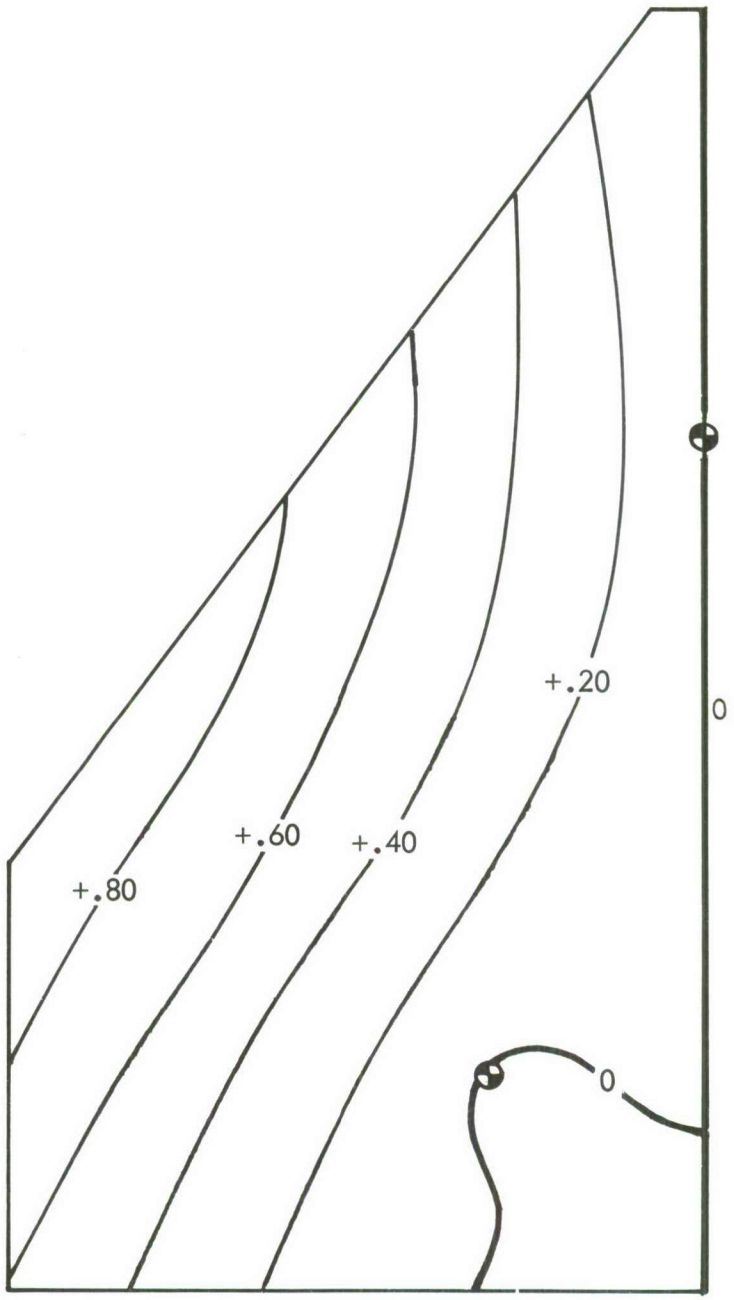

FREQUENCY 31.40 CPS

SUPPORT POINT

FIGURE 27: FIRST ANTISYMMETRIC MODE--COLD UNLOADED STRUCTURE

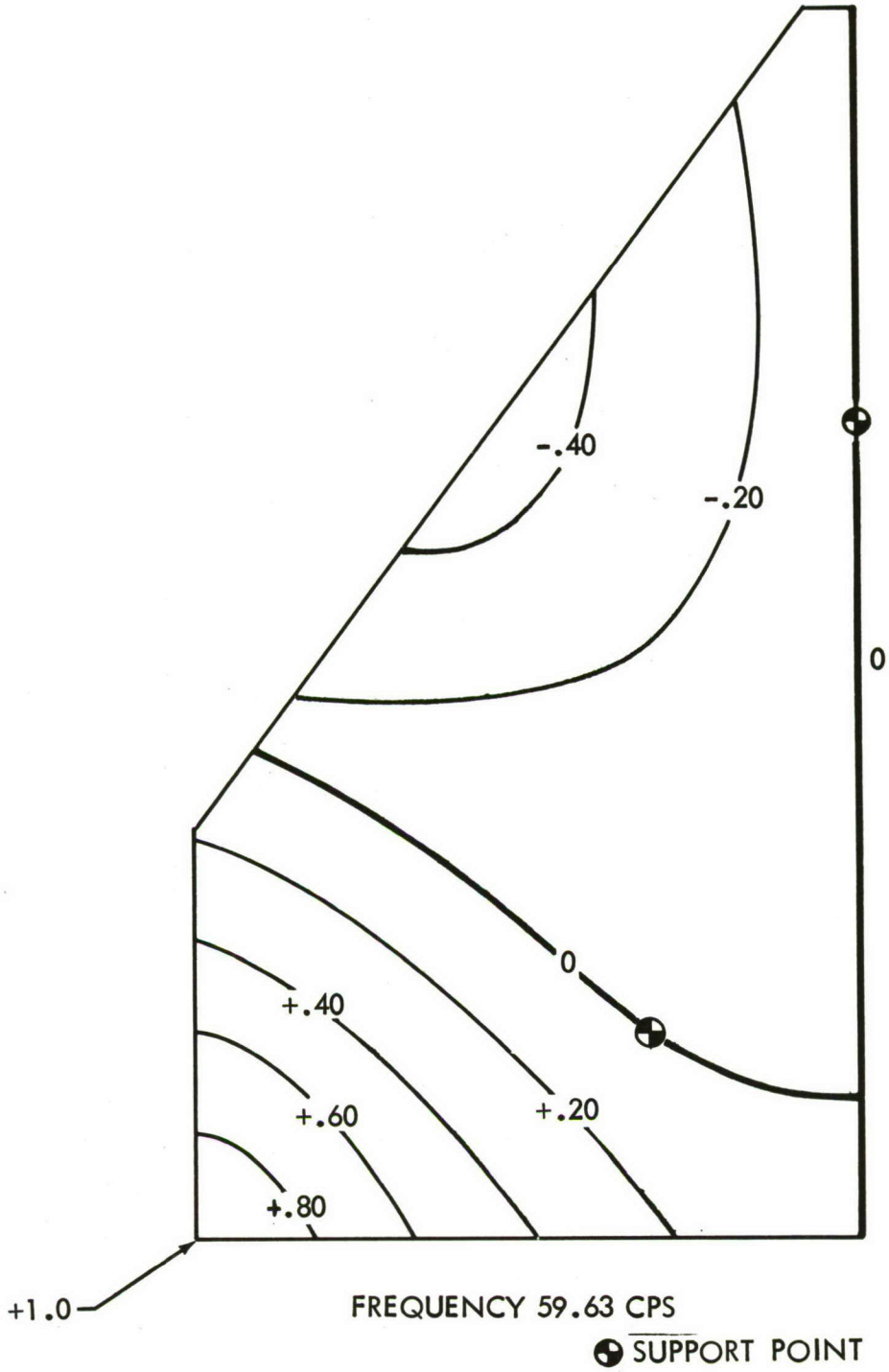

FIGURE 28: SECOND ANTISYMMETRIC MODE--COLD UNLOADED STRUCTURE

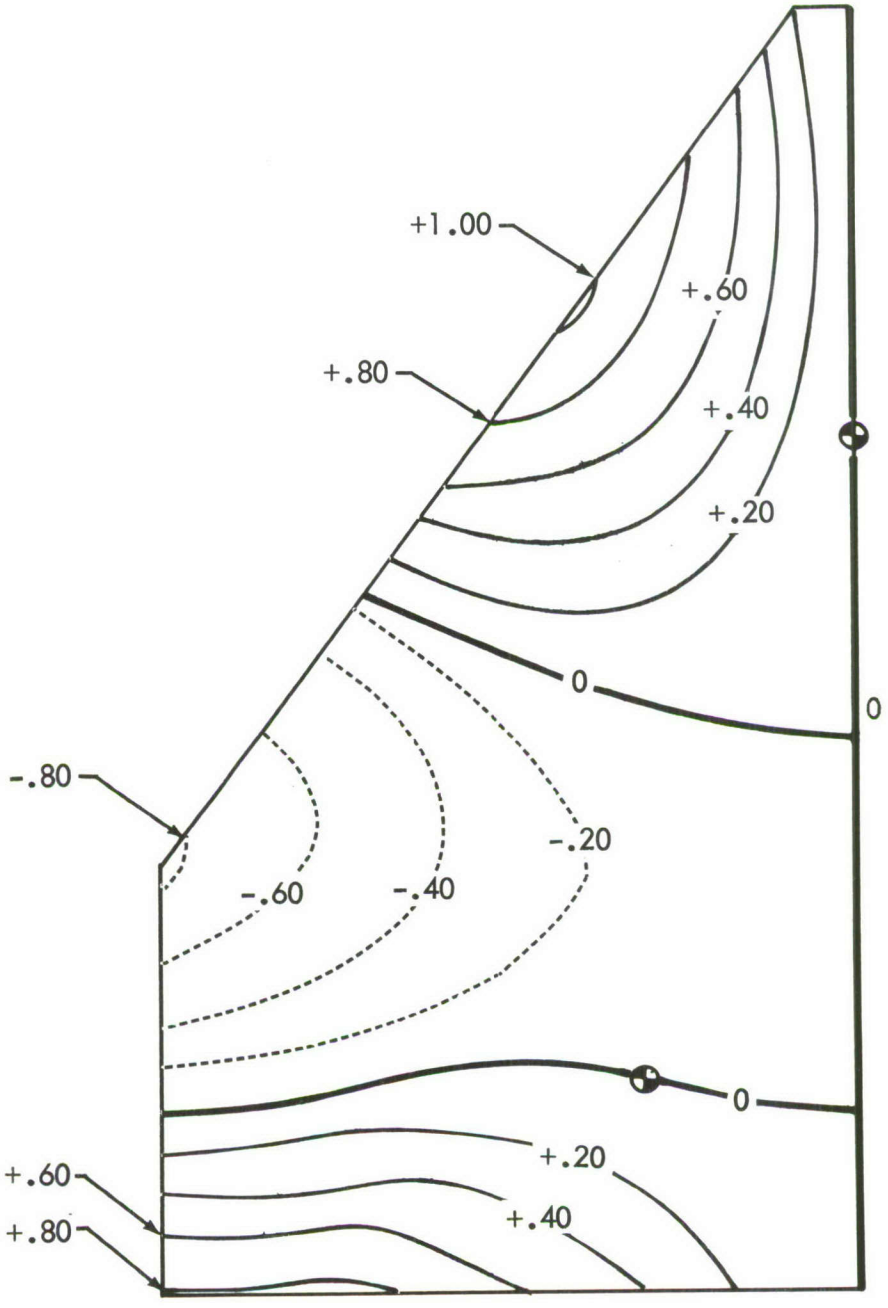

FREQUENCY 118.24 CPS

SUPPORT POINT

FIGURE 29: THIRD ANTISYMMETRIC MODE--COLD UNLOADED STRUCTURE

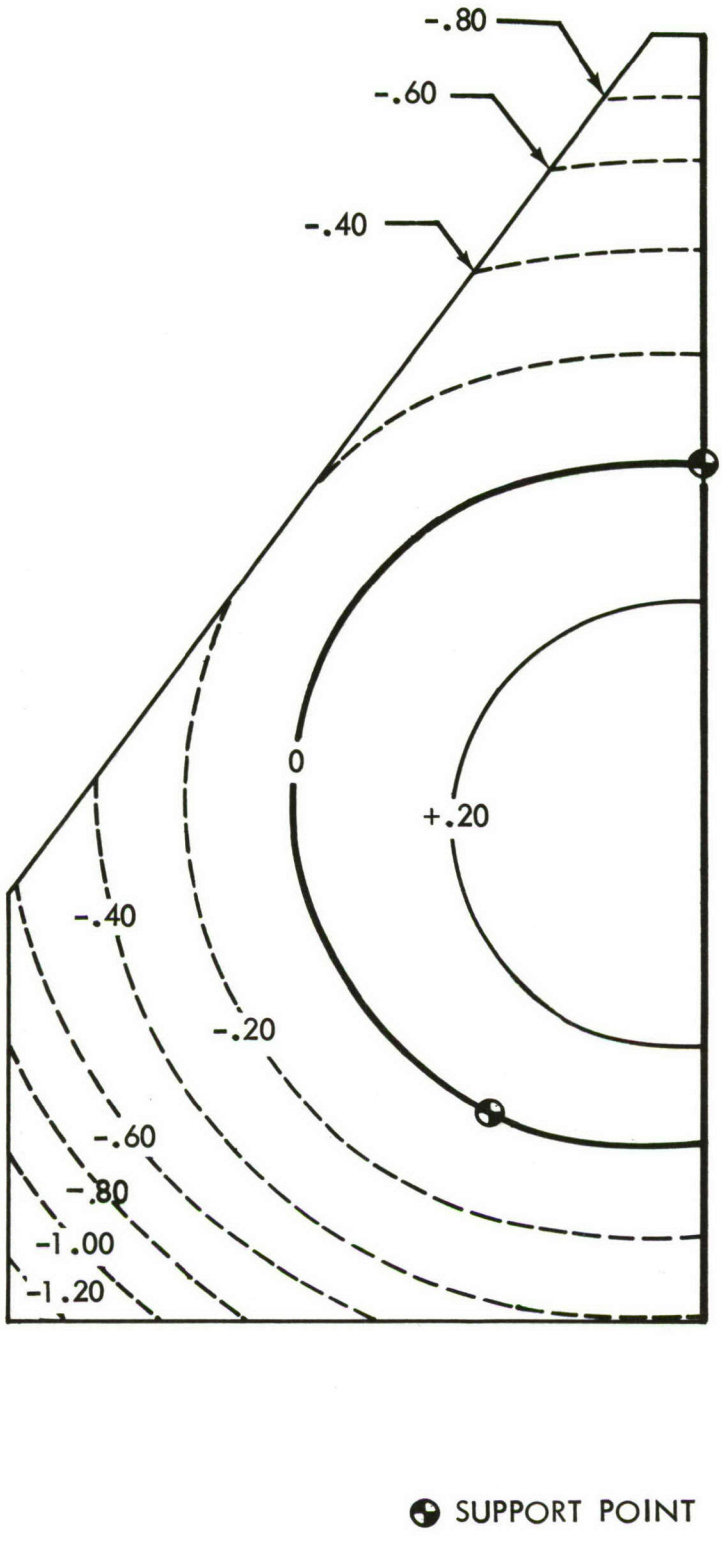

FIGURE 30: HOT STRUCTURE DEFLECTIONS

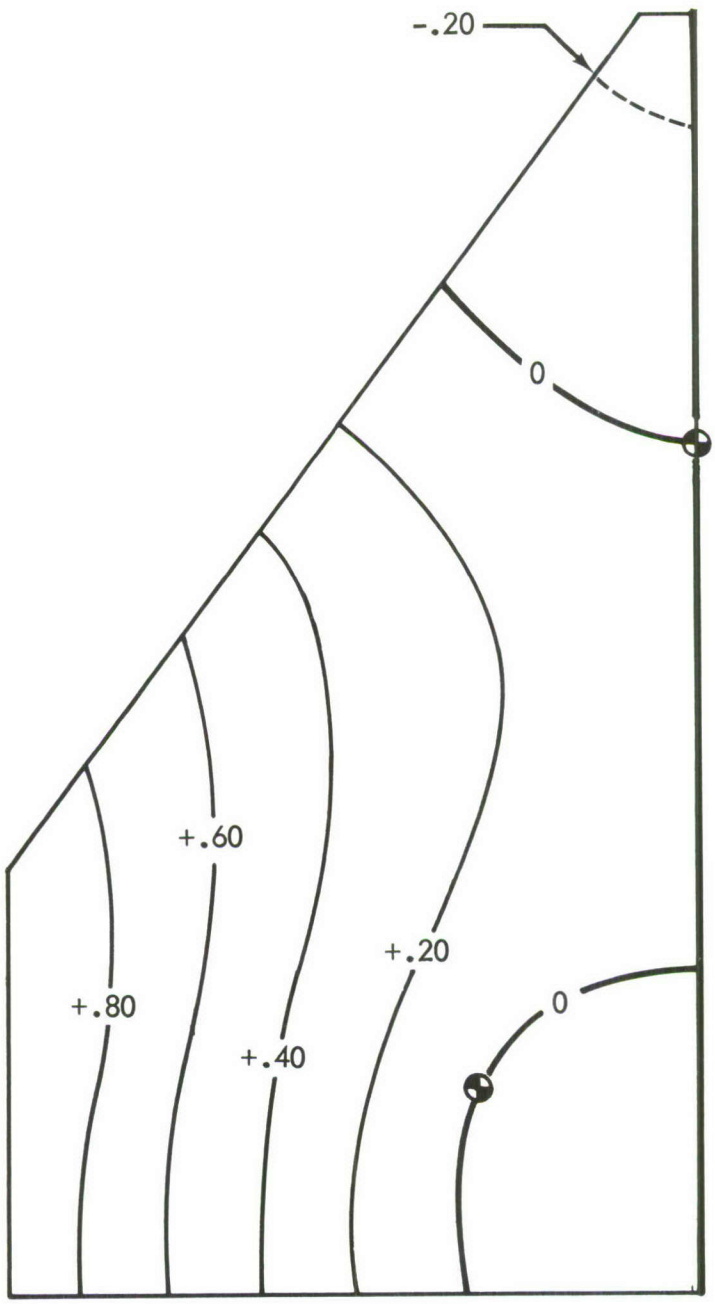

FREQUENCY 45.98 CPS

SUPPORT POINT

FIGURE 31: FIRST SYMMETRIC MODE--HOT STRUCTURE

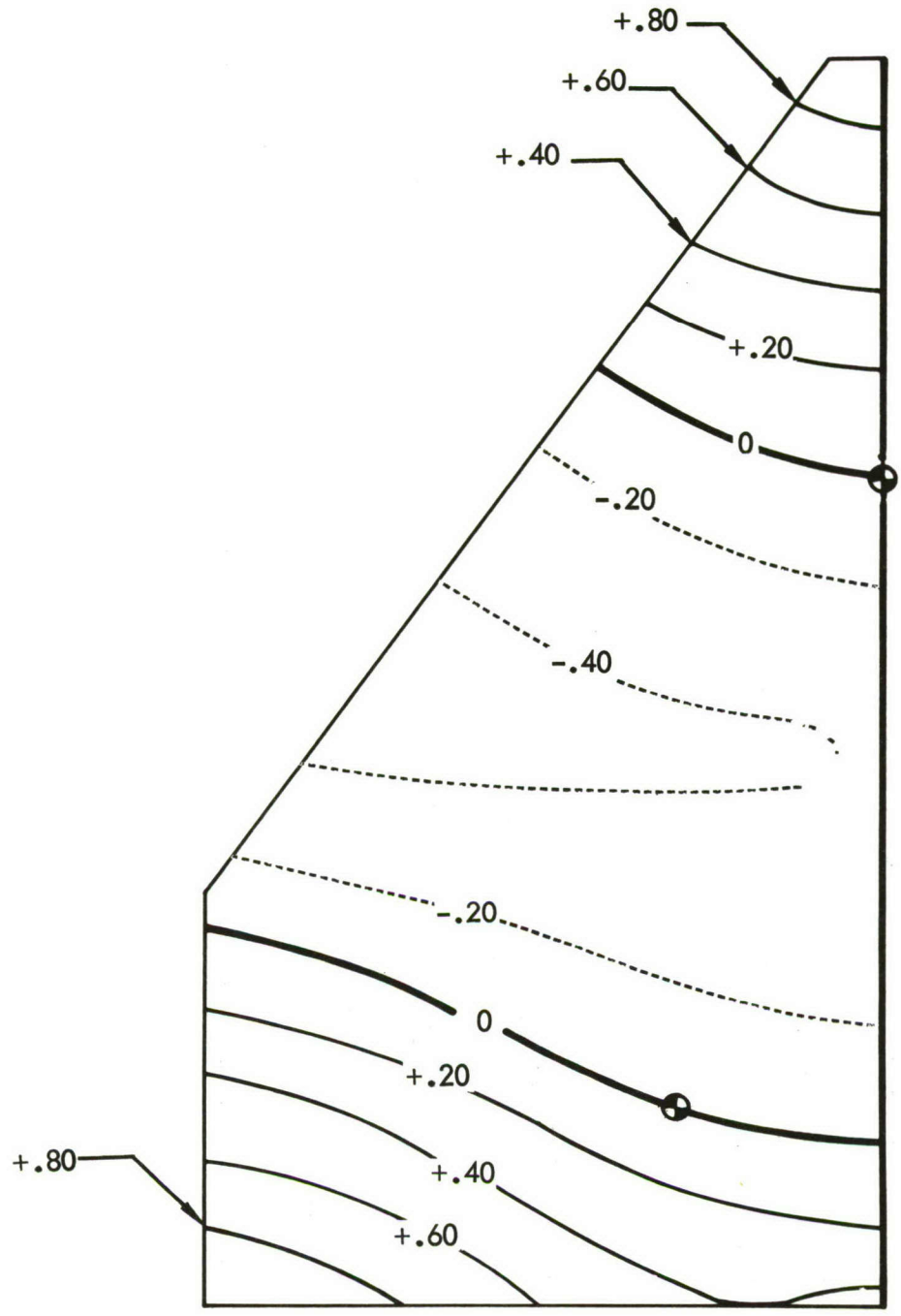

FREQUENCY 66.12 CPS

SUPPORT POINT

FIGURE 32: SECOND SYMMETRIC MODE--HOT STRUCTURE

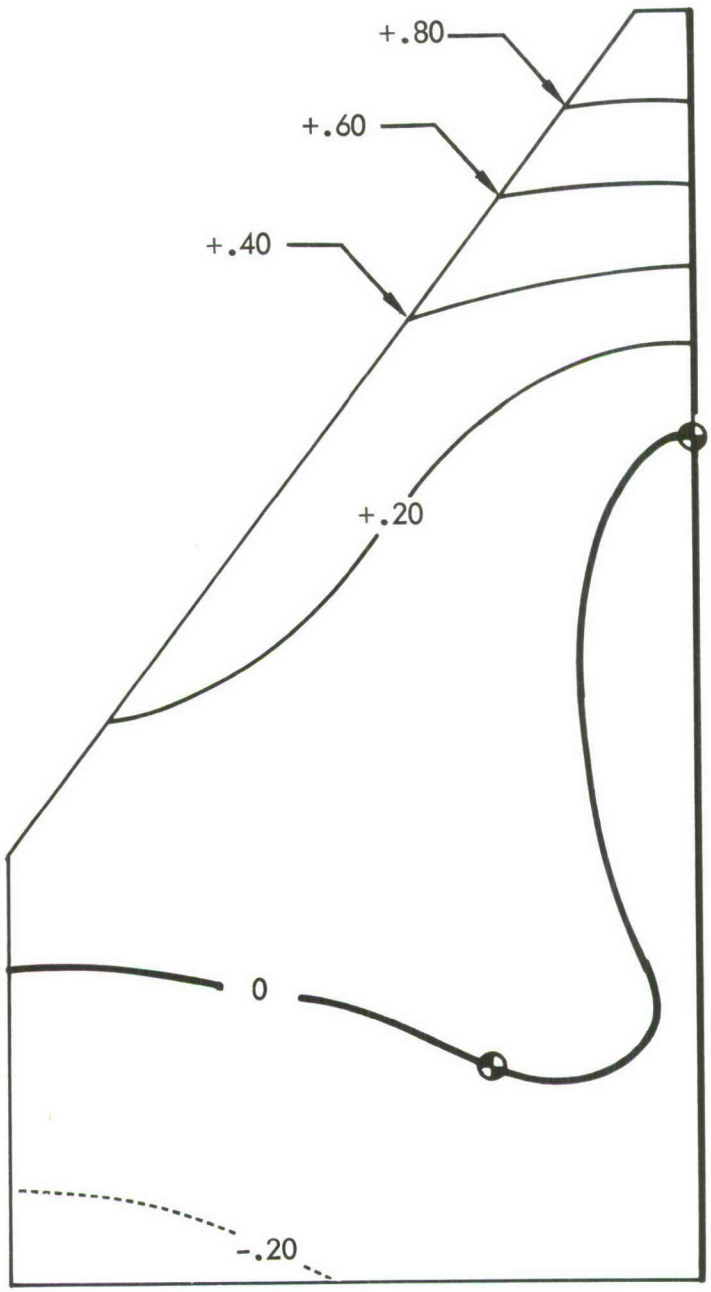

FREQUENCY 72.79 CPS

SUPPORT POINT

FIGURE 33: THIRD SYMMETRIC MODE--HOT STRUCTURE

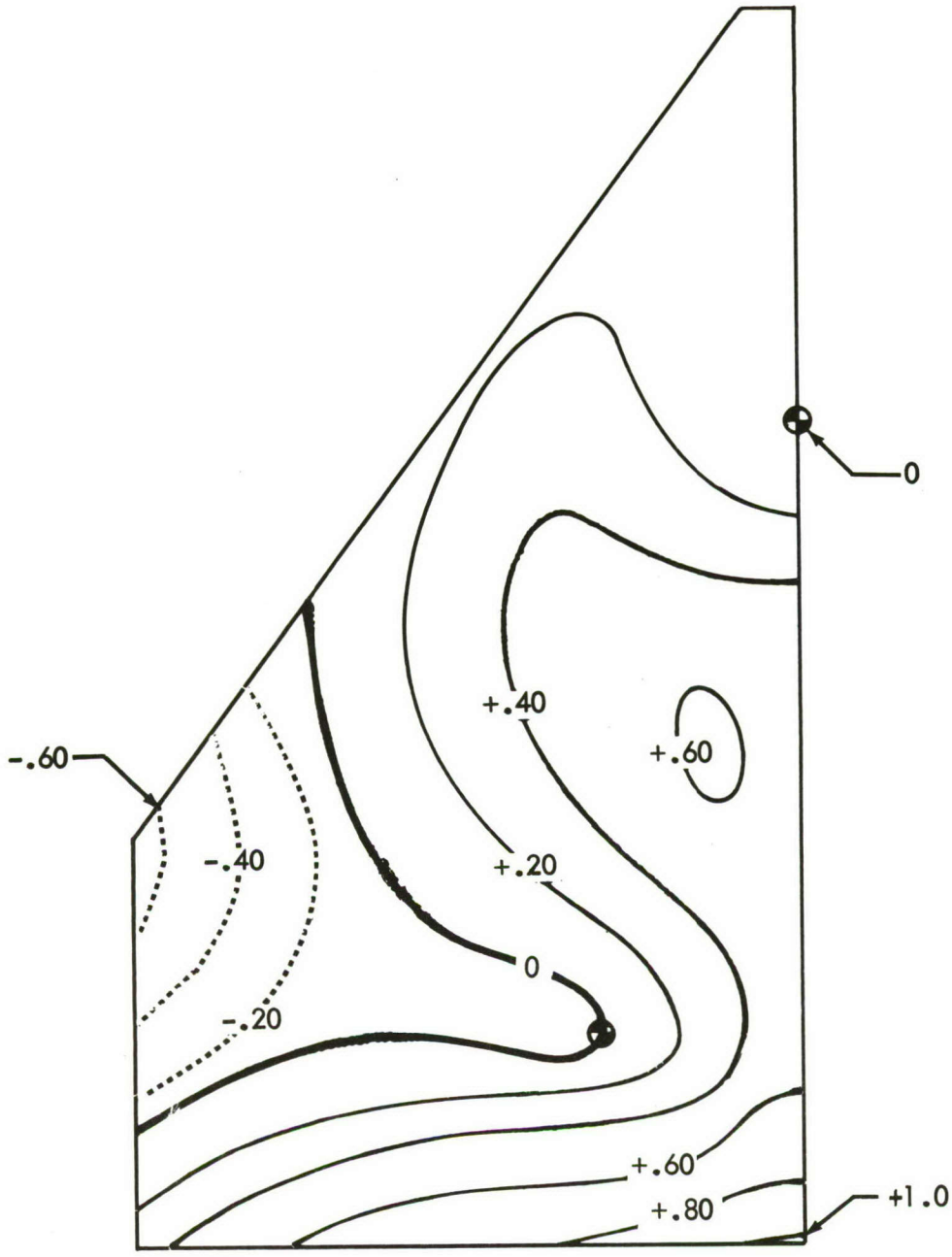

FREQUENCY 124.67 CPS

● SUPPORT POINT

FIGURE 34: FOURTH SYMMETRIC MODE--HOT STRUCTURE

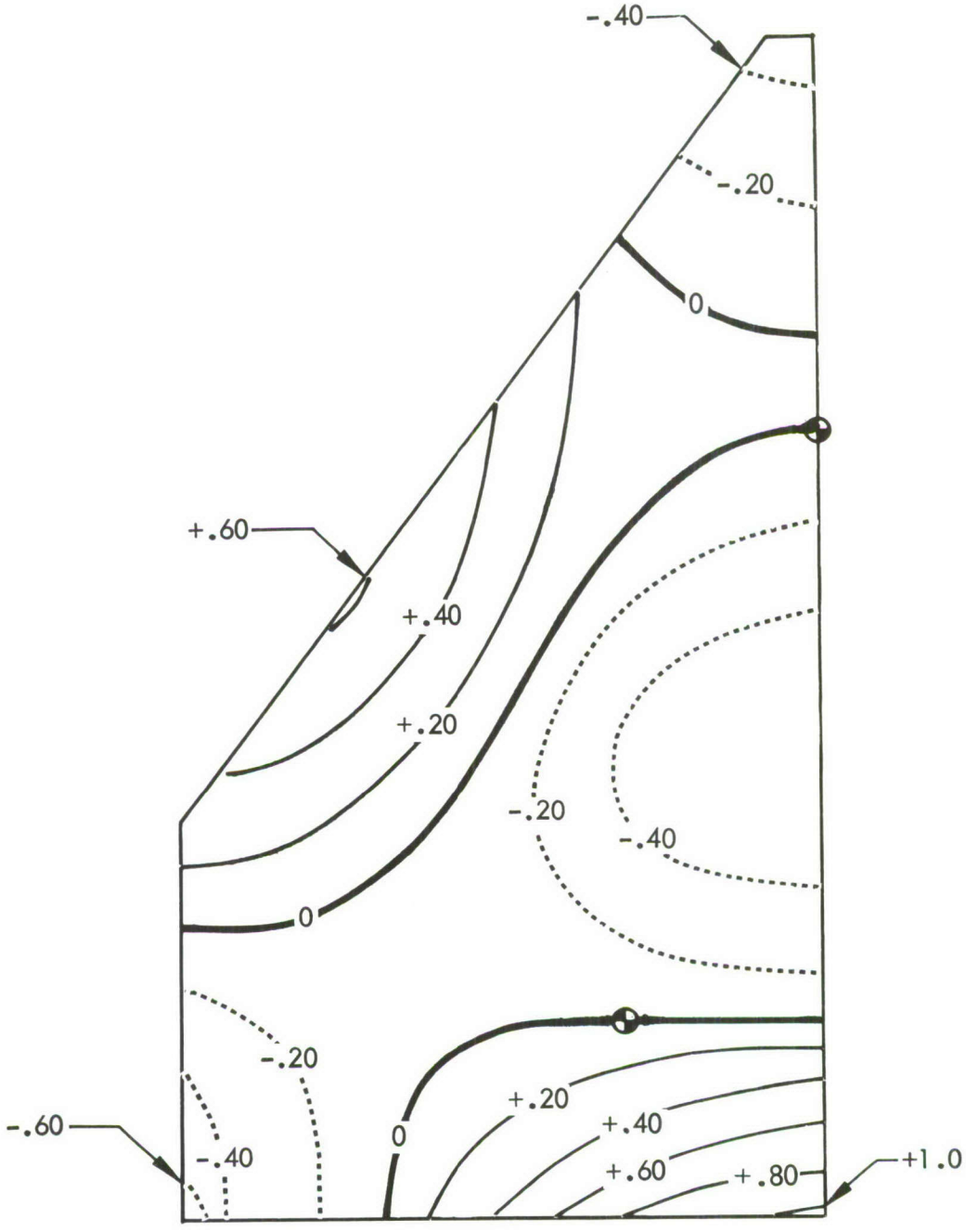

FREQUENCY 140.90 CPS

⊕ SUPPORT POINT

FIGURE 35: FIFTH SYMMETRIC MODE--HOT STRUCTURE

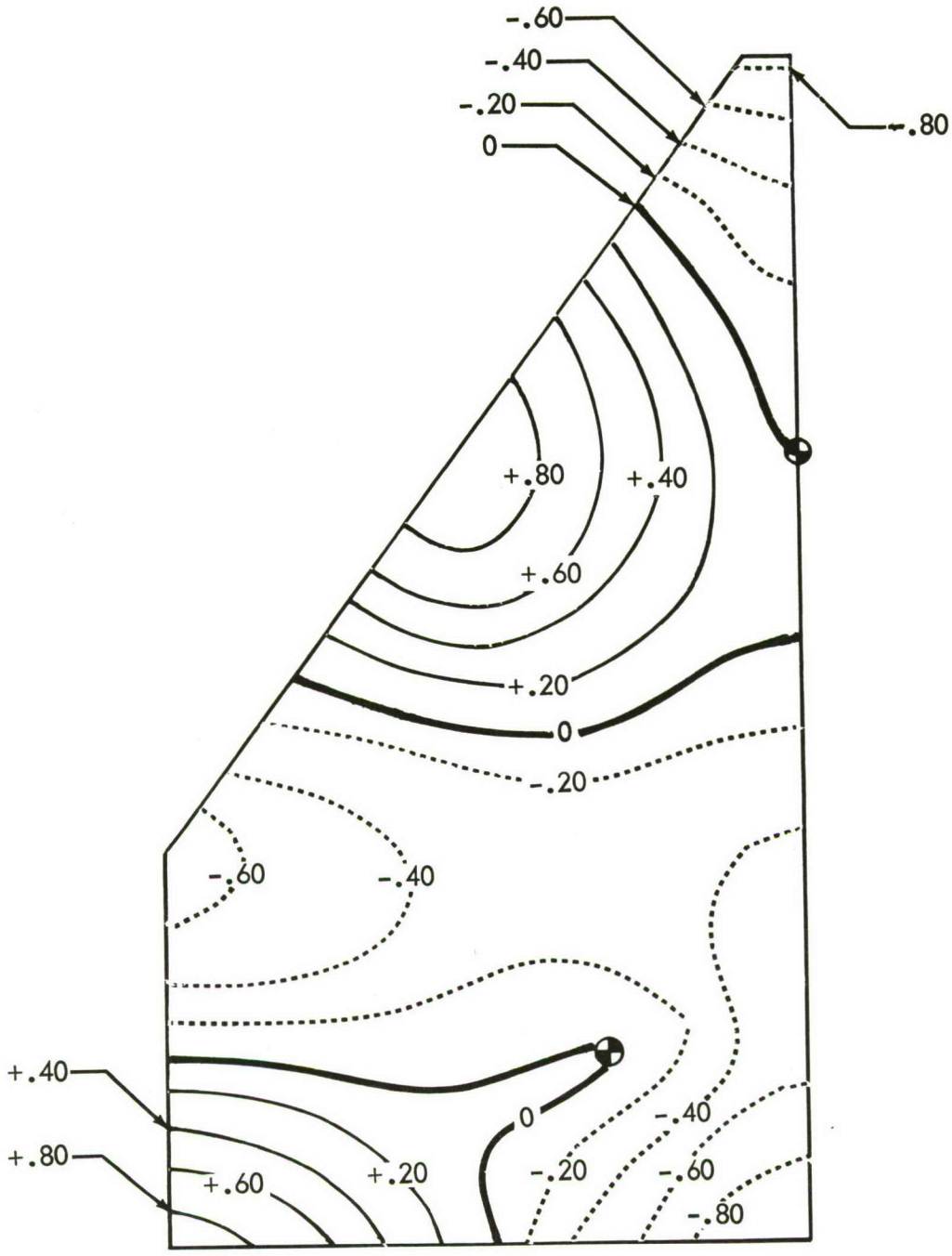

FIGURE 36: SIXTH SYMMETRIC MODE--HOT STRUCTURE

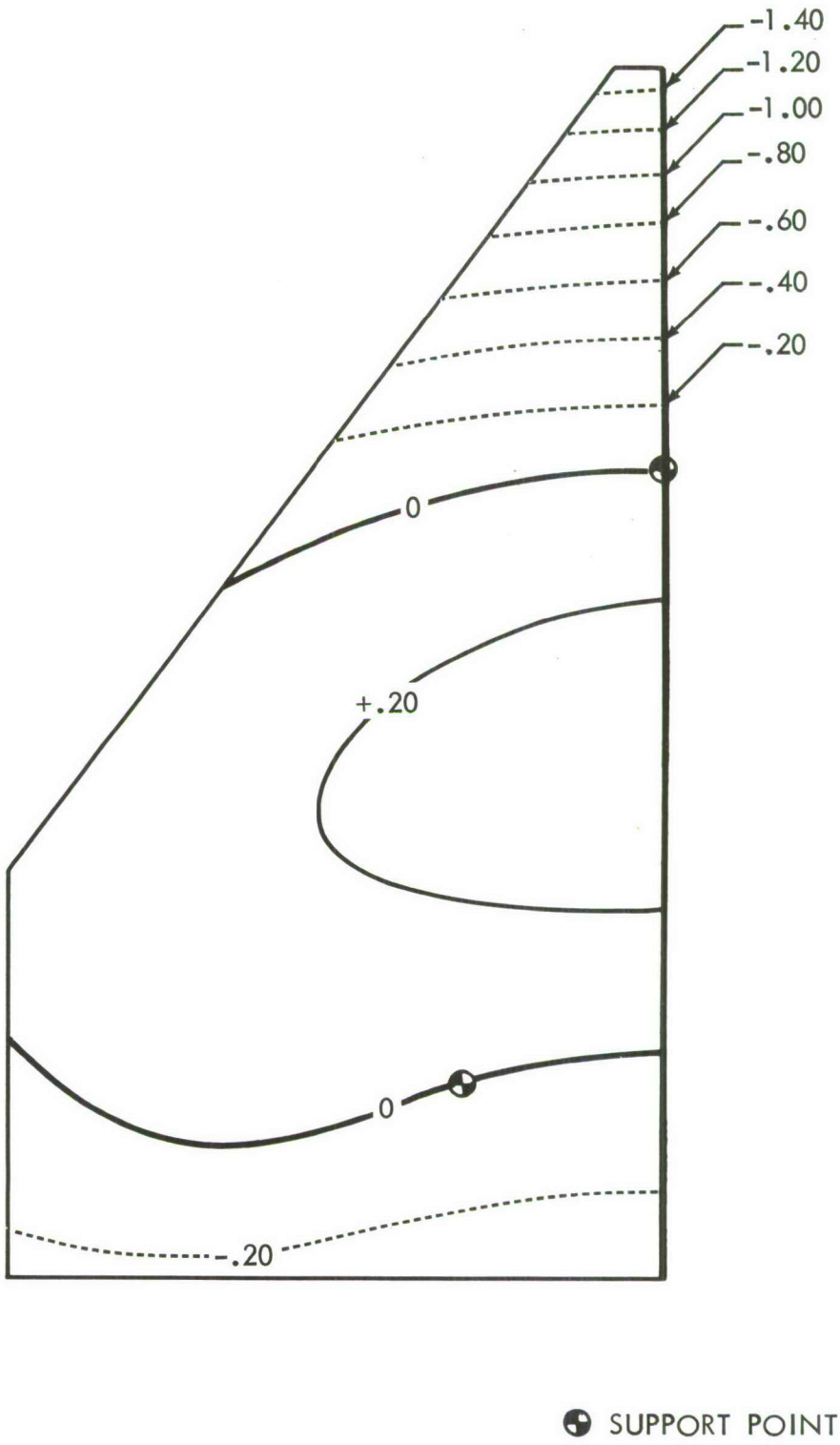

FIGURE 37: HOT STRUCTURE DEFLECTIONS--LINEAR DEFLECTION THEORY

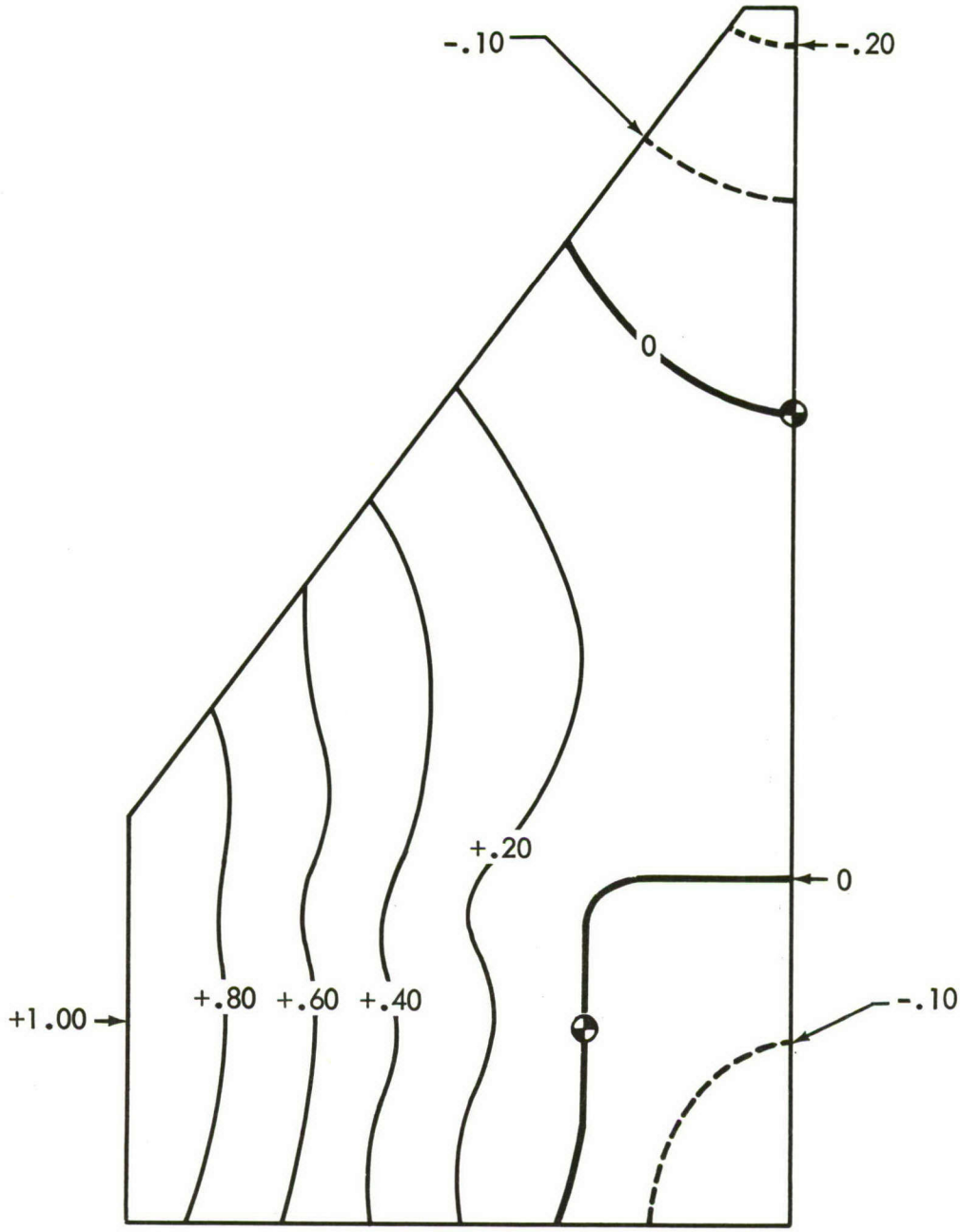

FIGURE 38: FIRST SYMMETRIC MODE--HOT STRUCTURE
LINEAR DEFLECTION THEORY(FLAT)

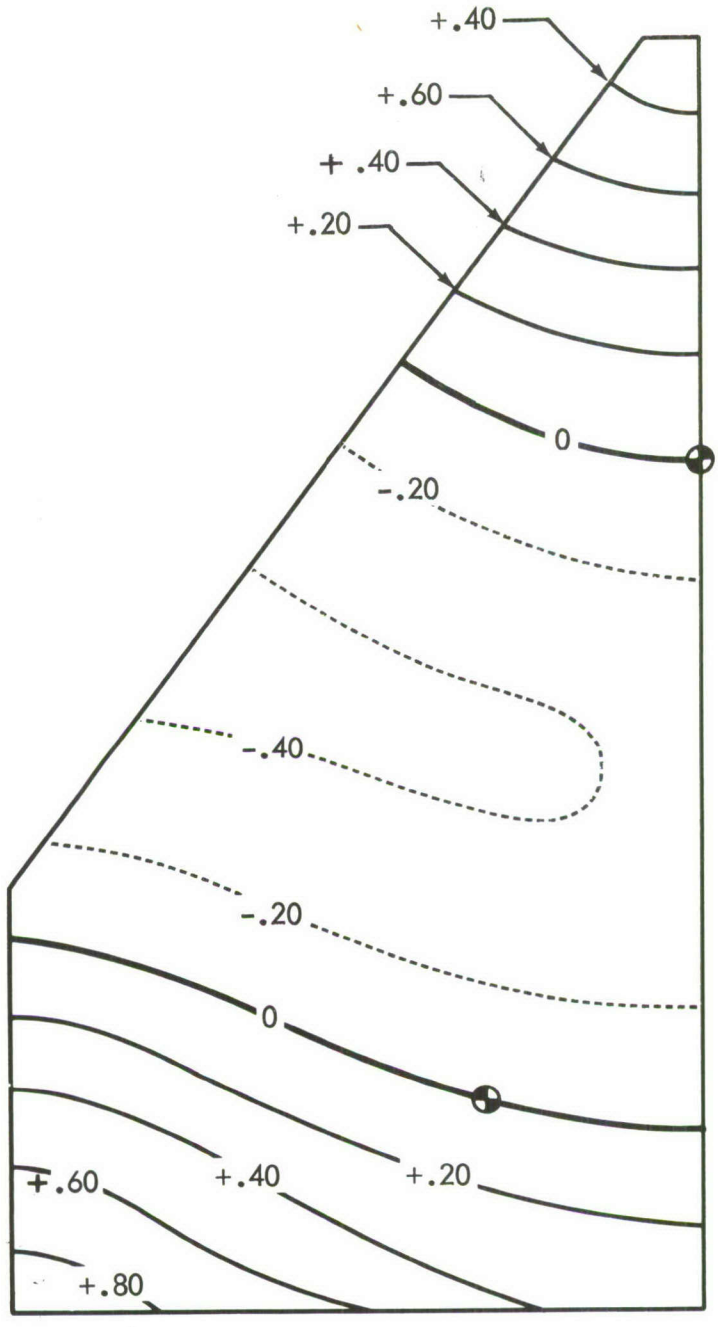

FREQUENCY 64.24 CPS

[K] COMPUTED IN TERMS OF FLAT SHAPE

SUPPORT POINT

FIGURE 39: SECOND SYMMETRIC MODE--HOT STRUCTURE LINEAR DEFLECTION THEORY(FLAT)

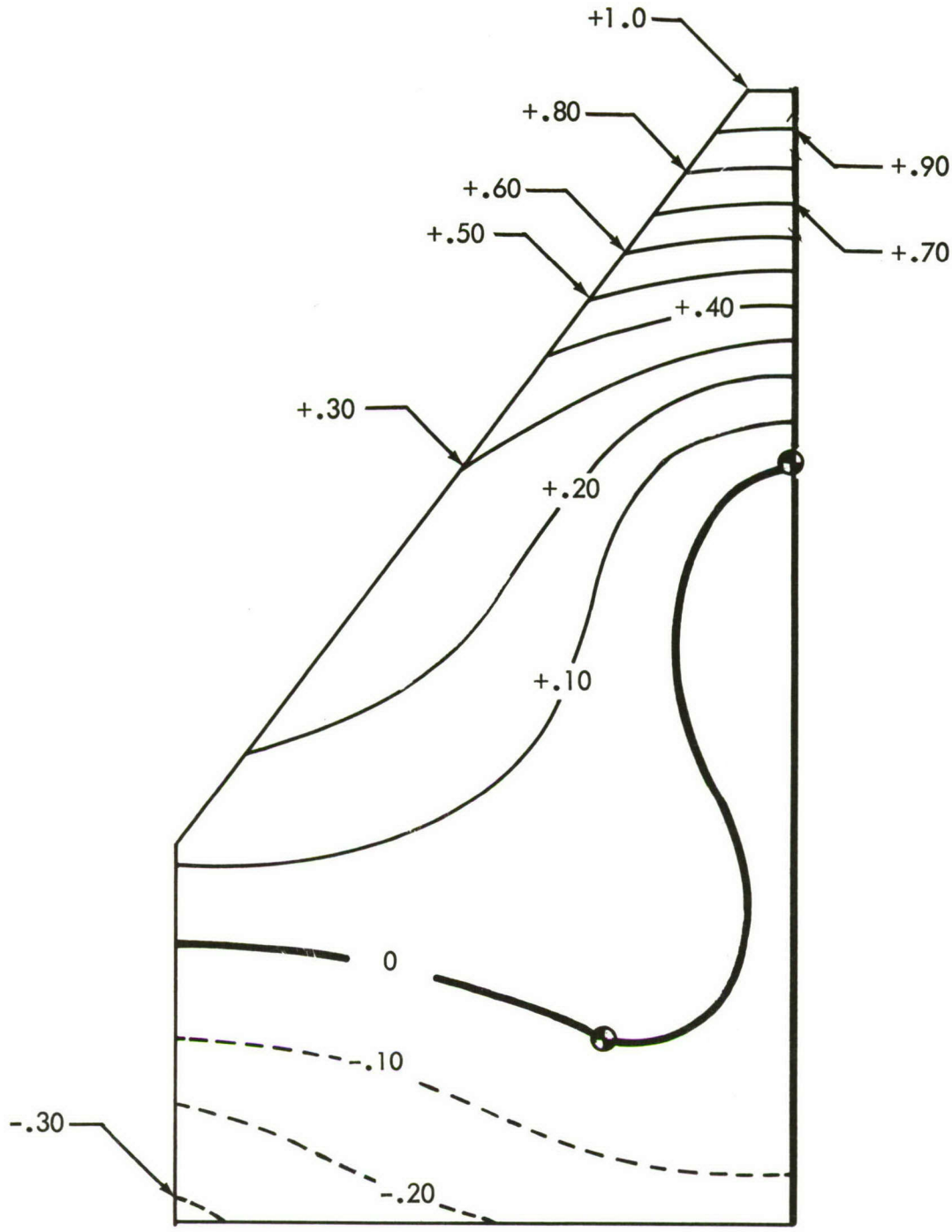

FREQUENCY 71.42 CPS

[K] COMPUTED IN TERMS OF FLAT SHAPE

SUPPORT POINT

FIGURE 40: THIRD SYMMETRIC MODE--HOT STRUCTURE
LINEAR DEFLECTION THEORY(FLAT)

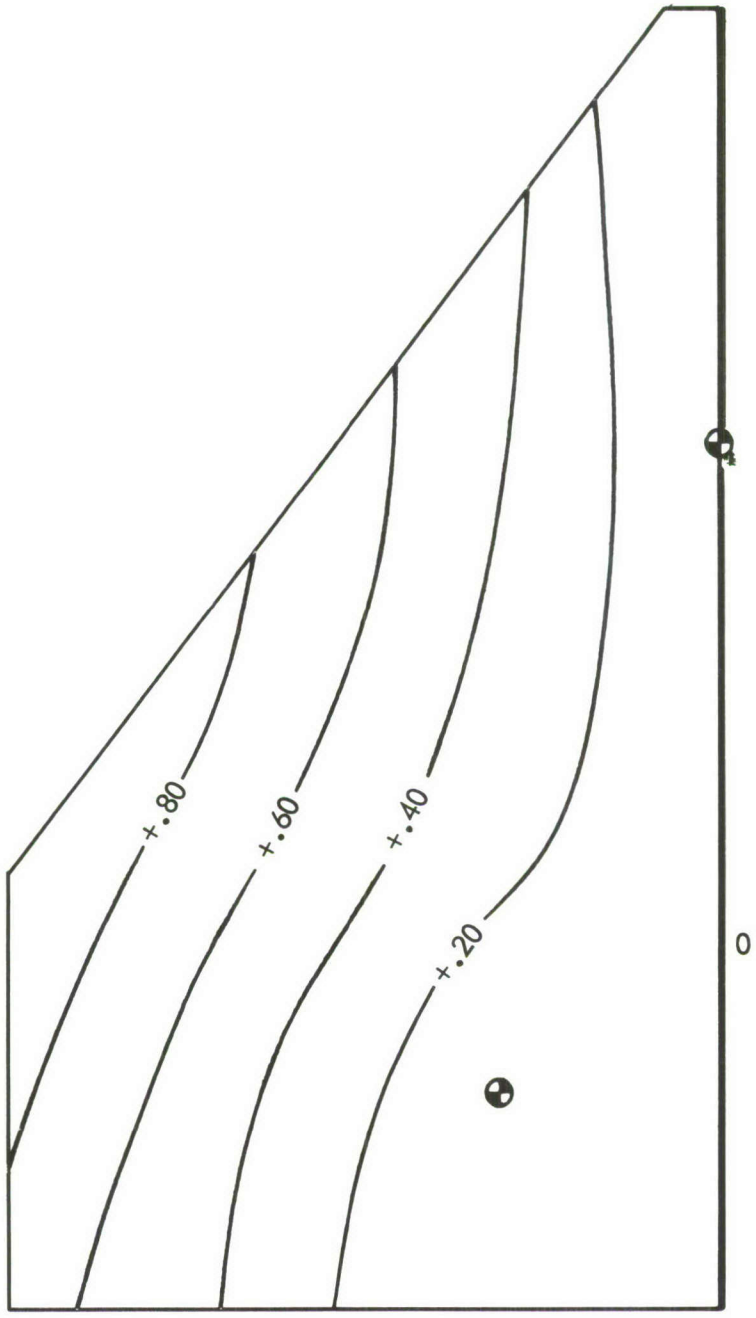

FREQUENCY 32.56 CPS

[K] COMPUTED IN TERMS OF FLAT SHAPE

SUPPORT POINT

FIGURE 41: FIRST ANTISYMMETRIC MODE--HOT STRUCTURE LINEAR DEFLECTION THEORY(FLAT)

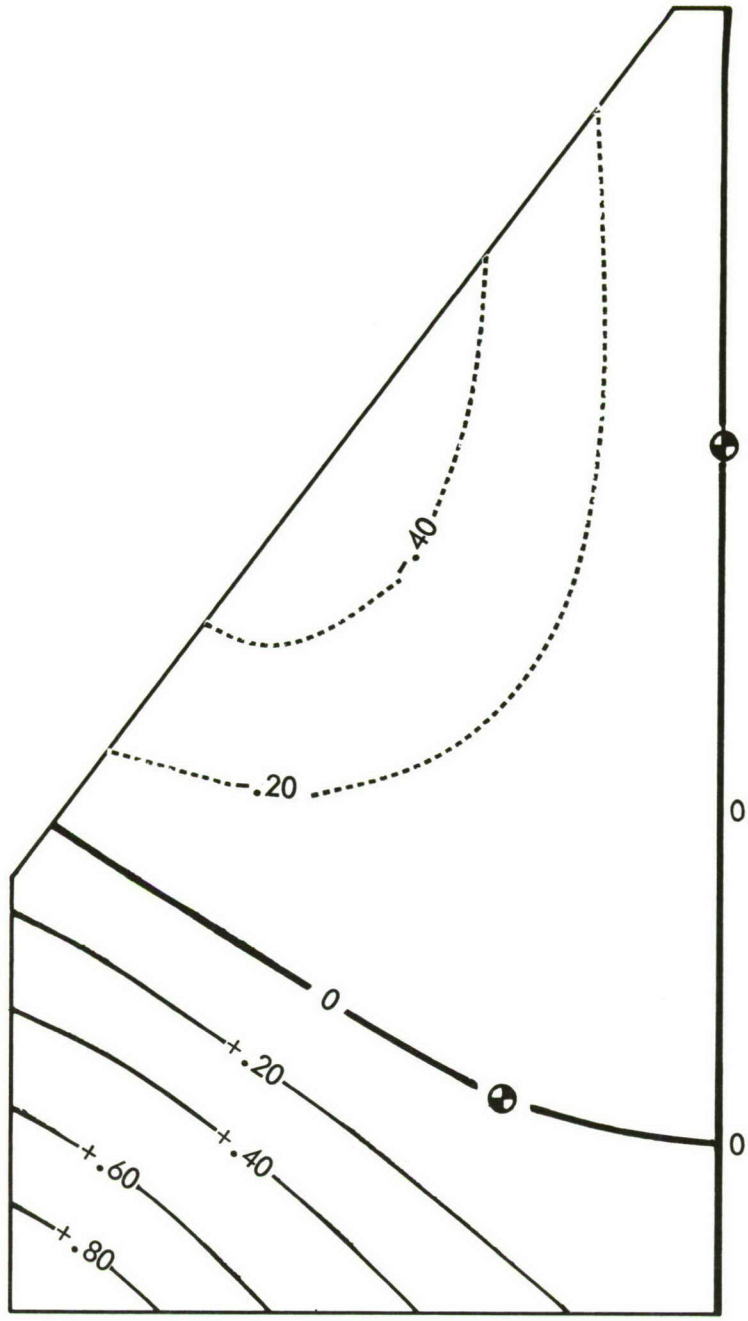

FREQUENCY 61.15 CPS

[K] COMPUTED IN TERMS OF FLAT SHAPE

SUPPORT POINT

FIGURE 42: SECOND ANTISYMMETRIC MODE--HOT STRUCTURE LINEAR DEFLECTION THEORY(FLAT)

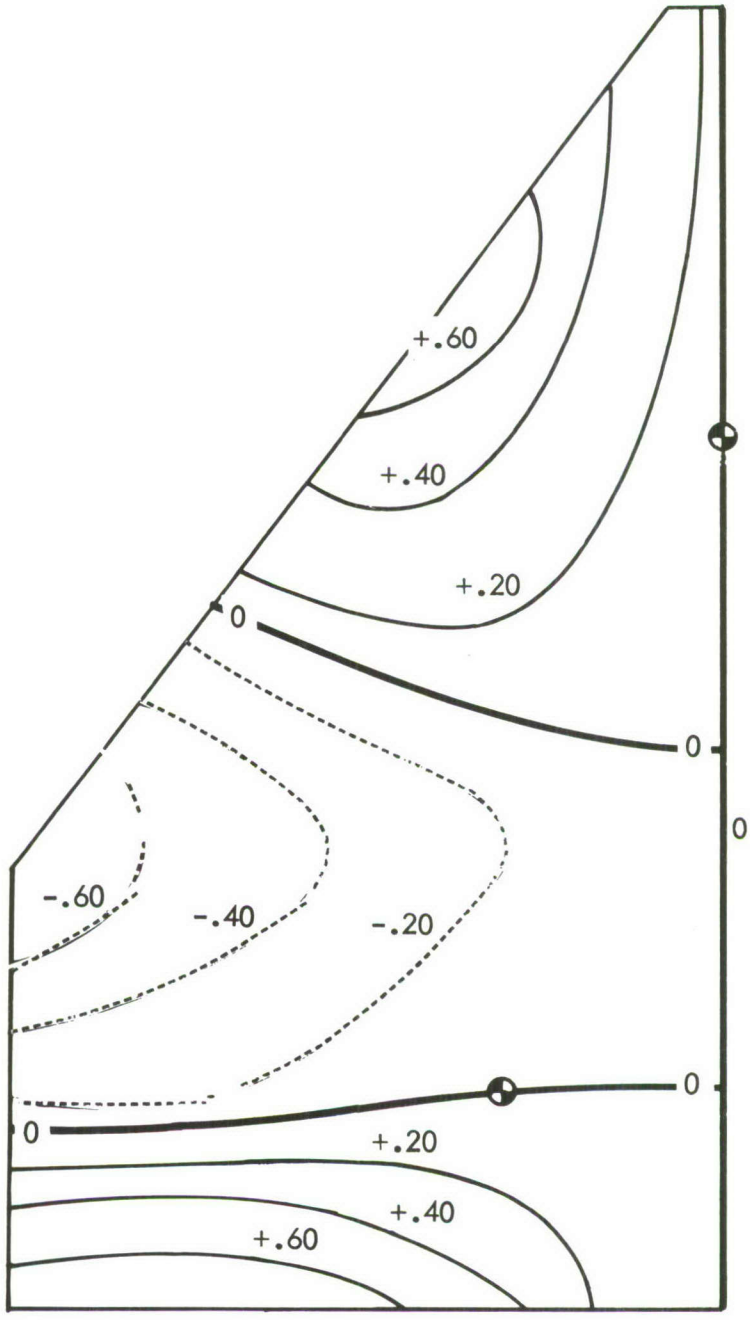

FREQUENCY 120.19 CPS

[K] COMPUTED IN TERMS OF FLAT SHAPE

SUPPORT POINT

FIGURE 43: THIRD ANTISYMMETRIC MODE--HOT STRUCTURE LINEAR DEFLECTION THEORY(FLAT)

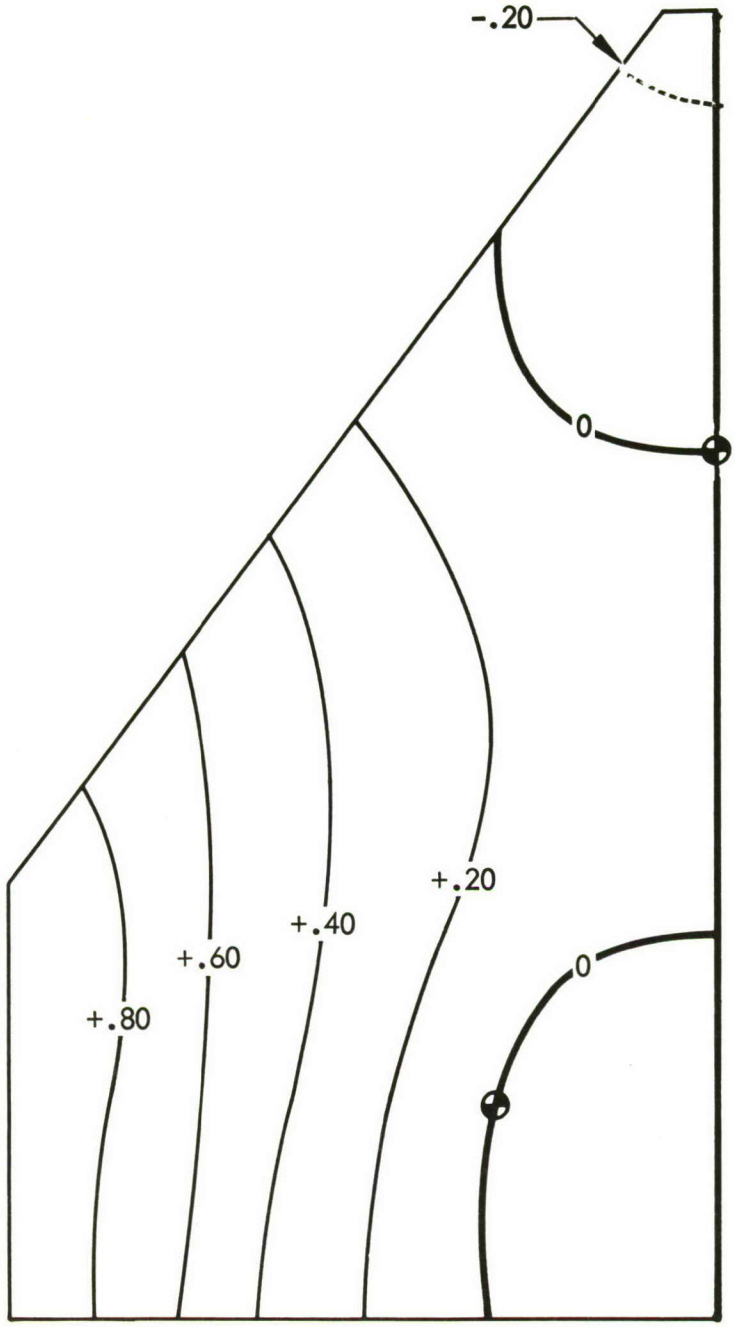

FREQUENCY 44.23

[K] COMPUTED IN TERMS OF DEFORMED SHAPE

SUPPORT POINT

FIGURE 44: FIRST SYMMETRIC MODE--HOT STRUCTURE
LINEAR DEFLECTION THEORY (FINAL SHAPE)

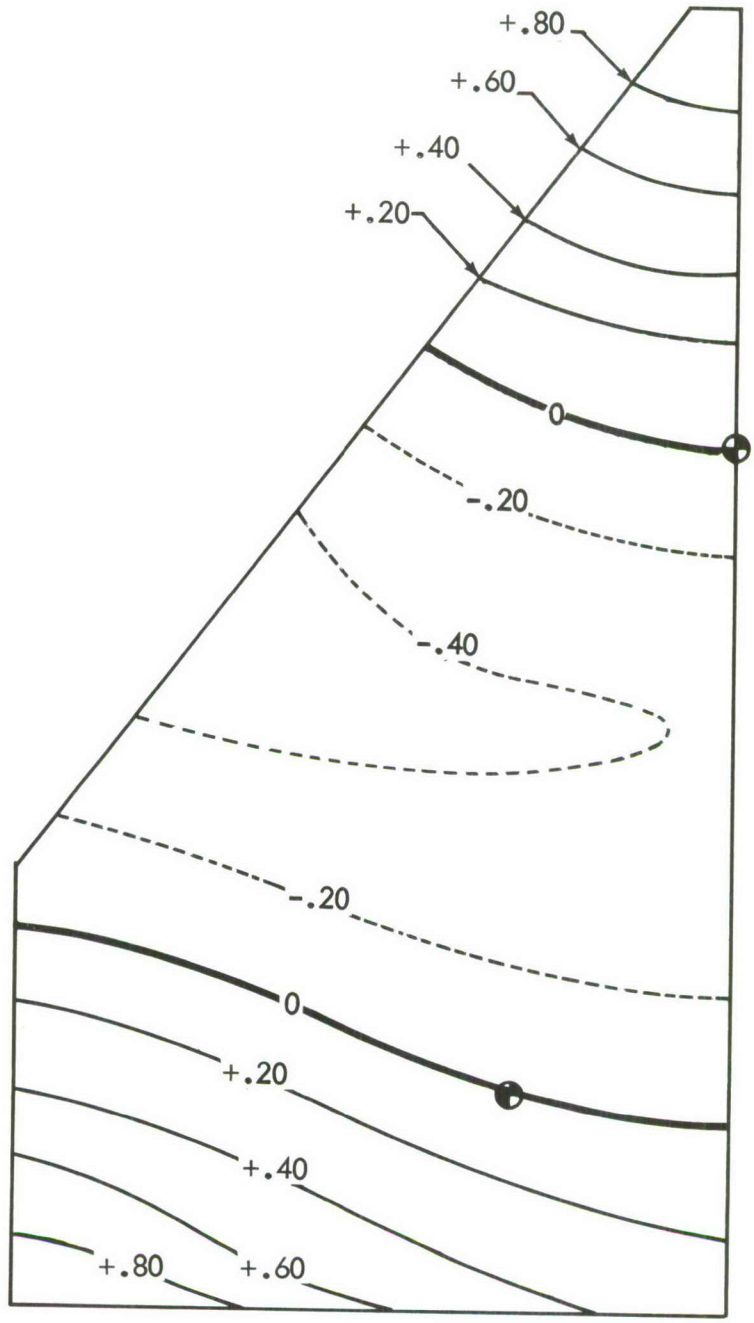

FREQUENCY 64.26 CPS

[K] COMPUTED IN TERMS OF DEFORMED SHAPE

SUPPORT POINT

FIGURE 45: SECOND SYMMETRIC MODE--HOT STRUCTURE LINEAR DEFLECTION THEORY (FINAL SHAPE)

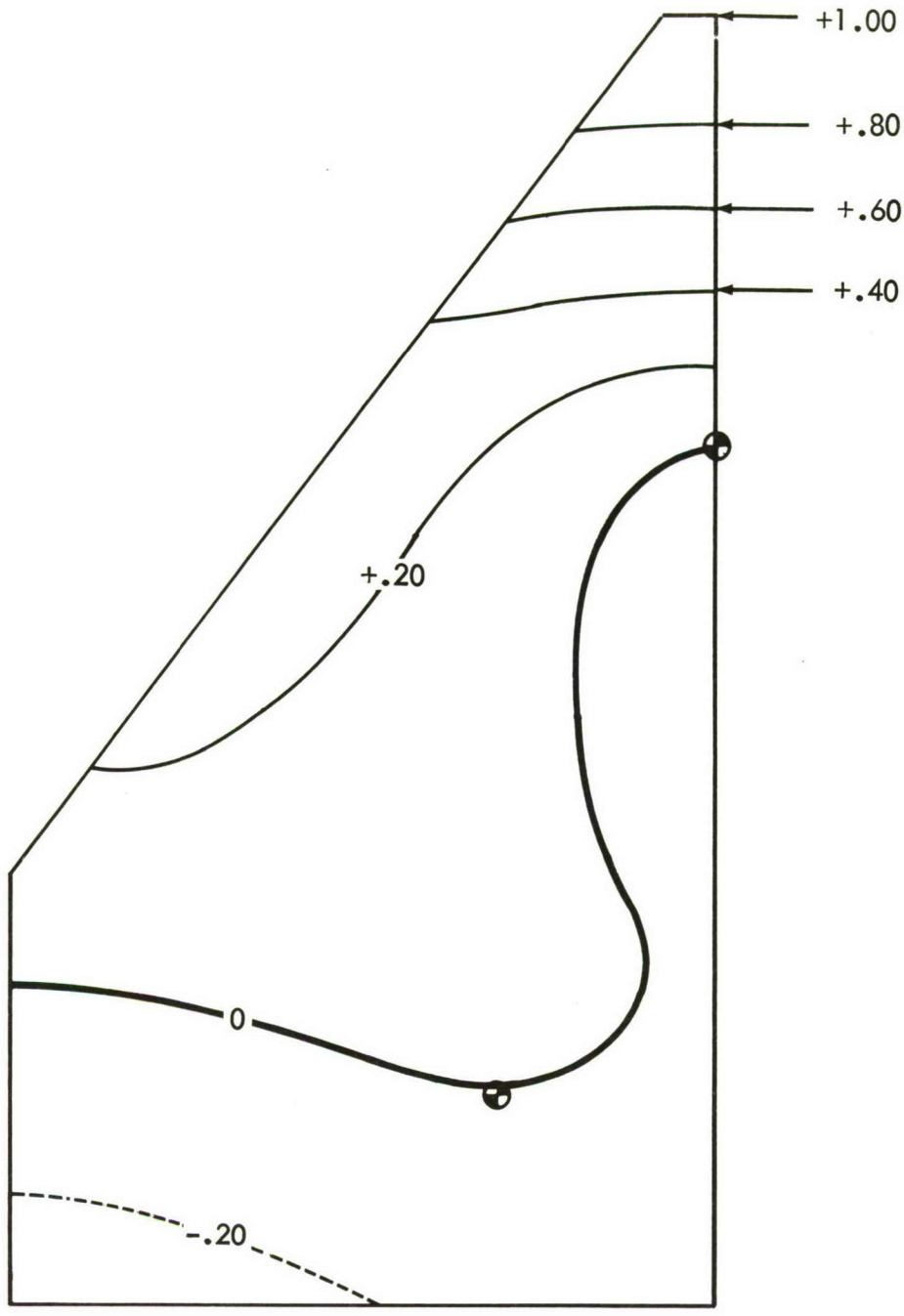

FIGURE 46: THIRD SYMMETRIC MODE--HOT STRUCTURE LINEAR DEFLECTION THEORY (FINAL SHAPE)

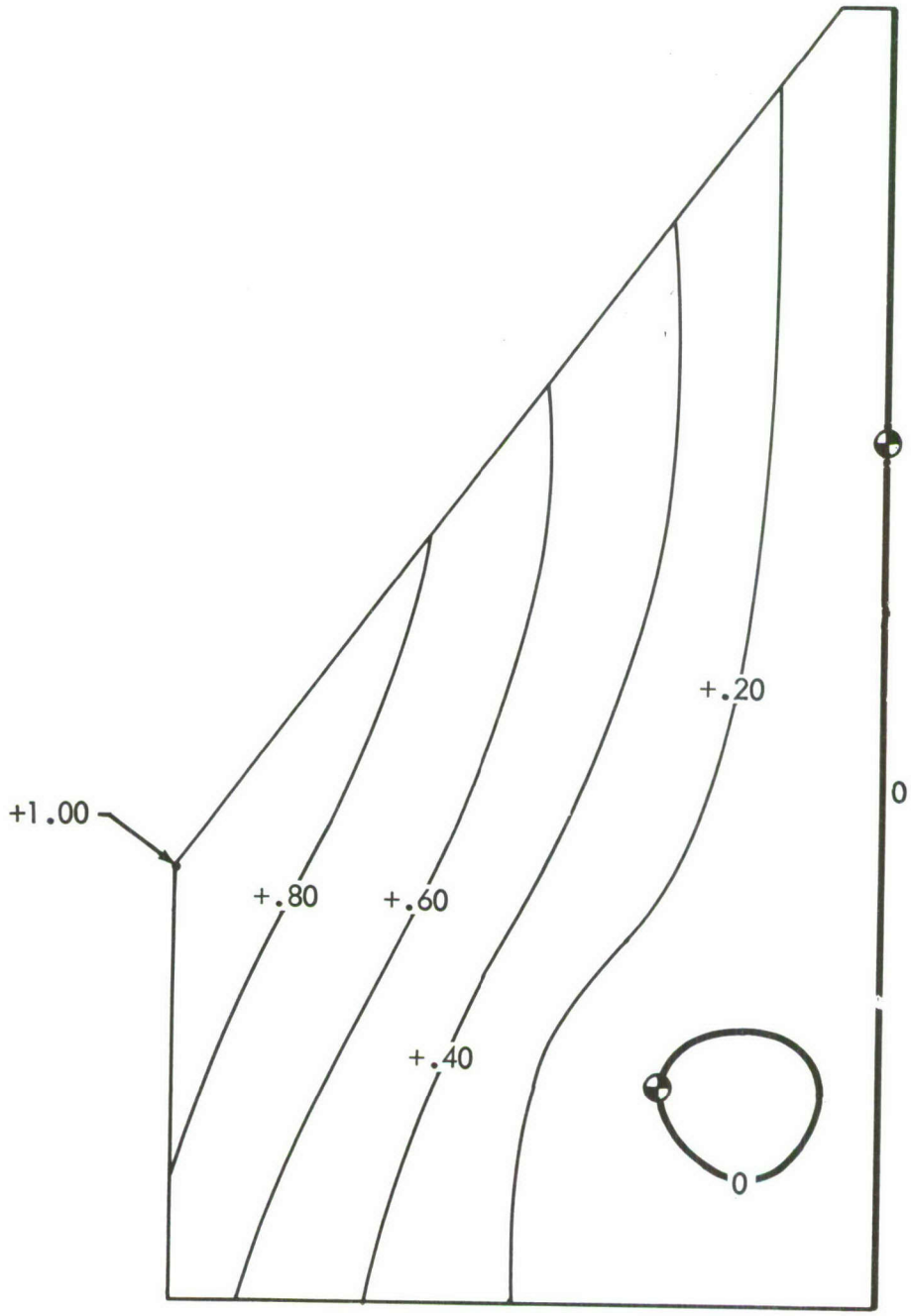

FREQUENCY 32.57 CPS

[K] COMPUTED IN TERMS OF DEFORMED SHAPE

SUPPORT POINT

FIGURE 47: FIRST ANTISYMMETRIC MODE--HOT STRUCTURE LINEAR DEFLECTION THEORY (FINAL SHAPE)

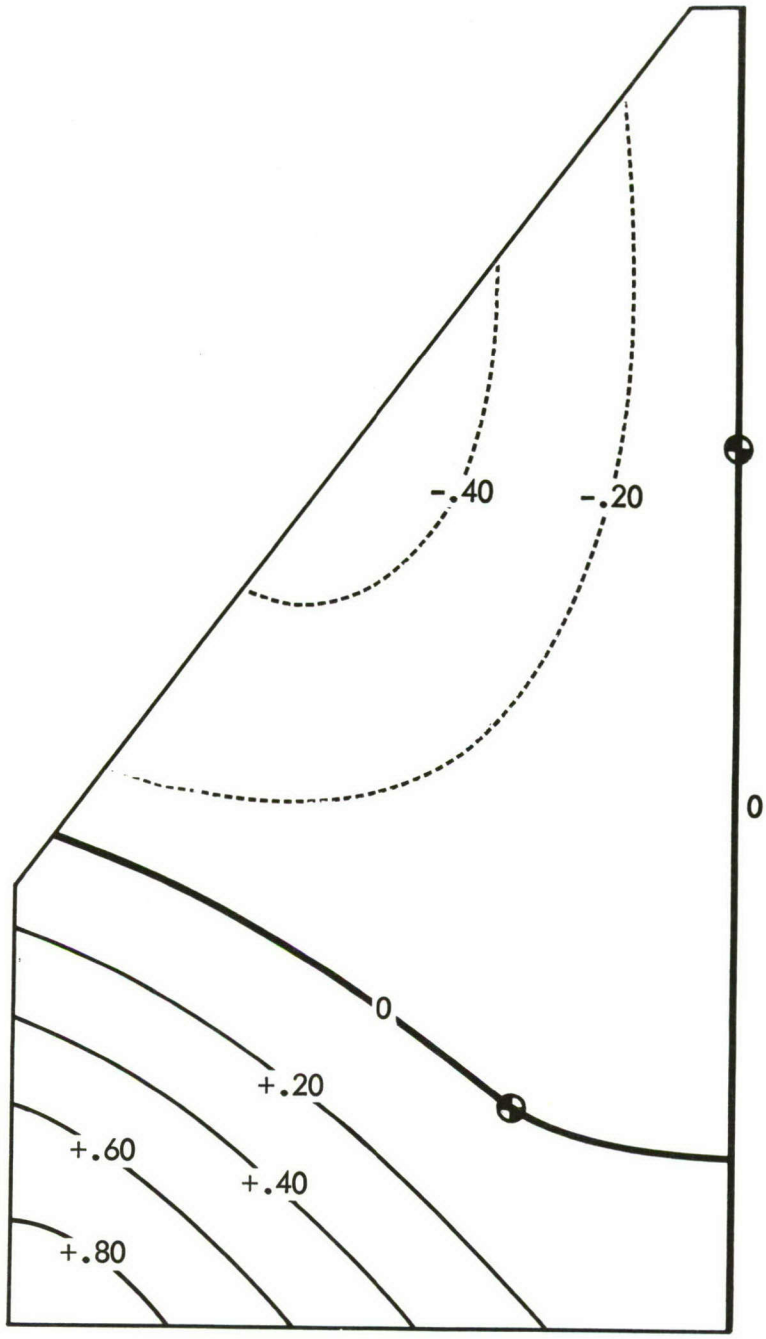

FREQUENCY 61.43 CPS

[K] COMPUTED IN TERMS OF DEFORMED SHAPE

SUPPORT POINT

FIGURE 48: SECOND ANTISYMMETRIC MODE--HOT STRUCTURE LINEAR DEFLECTION THEORY (FINAL SHAPE)

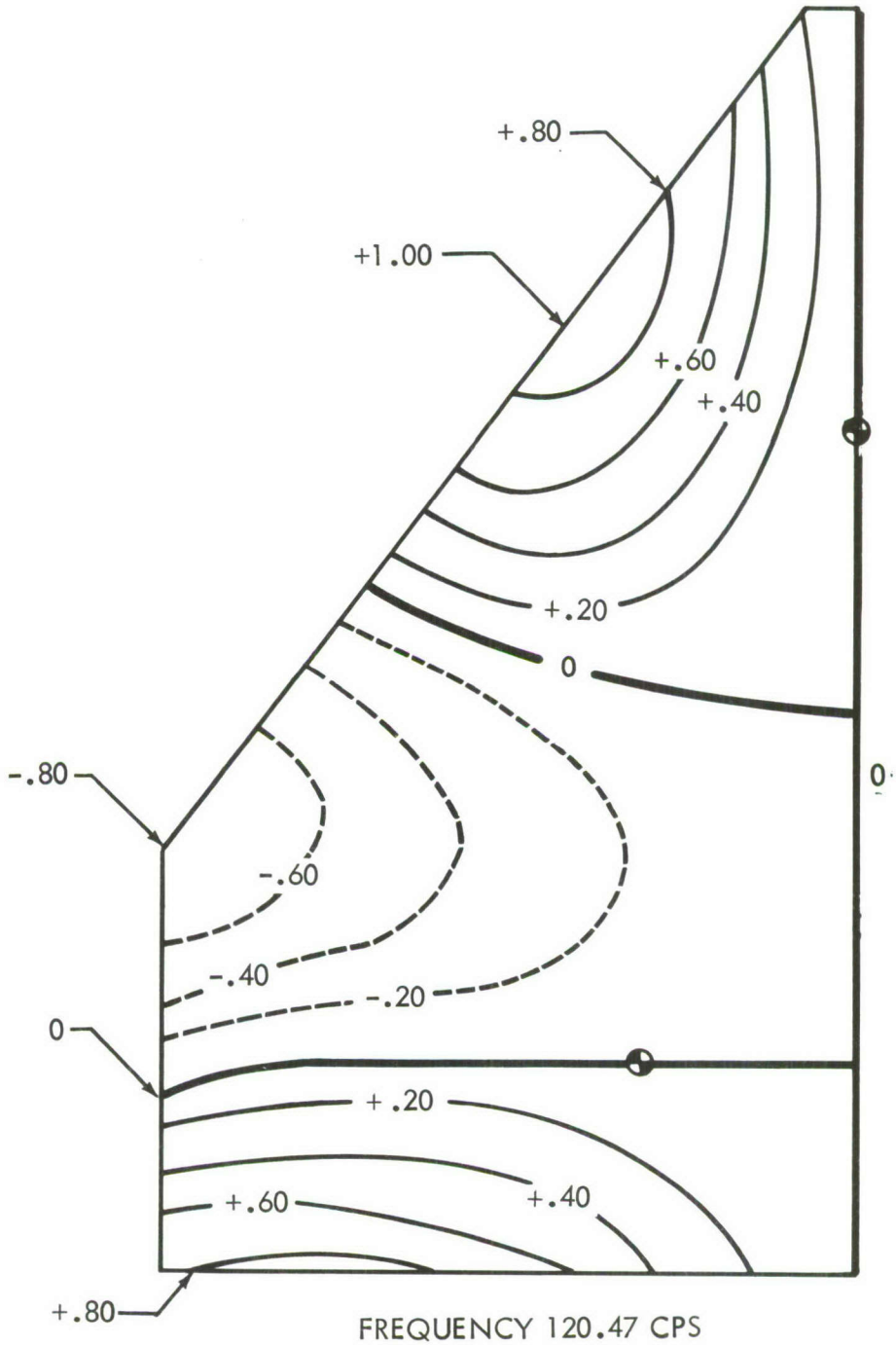

FIGURE 49: THIRD ANTISYMMETRIC MODE--HOT STRUCTURE LINEAR DEFLECTION THEORY (FINAL SHAPE)

REFERENCES

1. Novozhilov, V. V., "Foundations of the Nonlinear Theory of Elasticity," Graylock Press, Rochester, N. Y.
2. Turner, M. J., Clough, R. W., Martin, H. C., and Topp, L. J., "Stiffness and Deflection Analysis of Complex Structures," Journal of the Aeronautical Sciences, Vol. 23, September 1956, pp. 805-823.
3. Turner, M. J., "The Direct Stiffness Method of Structural Analysis," AGARD Meeting, Aachen, Germany, paper presented September 17, 1959.
4. Turner, M. J., Dill, E. H., Martin, H. C., and Melosh, R. J., "Large Deflections of Structures Subjected to Heating and External Loads," Journal of the Aero-Space Sciences, Vol. 27, February 1960, pp. 97-107.
5. Greene, B. E., Strome, D. R., and Weikel, R. C., "Application of the Stiffness Method to the Analysis of Shell Structures," Paper No. 61-AV-58, presented at Aviation Conference of the American Society of Mechanical Engineers, Los Angeles, California, March 12-16, 1961.
6. "Usage of COSMOS Systems for Structural and Vibration Analyses," Boeing document D2-4513.
7. Timoshenko, S., and Woinowsky-Krieger, "Theory of Plates and Shells," McGraw Hill Book Company.
8. Crandall, S. H., "Engineering Analysis," McGraw Hill Book Company.
9. Timoshenko, S., "Theory of Elastic Stability," McGraw Hill Book Company.
10. "Aerodynamic Heat Transfer Handbook," Vol. I., Boeing document D2-9514.
11. Hemp, W. S., "Fundamental Principles and Theorems of Thermo-Elasticity," The Aeronautical Quarterly, August 1956, pp. 184-192.
12. Bisplinghoff, R. L., Ashley, H., Halfman, R. L., "Aeroelasticity," Addison-Wesley Publishing Company.

APPENDIX A

DERIVATION OF TRIANGULAR-PLATE STIFFNESS MATRIX INCLUDING INITIAL MID-PLANE STRESSES AND HEATING

Let the triangular plate be oriented so that the middle surface of the plate is parallel to the x-y plane.

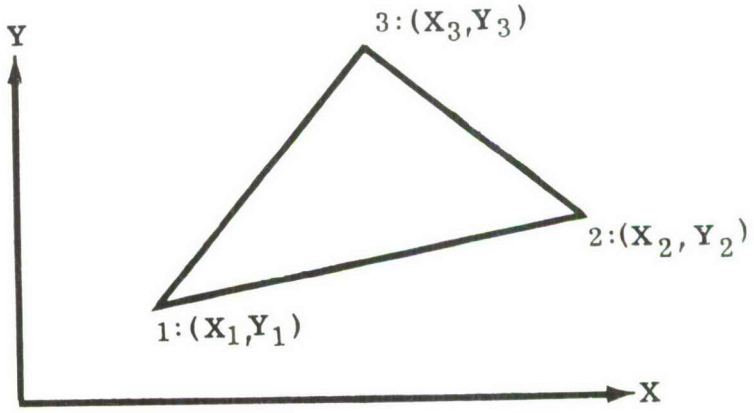

The strain components and the temperature are assumed constant throughout an individual triangular element. Furthermore, it is assumed that the elements of the structure are disconnected and allowed to expand upon heating; suitable constraints are then imposed to force the structure back to its original configuration. The basic problem then becomes that of determining the deflections due to relaxing the imposed constraints and applying external loads. For a nonlinear analysis the deformation will be divided into a series of steps so that changes in the displacement and rotations are small compared to unity. It will be necessary to consider the possibility that the rotations may be large compared to the strains. This type of assumption concerning the deformations is defined by Novozhilov (Reference 1) as representing geometrical nonlinearities.

In this analysis the displacements will be to the original configuration of the plate *before heating*. Coordinates of a typical point *before heating* will be represented by x and y, and displacements from the original

configuration will be given by u(x, y) and v(x, y). The strain components will be given by:

$$\epsilon_{xx} = \frac{\partial u}{\partial x} + 1/2 \left[\left(\frac{\partial u}{\partial x} \right)^2 + \left(\frac{\partial v}{\partial x} \right)^2 + \left(\frac{\partial w}{\partial x} \right)^2 \right]$$

$$\epsilon_{yy} = \frac{\partial v}{\partial y} + 1/2 \left[\left(\frac{\partial u}{\partial y} \right)^2 + \left(\frac{\partial v}{\partial y} \right)^2 + \left(\frac{\partial w}{\partial y} \right)^2 \right] \qquad \text{(A-1)}$$

$$\epsilon_{xy} = \frac{\partial u}{\partial y} + \frac{\partial v}{\partial x} + \frac{\partial u}{\partial x} \frac{\partial u}{\partial y} + \frac{\partial v}{\partial x} \frac{\partial v}{\partial y} + \frac{\partial w}{\partial x} \frac{\partial w}{\partial y}$$

These equations may be written in another form by introducing the notation:

$$e_{xx} = \frac{\partial u}{\partial x}, \quad e_{yy} = \frac{\partial v}{\partial y}, \quad e_{zz} = \frac{\partial w}{\partial z}$$

$$e_{xy} = \frac{\partial u}{\partial y} + \frac{\partial v}{\partial x}, \quad e_{xz} = \frac{\partial u}{\partial z} + \frac{\partial w}{\partial x}, \quad e_{yz} = \frac{\partial v}{\partial z} + \frac{\partial w}{\partial y} \qquad \text{(A-2)}$$

$$2\omega_x = \frac{\partial w}{\partial y} - \frac{\partial v}{\partial z}, \quad 2\omega_y = \frac{\partial u}{\partial z} - \frac{\partial w}{\partial x}, \quad 2\omega_z = \frac{\partial v}{\partial x} - \frac{\partial u}{\partial y}$$

to give:

$$\epsilon_{xx} = e_{xx} + 1/2 \left[e_{xx}^2 + \left(1/2\ e_{xy} + \omega_z \right)^2 + \left(1/2\ e_{yz} - \omega_x \right)^2 \right]$$

$$\epsilon_{yy} = e_{yy} + 1/2 \left[e_{yy}^2 + \left(1/2\ e_{xy} - \omega_z \right)^2 + \left(1/2\ e_{yz} + \omega_x \right)^2 \right]$$

$$\epsilon_{xy} = e_{xy} + e_{xx} \left(1/2\ e_{xy} - \omega_z \right) + e_{yy} \left(1/2\ e_{xy} + \omega_z \right) \qquad \text{(A-3)}$$

$$+ \left(1/2\ e_{xz} - \omega_y \right) \left(1/2\ e_{yz} + \omega_x \right)$$

Assuming that the rotations and strains are small compared to unity and that the rotations may be large compared to the strains, the terms represented by the strains squared may be neglected. However, the terms involving the rotations squared and the terms involving products of strains

and rotations must be retained. Using these assumptions, Equation A-3 becomes:

$$\epsilon_{xx} = e_{xx} + 1/2\left(\omega_y^2 + \omega_z^2\right) + 1/2\left(e_{xy}\omega_z - e_{xz}\omega_y\right)$$

$$\epsilon_{yy} = e_{yy} + 1/2\left(\omega_x^2 + \omega_z^2\right) + 1/2\left(e_{yz}\omega_x - e_{xy}\omega_z\right) \qquad \text{(A-4)}$$

$$\epsilon_{xy} = e_{xy} - \omega_x\omega_y + 1/2\left(e_{xz}\omega_x - e_{yz}\omega_y\right) + \omega_z\left(e_{yy} - e_{xx}\right)$$

The stress-strain relations and the strain energy will be expressed in terms of displacements from the *heated stress-free* state. Coordinates of a point in the *heated stress-free* state will be denoted by $(\bar{x}, \bar{y}, \bar{z})$. The displacements from that state are $(\bar{u}, \bar{v}, \bar{w})$.

$$\bar{x} = x(1 + {}_{\alpha}T) \qquad \bar{u} = u - \alpha Tx$$

$$\bar{y} = y(1 + {}_{\alpha}T) \qquad \bar{v} = v - \alpha Ty \qquad \text{displacements from the heated stress-free state.} \qquad \text{(A-5)}$$

$$\bar{z} = z(1 + {}_{\alpha}T) \qquad \bar{w} = w - \alpha Tz$$

The strains $\bar{\epsilon}_{xx}$, $\bar{\epsilon}_{yy}$, and $\bar{\epsilon}_{xy}$ from the *heated stress-free* state may be obtained by using Equation A-4 and letting these equations represent the prescribed strains.

$$\bar{\epsilon}_{xx} = \bar{e}_{xx} + 1/2\left(\bar{\omega}_y^2 + \bar{\omega}_z^2\right) + 1/2\left(\bar{e}_{xy}\bar{\omega}_z - \bar{e}_{xz}\bar{\omega}_y\right)$$

$$\bar{\epsilon}_{yy} = \bar{e}_{yy} + 1/2\left(\bar{\omega}_x^2 + \bar{\omega}_z^2\right) + 1/2\left(\bar{e}_{yz}\bar{\omega}_x - \bar{e}_{xy}\bar{\omega}_y\right) \qquad \text{(A-6)}$$

$$\bar{\epsilon}_{xy} = \bar{e}_{xy} - \bar{\omega}_x\bar{\omega}_y + 1/2\left(\bar{e}_{xz}\bar{\omega}_x - \bar{e}_{yz}\right) + \bar{\omega}_z\left(\bar{e}_{yy} - \bar{e}_{xx}\right)$$

Using Equation A-5 allows the temperature considerations to be incorporated into the expressions for the strains.

$$\bar{e}_{xx} = \frac{\partial \bar{u}}{\partial \bar{x}} = \frac{\partial \bar{u}}{\partial x}\frac{\partial x}{\partial \bar{x}} = \left(\frac{\partial u}{\partial x} - \alpha T\right)\left(\frac{1}{1 + \alpha T}\right)$$

$$\bar{e}_{yy} = \frac{\partial \bar{v}}{\partial \bar{y}} = \frac{\partial \bar{v}}{\partial y}\frac{\partial y}{\partial \bar{y}} = \left(\frac{\partial v}{\partial y} - \alpha T\right)\left(\frac{1}{1 + \alpha T}\right) \qquad \text{(A-7)}$$

$$\bar{e}_{xy} = \frac{\partial \bar{u}}{\partial \bar{y}} + \frac{\partial \bar{v}}{\partial \bar{x}} = \frac{\partial \bar{u}}{\partial y}\frac{\partial y}{\partial \bar{y}} + \frac{\partial \bar{v}}{\partial x}\frac{\partial x}{\partial \bar{x}} = \frac{\partial u}{\partial y}\left(\frac{1}{1 + \alpha T}\right) + \frac{\partial v}{\partial x}\left(\frac{1}{1 + \alpha T}\right)$$

By assuming that $\alpha T \ll 1$, the only strain-components affected by temperature are $\bar{e}_{xx}$ and $\bar{e}_{yy}$ which are given by:

$$\bar{e}_{xx} = \frac{\partial u}{\partial x} - \alpha T = e_{xx} - \alpha T$$

$$\bar{e}_{yy} = \frac{\partial v}{\partial y} - \alpha T = e_{yy} - \alpha T \qquad \text{(A-8)}$$

$$\bar{e}_{xy} = \frac{\partial u}{\partial y} + \frac{\partial v}{\partial x} = e_{xy}$$

Thus, it follows that:

$$\bar{\epsilon}_{xx} = \epsilon_{xx} - \alpha T$$

$$\bar{\epsilon}_{yy} = \epsilon_{yy} - \alpha T \qquad \text{(A-9)}$$

$$\bar{\epsilon}_{xy} = \epsilon_{xy}$$

The stress-strain relations in terms of the displacements from the heated stress-free state are given by:

$$\begin{Bmatrix} \sigma_{xx} \\ \sigma_{yy} \\ \tau_{xy} \end{Bmatrix} = \frac{E}{(1 - \nu^2)} \begin{bmatrix} 1 & \nu & 0 \\ \nu & 1 & 0 \\ 0 & 0 & \lambda_1 \end{bmatrix} \begin{Bmatrix} \bar{\epsilon}_{xx} \\ \bar{\epsilon}_{yy} \\ \bar{\epsilon}_{xy} \end{Bmatrix} \qquad \text{(A-10)}$$

Where: $\lambda_1 = \frac{(1 - \nu)}{2}$

Substituting Equation A-9 into A-10 gives the stresses in terms of the initial strains (unheated state):

$$\begin{Bmatrix} \sigma_{xx} \\ \sigma_{yy} \\ \tau_{xy} \end{Bmatrix} = \frac{E}{(1-\nu^2)} \begin{bmatrix} 1 & \nu & 0 \\ \nu & 1 & 0 \\ 0 & 0 & \lambda_1 \end{bmatrix} \begin{Bmatrix} \bar{\epsilon}_{xx} \\ \bar{\epsilon}_{yy} \\ \bar{\epsilon}_{xy} \end{Bmatrix} - \frac{E\,\alpha\,T}{(1-\nu)} \begin{Bmatrix} 1 \\ 1 \\ 0 \end{Bmatrix} \quad \text{(A-11)}$$

The strain energy for the heated plate may be written:

$$U = \frac{1}{2}\,At\left[\sigma_{xx}\,\epsilon_{xx} + \sigma_{yy}\,\epsilon_{yy} + \tau_{xy}\,\epsilon_{xy} - (\sigma_{xx} + \sigma_{yy})\,\alpha T\right] \quad \text{(A-12)}$$

where: A = original plate area in the unheated, unstrained state;

t = original plate thickness.

Equation A-12 may now be written in the following form making use of Equation A-10:

$$U = \frac{EAt}{2(1-\nu^2)} \left[\epsilon_{xx} \quad \epsilon_{yy} \quad \epsilon_{xy}\right] \begin{bmatrix} 1 & \nu & 0 \\ \nu & 1 & 0 \\ 0 & 0 & \lambda_1 \end{bmatrix} \begin{Bmatrix} \epsilon_{xx} \\ \epsilon_{yy} \\ \epsilon_{xy} \end{Bmatrix} \quad \text{(A-13)}$$

$$- \frac{EAt\,\alpha T}{2(1-\nu)} \left[\epsilon_{xx} + \epsilon_{yy}\right] + \frac{EAt}{2(1-\nu^2)} \left[\epsilon_{xx} + \epsilon_{yy} + \epsilon_{xx} + \epsilon_{yy}\right](-\alpha T)$$

$$- \left[-\frac{E\,\alpha\,T}{(1-\nu)} - \frac{E\,\alpha\,T}{(1-\nu)}\right](\alpha T)\left(\frac{At}{2}\right)$$

Simplifying Equation A-13 gives the strain energy in the desired form:

$$U = \frac{EAt}{2(1-\nu^2)} \left[\epsilon_{xx} \quad \epsilon_{yy} \quad \epsilon_{xy}\right] \begin{bmatrix} 1 & \nu & 0 \\ \nu & 1 & 0 \\ 0 & 0 & \lambda_1 \end{bmatrix} \begin{Bmatrix} \epsilon_{xx} \\ \epsilon_{yy} \\ \epsilon_{xy} \end{Bmatrix} \quad \text{(A-14)}$$

$$- \frac{AET \quad a\,t}{(1-\nu)} \left[\epsilon_{xx} + \epsilon_{yy} \right] + \frac{AEt}{(1-\nu)} \left(a\,T \right)^2 \qquad \text{(A-14 Cont'd)}$$

At an intermediate step in the deformation process, the plate element is in a state of initial strain designated by ϵ^{o}_{xx}, ϵ^{o}_{yy}, ϵ^{o}_{xy}. With the addition of small additional displacements, it becomes necessary to obtain the changes in the components of the nodal forces. Ultimately, the total strain from the undeformed state must be determined.

A plate with small initial strains may be obtained from a neighborhood configuration with zero strains by a linear transformation involving no rotations. Thus, $\omega^{o}_{x} = \omega^{o}_{y} = \omega^{o}_{z} = 0$. Therefore, from Equation A-4 the expansion for the initial strain is:

$$\begin{aligned} \epsilon^{o}_{xx} &= e^{o}_{xx} = \frac{\partial u^{o}}{\partial x} \\ \epsilon^{o}_{yy} &= e^{o}_{yy} = \frac{\partial v^{o}}{\partial y} \\ \epsilon^{o}_{xy} &= e^{o}_{xy} = \frac{\partial u^{o}}{\partial y} + \frac{\partial v^{o}}{\partial x} \end{aligned} \qquad \text{(A-15)}$$

The coordinates of a typical point in the middle surface of the strained element are denoted by (x, y); the corresponding point of the unstrained element is (x^{o}, y^{o}), where:

$$\begin{aligned} x &= x^{o} + u^{o} \quad (x^{o}, y^{o}) \\ y &= y^{o} + v^{o} \quad (x^{o}, y^{o}) \end{aligned} \qquad \text{(A-16)}$$

In further development, no distinction will be made between integration and differentiation with respect to x and y and with respect to x^{o} and y^{o}. Additional displacements u', v', w' are now introduced so that the total displacement from the unstrained state is given by:

$$\begin{aligned} u &= u^{o} + u' \\ v &= v^{o} + v' \\ w &= w' \end{aligned} \qquad \text{(A-17)}$$

If additional strains and rotations are assumed to be small compared to unity, but not necessarily of the same order of magnitude, then the

terms of order $e'_{xy}\,\omega'_z$, $e'_{xz}\,\omega'_y$, etc. can be neglected. As a result, the total strains may be written:

$$\epsilon_{xx} = e^o_{xx} + e'_{xx} + \frac{1}{2}(\omega'^2_y + \omega'^2_z) + \frac{1}{2}(e^o_{xy} + e'_{xy})\omega'_z - \frac{1}{2}(e'_{xz} + \frac{\partial u^o}{\partial z})\,\omega'_y$$

$$\epsilon_{yy} = e^o_{yy} + e'_{yy} + \frac{1}{2}(\omega'^2_x + \omega'^2_z) - \frac{1}{2}(e^o_{xy} + e'_{xy})\omega'_z + \frac{1}{2}(e'_{yz} + \frac{\partial v^o}{\partial z})\,\omega'_x \qquad \text{(A-18)}$$

$$\epsilon_{xy} = e^o_{xy} + e'_{xy} - \omega'_x\omega'_y + (e^o_{yy} + e'_{yy} - e^o_{xx} - e'_{xx})\,\omega'_z$$

$$+\frac{1}{2}\left[(e'_{xz} + \frac{\partial u^o}{\partial z})\,\omega'_x - (e'_{yz} + \frac{\partial v^o}{\partial z})\omega'_z\right]$$

Neglecting the terms whose order of magnitude is not significant gives the following results:

$$\epsilon_{xx} = e^o_{xx} + e'_{xx} + \frac{1}{2}(\omega'^2_y + \omega'^2_z) + \frac{1}{2}e^o_{xy}\,\omega'_z$$

$$\epsilon_{yy} = e^o_{yy} + e'_{yy} + \frac{1}{2}(\omega'^2_x + \omega'^2_z) - \frac{1}{2}e^o_{xy}\,\omega'_z \qquad \text{(A-19)}$$

$$\epsilon_{xy} = e^o_{xy} + e'_{xy} - \omega'_x\omega'_y + (e^o_{yy} - e^o_{xx})\,\omega'_z$$

Prior to the additional deflections u', v', w', the plate is situated with the middle surface in the x-y plane. If the strains are assumed constant in the triangular plate, then the additional displacements from the unstrained state will be given by:

$$\begin{aligned} u' &= a\,x + b\,y + c \\ v' &= d\,x + e\,y + f \\ w' &= g\,x + h\,y + k \end{aligned} \qquad \text{(A-20)}$$

These constants can be evaluated in terms of nodal displacements and coordinates of the triangle. Assume that prior to the small additional

displacements (u' , v' , w') the triangular plate is situated with the following nodal coordinates: (x_1 , y_1) ; (x_2 , y_2) ; and (x_3 , y_3). Evaluating the constants gives:

$$u'_1 = ax_1 + by_1 + c \qquad u'_2 = ax_2 + by_2 + c \qquad u'_3 = ax_3 + by_3 + c$$

$$v'_1 = dx_1 + ey_1 + f \qquad v'_2 = dx_2 + ey_2 + f \qquad v'_3 = dx_3 + ey_3 + f \qquad \text{(A-21)}$$

$$w'_1 = gx_1 + hy_1 + k \qquad w'_2 = gx_2 + hy_2 + k \qquad w'_3 = gx_3 + hy_3 + k$$

If Equation A-21 is used to evaluate the strains $\epsilon_{ij}(i, j = x, y,$ respectively) in terms of the corner displacements, the strain energy for the triangle may be evaluated in terms of the corner displacements by integrating Equation A-12 over the area of the triangle. Having the strain energy in terms of corner displacements, the stiffness matrix may be computed from:

$$\left[K_{ij}\right] = \left[\frac{\partial^2 U}{\partial u_i \partial u_j}\right] \qquad \text{(A-22)}$$

The final stiffness equation can be arranged:

$$\left\{\Delta F\right\} = \left(\left[K^0\right] + \left[K^1\right]\right)\left\{\Delta f\right\} \qquad \text{(A-23)}$$

where:

$$\left\{\Delta f\right\} = \left\{\Delta u_1 , \Delta v_1 , \Delta w_1 , \Delta u_2 , \Delta v_2 , \Delta w_2 , \Delta u_3 , \Delta v_3 , \Delta w_3\right\}$$

and K^0 is associated with the stress-free state at the beginning of loading and K^1 is associated with the residual stresses present at the beginning of loading. The expanded values of K^0 are given on Page 110. K^1 may be written in terms of the initial stresses as follows:

$$\left[K^1\right] = \frac{t}{16A}\ \sigma^o_{xx}\ \left[K^1_1\right] + \frac{t}{16A}\ \sigma^o_{yy}\ \left[K^1_2\right] + \frac{t}{8A}\ \tau^o_{xy}\ \left[K^1_3\right] \qquad \text{(A-24)}$$

where (σ^{o}_{xx}, σ^{o}_{yy}, τ^{o}_{xy}) represent the initial stresses; K_1^1, K_2^1, and K_3^1 are given in expanded form on Pages 107, 108, and 109, respectively.

APPENDIX B

NONLINEAR DIGITAL PROCEDURE

Let $[K^o]$ be an element stiffness matrix for any unstressed element in its assumed local coordinate system. Explicit formulas for these matrices are given in Reference 6. Let $\{\Delta T_i\}$ be the column of incremental temperatures at each node which is applied to the structure during the i^{th} step in a nonlinear analysis. Let $\{\Delta \hat{L}_i\}$ be the column of incremental loads applied to the structure during the i^{th} step. If $\{\Delta T_i\}$ is of order n, $\{\Delta \hat{L}_i\}$ may be of order n, 2n, 3n, 4n, 5n, or 6n.

Let:

$$\frac{t}{2}\begin{bmatrix} y_{23} & 0 & x_{32} \\ 0 & x_{32} & y_{23} \\ 0 & 0 & 0 \\ y_{31} & 0 & x_{13} \\ 0 & x_{13} & y_{31} \\ 0 & 0 & 0 \\ y_{12} & 0 & x_{21} \\ 0 & x_{21} & y_{12} \\ 0 & 0 & 0 \end{bmatrix} = [G_p] \qquad \text{(B-1)}$$

where t = plate thickness; x_i, y_i are plate local nodal coordinates; and $x_{ij} = x_i - x_j$ etc. $[G_p]$ is a geometry matrix which, when multiplied on the right by the column $\begin{Bmatrix} \sigma_x \\ \sigma_y \\ \sigma_{xy} \end{Bmatrix}$ of local element stresses, gives element corner forces for a 3-node plate. Let:

$$A_s \begin{Bmatrix} -\lambda \\ -\mu \\ \lambda \\ \mu \end{Bmatrix} = \{G_s\} \qquad \text{(B-2)}$$

where A_s = x-sectional area of a stringer; $\lambda = \frac{\ell}{L}$, $\mu = \frac{d_{12}}{L}$,

$\ell = (L^2 - d_{12}^2)^{\frac{1}{2}}$, $L = (x_{34}^2 + y_{34}^2 + z_{34}^2)^{\frac{1}{2}}$, d_1 and d_2 are shear-web half widths; and (x_3, y_3, z_3) and (x_4, y_4, z_4) are the nodal coordinates at the stringer ends. (See Reference 6.) As for the plate, $[G_s]$ is a pure geometry matrix in local coordinates which transforms a stringer stress into equivalent local corner forces.

Let $[B]$ be the (3 by 3) matrix which transforms a vector in the overall coordinate system into a vector in the local coordinate system. Since $[B]$ is a unitary matrix, $[B]^T = [B]^{-1} \equiv [A]$. Then, if $\{V\}$ is any vector in a local coordinate system and if $\{\hat{V}\}$ is the transformed vector in an overall coordinate system,

$$[B] \{\hat{V}\} = \{V\}, \text{ or } \{\hat{V}\} = [A]\{V\} = [B]^{-1}\{V\}$$

The elements of B are cosines of the angles between local and overall coordinate axes. Let $\{u_i\}$ be the column of nodal coordinates in the overall coordinate system after the i^{th} step, and $\{\hat{\Delta u}_i\}$ be the incremental deflections which occur during the i^{th} step. Let $\{\sigma_i\}$ be the total stresses present in the structure after the i^{th} step, and $\{\Delta\sigma_i\}$ be the incremental stresses which occur during the i^{th} step. Stresses are always in the local coordinate system of each structural element. Let $[K^1]$ be the matrix for any element which, when multiplied by the local element stresses, accounts for the change in $[K_i]$ in the presence of the stresses. Thus, the total stiffness matrix for any element during the i^{th} step would be $[K_i] \equiv [K^0] + [K^1]\{\sigma_{i-1}\}$ in the local coordinate

system of the structural element. Specific K^1 formulas for the 2-node stringer and 3-node plate are:

$$\left[K^1\right]\text{Stringer} = \frac{A_s}{L}\begin{bmatrix} 1-\lambda^2 & & & & & & u_1 \\ 0 & 0 & & \text{SYMMETRIC} & & & v_1 \\ -\lambda\mu & 0 & 1-\mu^2 & & & & w_1 \\ -(1-\frac{2}{\lambda}) & 0 & \lambda\mu & 1-\lambda^2 & & & u_2 \\ 0 & 0 & 0 & 0 & 0 & & v_2 \\ \lambda\mu & 0 & -(1-\mu^2) & -\lambda\mu & 0 & 1-\mu^2 & w_2 \end{bmatrix} \qquad \text{(B-3)}$$

$$\left[K^1\right]\text{Plate} = \frac{t}{16A}\left[\sigma^{\,o}_{xx}\,K^1_1 + \sigma^{\,o}_{yy}\,K^1_2 + 2\,\tau^{\,o}_{xy}\,K^1_3\right] \qquad \text{(B-4)}$$

Where A is the plate area; and K^1_1, K^1_2, and K^1_3 are defined on Pages 107, 108, and 109. (Also, see Equation A-24.)

Let E be Young's modulus and let α be the linear coefficient of thermal expansion—E and α are considered functions of temperature by COSMOS.

A nonlinear analysis with COSMOS starts with a set of data which looks exactly like the usual linear COSMOS input. (See Reference 6.) These data consist of control data, nodal data, structural data, and state data. When the data are organized and the job card "Prepare for a Non-Linear Analysis" is read, the program goes through certain preliminary steps before doing any nonlinear step. The $\left[K^o\right]$, $\left[K^1\right]$, and $\left[G\right]$ matrices for each structural element are generated in their respective local coordinate systems and stored on tape. These matrices will never be changed during a nonlinear analysis. The E and ν for each element are determined from a material table at the assumed uniform temperature of the element. This temperature is determined from the state data in the usual manner.

Each step in the nonlinear analysis is initiated by a job card which reads "Apply Partial Loads" or "Repeat Partial Loads." A new set of state data is read into the machine, or the set from the last step is used. Assume completed i-1 steps and describe the computations during the i^{th} step. The columns $\left\{\hat{u}_{i-1}\right\}$ and $\left\{\sigma_{i-1}\right\}$ resulting from the $(i-1)^{\text{th}}$ step are saved.

(1) Generate in local coordinates, for each structural element, a column of nodal forces which would produce the required thermal expansion. Call this column $\left\{F_{\Delta T_i}\right\}$. For a 3-node plate:

$$\left\{F_{\Delta T_i}\right\} = -\left(\frac{E \quad \alpha \Delta T_i}{1-\nu}\right) \left[G_p\right] \begin{Bmatrix} 1 \\ 1 \\ 0 \end{Bmatrix} \tag{B-5}$$

and for a stringer:

$$\left\{F_{\Delta T_i}\right\} = - (E \alpha \Delta T_i) \left\{G_s\right\} \tag{B-6}$$

In Equations B-5 and B-6 the subscript ΔT_i is intended to imply the state-data temperature, and the factor ΔT_i is intended to mean the structural-element temperature increment for this step.

(2) Transform $\left\{F_{\Delta T_i}\right\}$ to overall coordinates by $\left\{\hat{F}_{\Delta T_i}\right\} = \left[A\right] \left\{F_{T_i}\right\}$ where the elements of A are calculated based on $\left\{\hat{u}_{i-1}\right\}$

(3) Calculate $\left\{\hat{\Delta} L_i\right\} - \left\{\hat{F}_{\Delta T_i}\right\}$

(4) Calculate the local element stiffness matrix for this step:

$$\left[K_i\right] = \left[K^0\right] + \left[K^1\right] \left\{\sigma_{i-1}\right\}$$

and transform to the overall coordinate system

$$\left[\hat{K}_i\right] = \left[A\right] \left[K_i\right] \left[B\right]$$

(5) Merge the element stiffness matrices into the gross stiffness matrix for the structure. Perform deletions and reductions as required by boundary conditions.

(6) Repeat Steps (1) through (5) until all the elements have been handled.

(7) Use the job cards "Invert the Stiffness Matrix," "Obtain Deflections from the Inverse," or "Form a Back Substitution Solution," as needed, to find $\left\{\hat{\Delta} u_i\right\} = \left[\hat{K}_i\right]^{-1} \left\{\left\{\hat{\Delta} L_i\right\} - \left\{F \hat{\Delta} T_i\right\}\right\}$

(8) Calculate incremental stresses for each element, using the job card "Perform a Stress Analysis."

$$\left\{\Delta \sigma_i\right\}_{plate} = \left[G_1\right] \left[B\right] \left\{\hat{\Delta} u_i\right\} - \frac{E \alpha \Delta T_i}{1 - \nu} \begin{Bmatrix} 1 \\ 1 \\ 0 \end{Bmatrix}$$

$$\Delta \sigma_{i\,stringer} = \left[G_2\right] \left[B\right] \left\{\hat{\Delta} u_i\right\} - E \alpha \Delta T_i$$

where $\left[G_1\right]$ and $\left[G_2\right]$ are the usual stress matrices used in linear COSMOS and are found in LARM No. 24.

(9) Find $\left\{\sigma_i\right\} = \left\{\sigma_{i-1}\right\} + \left\{\Delta \sigma_i\right\}$

(10) Find $\left\{u_i\right\} = \left\{\hat{u}_{i-1}\right\} + \left\{\hat{\Delta} u_i\right\}$ using the job card "Deflect Nodes Internally."

This is the end of step i.

Any of the following may be extracted at the end of any step by using the normal list of linear COSMOS job cards and the additional job cards, "Print Nodal Coordinates" or "Output Stress."

(1) $\left[\hat{K}_i\right]$ —Final stiffness matrix in the overall coordinate system;

(2) $\left[\hat{K}_i\right]^{-1}$ —Inverse of final stiffness matrix;

(3) $\left\{\hat{u}_i\right\}$ —Displacements;

(4) $\left\{\hat{\Delta} u_i\right\}$ —Incremental displacements;

(5) $\left\{\sigma_i\right\}$ —Stresses;

(6) $\left\{\left\{\hat{\Delta} L_i\right\} - \left\{F \hat{\Delta} T_i\right\}\right\}$ —Column of net nodal forces.

$$
\left[K_1\right] =
\begin{bmatrix}
3x_{32}^2 & & & & & & & & & \\
x_{23}y_{23} & -y_{23}^2 & & & & & & & & \\
0 & 0 & 4y_{23}^2 & & & & & & & \\
3x_{13}x_{32} & x_{31}y_{23} & 0 & 3x_{13}^2 & & & & & & \\
x_{23}y_{31} & y_{23}y_{13} & 0 & x_{31}y_{31} & -y_{31}^2 & & & & & \\
0 & 0 & 4y_{31}y_{23} & 0 & 0 & 4y_{31}^2 & & & & \\
3x_{21}x_{32} & x_{12}y_{23} & 0 & 3x_{21}x_{13} & x_{12}y_{31} & 0 & 3x_{21}^2 & & & \\
x_{23}y_{12} & y_{32}y_{12} & 0 & x_{31}y_{12} & y_{13}y_{12} & 0 & x_{12}y_{12} & -y_{12}^2 & & \\
0 & 0 & 4y_{12}y_{23} & 0 & 0 & 4y_{12}y_{31} & 0 & 0 & 4y_{12}^2 &
\end{bmatrix}
$$

SYMMETRIC

$$
\left[K_2^1\right] =
\begin{bmatrix}
-X_{32}^2 & & & & & & & & & \\
x_{23}y_{23} & 3\,y_{23}^2 & & & & & & & & \\
0 & 0 & 4\,x_{32}^2 & & & & & & & \\
x_{31}x_{32} & x_{31}y_{23} & 0 & -x_{13}^2 & & & & & & \\
x_{23}y_{31} & 3\,y_{23}y_{31} & 0 & x_{31}y_{31} & 3\,y_{31}^2 & & & & & \\
0 & 0 & 4\,x_{13}x_{32} & 0 & 0 & 4\,x_{13}^2 & & & & \\
x_{12}x_{32} & x_{12}y_{23} & 0 & x_{12}x_{13} & x_{12}y_{31} & 0 & -x_{21}^2 & & & \\
x_{23}y_{12} & 3\,y_{23}y_{12} & 0 & x_{31}y_{12} & 3\,y_{31}y_{12} & 0 & x_{12}y_{12} & 3\,y_{12}^2 & & \\
0 & 0 & -x_{21}x_{32} & 0 & 0 & 4x_{13}x_{21} & 0 & 0 & 4\,x_{21}^2
\end{bmatrix}
$$

SYMMETRIC

$$
[K_3'] =
\begin{bmatrix}
y_{23}^2 + x_{23}^2 & 2x_{23}y_{23} & & & & & & & & & & \\
0 & 0 & 4x_{32}y_{23} & & & & & & & & & \\
x_{31}y_{23} + x_{23}y_{31} & y_{23}y_{31} + x_{23}x_{31} & 0 & 2x_{31}y_{31} & & & & & & & & \\
y_{23}y_{31} + x_{23}x_{31} & x_{23}y_{31} + y_{23}x_{31} & 0 & y_{31}^2 + x_{31}^2 & 2x_{31}y_{31} & & & & & & & \\
0 & 0 & 2(x_{32}y_{31} + x_{13}y_{23}) & 0 & 0 & 4x_{13}y_{31} & & & & & & \\
x_{12}y_{23} + x_{23}y_{12} & y_{23}y_{12} + x_{23}x_{12} & 0 & x_{12}y_{31} + x_{31}y_{12} & y_{12}y_{31} + x_{12}x_{31} & 0 & 2x_{12}y_{12} & & & & & \\
y_{23}y_{12} + x_{23}x_{12} & x_{23}y_{12} + y_{23}x_{12} & 0 & y_{31}y_{12} + x_{31}x_{12} & x_{31}y_{12} + x_{12}y_{31} & 0 & y_{12}^2 + x_{12}^2 & 2x_{12}y_{12} & & & \\
0 & 0 & 2(x_{32}y_{12} + x_{21}y_{23}) & 0 & 0 & 2(x_{13}y_{12} + x_{21}y_{31}) & 0 & 0 & 4x_{21}y_{12} & & \\
\end{bmatrix}
$$

SYMMETRIC

$$
[K^{\circ}] = \frac{Et}{4A(1-\nu^2)}
\begin{bmatrix}
y_{23}^2 + \lambda_1 x_{32}^2 & & & & & & & & & & & \\
\lambda_1 x_{32} y_{23} - \nu x_{23} y_{23} & x_{23}^2 + \lambda_1 y_{23}^2 & & & & & & & & & & \\
0 & 0 & 0 & & & & & & & & & \\
y_{31} y_{23} + \lambda_1 x_{13} x_{32} & \lambda_1 x_{13} y_{23} - \nu x_{23} y_{31} & 0 & y_{31}^2 + \lambda_1 x_{13}^2 & & & & & & & & \\
\lambda_1 x_{32} y_{31} - \nu x_{31} y_{23} & x_{23} x_{31} + \lambda_1 y_{23} y_{31} & 0 & \lambda_1 x_{13} y_{31} - \nu x_{31} y_{31} & x_{31}^2 + \lambda_1 y_{31}^2 & & & & & & & \\
0 & 0 & 0 & 0 & 0 & 0 & & & & & & \\
y_{23} y_{12} + \lambda_1 x_{32} x_{21} & \lambda_1 x_{21} y_{23} - \nu x_{23} y_{12} & 0 & y_{31} y_{12} + \lambda_1 x_{13} x_{21} & \lambda_1 x_{21} y_{31} - \nu x_{31} y_{12} & 0 & y_{12}^2 + \lambda_1 x_{21}^2 & & & & & \\
\lambda_1 x_{32} y_{12} - \nu x_{12} y_{23} & x_{12} x_{23} + \lambda_1 y_{23} y_{12} & 0 & \lambda_1 x_{13} y_{12} - \nu x_{12} y_{31} & x_{31} x_{12} + \lambda_1 y_{31} y_{12} & 0 & \lambda_1 y_{12} x_{21} - \nu x_{12} y_{12} & x_{12}^2 + \lambda_1 y_{12}^2 & & & & \\
0 & 0 & 0 & 0 & 0 & 0 & 0 & 0 & 0 & & & \\
\vdots & \vdots & \vdots & \vdots & \vdots & \vdots & \vdots & \vdots & \vdots & \vdots & \vdots & \\
0 & 0 & 0 & 0 & 0 & 0 & 0 & 0 & 0 & 0 & 0 & 0
\end{bmatrix}
$$

SYMMETRIC

APPENDIX C

NODAL TEMPERATURES

Table 1: MODEL TEMPERATURES—COLD SIDE

TIME—1.5 MINUTES					
NODE NUMBER	TEMP. (°RANKINE)	NODE NUMBER	TEMP. (°RANKINE)	NODE NUMBER	TEMP. (°RANKINE)
2	532.1	50	535.0	98	532.1
4	532.0	52	533.2	100	532.0
6	532.0	54	532.1	102	535.0
8	532.0	56	532.0	104	534.0
10	532.0	58	532.0	106	532.5
12	532.0	60	532.0	108	532.4
14	532.5	62	535.0	110	535.0
16	532.0	64	534.0	112	533.2
18	532.0	66	532.5	114	532.9
20	532.0	68	532.0	116	535.0
22	532.0	70	532.0	118	534.0
24	532.0	72	532.0	120	533.7
26	533.2	74	535.0	122	535.0
28	532.1	76	533.2	124	534.3
30	532.0	78	532.1		
32	532.0	80	532.0		
34	532.0	82	532.0		
36	532.0	84	535.0		
38	534.0	86	534.0		
40	532.5	88	532.5		
42	532.0	90	532.0		
44	532.0	92	532.0		
46	532.0	94	535.0		
48	532.0	96	533.2		

Table 2: MODEL TEMPERATURES—COLD SIDE

TIME—3.0 MINUTES					
NODE NUMBER	TEMP. (°RANKINE)	NODE NUMBER	TEMP. (°RANKINE)	NODE NUMBER	TEMP. (°RANKINE)
2	546.0	50	550.0	98	546.0
4	545.2	52	547.5	100	545.8
6	545.0	54	546.0	102	550.0
8	545.0	56	545.2	104	548.5
10	545.0	58	545.0	106	546.5
12	545.0	60	545.0	108	546.2
14	546.5	62	550.0	110	550.0
16	545.5	64	548.5	112	547.5
18	545.0	66	546.5	114	547.1
20	545.0	68	545.5	116	550.0
22	545.0	70	545.0	118	548.5
24	545.0	72	545.0	120	548.0
26	547.5	74	550.0	122	550.0
28	546.0	76	547.5	124	549.0
30	545.2	78	546.0		
32	545.0	80	545.2		
34	545.0	82	545.1		
36	545.0	84	550.0		
38	548.5	86	548.5		
40	546.5	88	546.5		
42	545.5	90	545.5		
44	545.0	92	545.3		
46	545.0	94	550.0		
48	545.0	96	547.5		

Table 3: MODEL TEMPERATURE—COLD SIDE

TIME—4.5 MINUTES					
NODE NUMBER	TEMP. (°RANKINE)	NODE NUMBER	TEMP. (°RANKINE)	NODE NUMBER	TEMP. (°RANKINE)
2	574.0	50	579.0	98	574.0
4	572.0	52	576.0	100	573.0
6	572.0	54	574.0	102	579.0
8	572.0	56	572.0	104	577.0
10	572.0	58	572.0	106	575.0
12	572.0	60	572.0	108	574.0
14	575.0	62	579.0	110	579.0
16	572.5	64	577.0	112	576.0
18	572.0	66	575.0	114	575.0
20	572.0	68	572.5	116	579.0
22	572.0	70	572.0	118	577.0
24	572.0	72	572.0	120	577.0
26	576.0	74	579.0	122	579.0
28	574.0	76	576.0	124	578.0
30	572.0	78	574.0		
32	572.0	80	572.0		
34	572.0	82	572.0		
36	572.0	84	579.0		
38	577.0	86	577.0		
40	575.0	88	575.0		
42	572.5	90	572.5		
44	572.0	92	572.2		
46	572.0	94	579.0		
48	572.0	96	576.0		

Table 4: MODEL TEMPERATURES—COLD SIDE

TIME—6.0 MINUTES					
NODE NUMBER	TEMP. (°RANKINE)	NODE NUMBER	TEMP. (°RANKINE)	NODE NUMBER	TEMP. (°RANKINE)
2	622.0	50	634.5	98	622.0
4	621.0	52	624.0	100	621.8
6	620.0	54	622.0	102	634.5
8	620.0	56	621.0	104	627.5
10	620.0	58	620.0	106	622.5
12	620.0	60	620.0	108	622.5
14	622.5	62	634.5	110	634.5
16	621.5	64	627.5	112	624.0
18	620.5	66	622.5	114	623.4
20	620.0	68	621.5	116	634.5
22	620.0	70	620.5	118	627.5
24	620.0	72	620.2	120	626.0
26	624.0	74	634.5	122	634.5
28	622.0	76	624.0	124	629.5
30	621.0	78	622.0		
32	620.0	80	621.0		
34	620.0	82	620.7		
36	620.0	84	634.5		
38	627.5	86	627.5		
40	622.5	88	622.5		
42	621.5	90	621.5		
44	620.5	92	621.2		
46	620.0	94	634.5		
48	620.0	96	624.0		

Table 5: MODEL TEMPERATURES—COLD SIDE

TIME—7.5 MINUTES					
NODE NUMBER	TEMP. (°RANKINE)	NODE NUMBER	TEMP. (°RANKINE)	NODE NUMBER	TEMP. (°RANKINE)
2	741.0	50	660.0	98	741.0
4	737.0	52	746.0	100	740.0
6	735.0	54	741.0	102	666.0
8	734.0	56	737.0	104	730.0
10	734.0	58	735.0	106	744.0
12	734.0	60	734.0	108	745.0
14	744.0	62	666.0	110	666.0
16	739.0	64	730.0	112	746.0
18	736.0	66	744.0	114	747.0
20	734.0	68	739.0	116	666.0
22	734.0	70	736.0	118	730.0
24	734.0	72	734.0	120	738.0
26	746.0	74	666.0	122	666.0
28	741.0	76	746.0	124	720.0
30	737.0	78	741.0		
32	735.0	80	737.0		
34	734.0	82	734.0		
36	734.0	84	666.0		
38	730.0	86	730.0		
40	744.0	88	744.0		
42	739.0	90	739.0		
44	736.0	92	737.0		
46	734.0	94	666.0		
48	734.0	96	746.0		

Table 6: MODEL TEMPERATURES—COLD SIDE

TIME—9.0 MINUTES					
NODE NUMBER	TEMP. (°RANKINE)	NODE NUMBER	TEMP. (°RANKINE)	NODE NUMBER	TEMP. (°RANKINE)
2	870.0	50	790.0	98	870.0
4	864.0	52	874.0	100	867.0
6	860.0	54	870.0	102	790.0
8	858.0	56	864.0	104	851.0
10	858.0	58	860.0	106	874.0
12	855.0	60	860.0	108	868.0
14	874.0	62	790.0	110	790.0
16	866.0	64	851.0	112	874.0
18	862.0	66	874.0	114	870.0
20	859.0	68	866.0	116	790.0
22	858.0	70	862.0	118	851.0
24	858.0	72	861.0	120	867.0
26	874.0	74	890.0	122	790.0
28	870.0	76	874.0	124	847.0
30	864.0	78	870.0		
32	860.0	80	864.0		
34	858.0	82	862.0		
36	858.0	84	790.0		
38	851.0	86	851.0		
40	874.0	88	874.0		
42	866.0	90	866.0		
44	862.0	92	864.0		
46	859.0	94	790.0		
48	859.0	96	874.0		

Table 7: MODEL TEMPERATURES—COLD SIDE

TIME—10.5 MINUTES					
NODE NUMBER	TEMP. (°RANKINE)	NODE NUMBER	TEMP. (°RANKINE)	NODE NUMBER	TEMP. (°RANKINE)
2	933.0	50	975.0	98	933.0
4	926.0	52	860.0	100	931.0
6	920.0	54	933.0	102	975.0
8	920.0	56	926.0	104	848.0
10	920.0	58	920.0	106	900.0
12	920.0	60	920.0	108	918.0
14	900.0	62	975.0	110	975.0
16	930.0	64	848.0	112	860.0
18	923.0	66	900.0	114	872.0
20	920.0	68	930.0	116	975.0
22	920.0	70	923.0	118	848.0
24	920.0	72	920.0	120	845.0
26	860.0	74	975.0	122	975.0
28	933.0	76	860.0	124	846.0
30	926.0	78	933.0		
32	920.0	80	926.0		
34	920.0	82	922.0		
36	920.0	84	975.0		
38	848.0	86	848.0		
40	900.0	88	900.0		
42	930.0	90	930.0		
44	923.0	92	928.0		
46	920.0	94	975.0		
48	920.0	96	860.0		

Table 8: MODEL TEMPERATURES—COLD SIDE

TIME—12.0 MINUTES					
NODE NUMBER	TEMP. (°RANKINE)	NODE NUMBER	TEMP. (°RANKINE)	NODE NUMBER	TEMP. (°RANKINE)
2	885.0	50	830.0	98	885.0
4	960.0	52	830.0	100	905.0
6	975.0	54	885.0	102	830.0
8	970.0	56	960.0	104	820.0
10	965.0	58	975.0	106	840.0
12	962.0	60	980.0	108	853.0
14	840.0	62	830.0	110	830.0
16	930.0	64	820.0	112	830.0
18	975.0	66	840.0	114	829.0
20	975.0	68	930.0	116	830.0
22	968.0	70	975.0	118	820.0
24	968.0	72	979.0	120	819.0
26	830.0	74	830.0	122	830.0
28	885.0	76	830.0	124	820.0
30	960.0	78	885.0		
32	975.0	80	960.0		
34	970.0	82	968.0		
36	973.0	84	830.0		
38	820.0	86	820.0		
40	840.0	88	840.0		
42	930.0	90	930.0		
44	975.0	92	942.0		
46	975.0	94	830.0		
48	973.0	96	830.0		

Table 9: MODEL TEMPERATURE—COLD SIDE

TIME—13.5 MINUTES					
NODE NUMBER	TEMP. (°RANKINE)	NODE NUMBER	TEMP. (°RANKINE)	NODE NUMBER	TEMP. (°RANKINE)
2	820.0	50	810.0	98	820.0
4	900.0	52	800.0	100	828.0
6	985.0	54	820.0	102	810.0
8	1000.0	56	900.0	104	800.0
10	995.0	58	985.0	106	805.0
12	992.0	60	992.0	108	808.0
14	805.0	62	810.0	110	810.0
16	850.0	64	800.0	112	800.0
18	950.0	66	805.0	114	800.0
20	1000.0	68	850.0	116	810.0
22	995.0	70	950.0	118	800.0
24	998.0	72	968.0	120	798.0
26	800.0	74	810.0	122	810.0
28	820.0	76	800.0	124	802.0
30	900.0	78	820.0		
32	985.0	80	900.0		
34	1000.0	82	922.0		
36	1003.0	84	810.0		
38	800.0	86	800.0		
40	805.0	88	805.0		
42	850.0	90	850.0		
44	950.0	92	869.0		
46	1000.0	94	810.0		
48	1003.0	96	800.0		

Table 10: MODEL TEMPERATURES—COLD SIDE

TIME—15.0 MINUTES					
NODE NUMBER	TEMP. (°RANKINE)	NODE NUMBER	TEMP. (°RANKINE)	NODE NUMBER	TEMP. (°RANKINE)
2	808.0	50	835.0	98	808.0
4	845.0	52	808.0	100	809.0
6	932.0	54	808.0	102	835.0
8	1013.0	56	845.0	104	817.0
10	1060.0	58	932.0	106	800.0
12	1060.0	60	947.0	108	800.0
14	800.0	62	835.0	110	835.0
16	820.0	64	817.0	112	808.0
18	880.0	66	800.0	114	802.0
20	980.0	68	820.0	116	835.0
22	1037.0	70	880.0	118	817.0
24	1050.0	72	900.0	120	812.0
26	808.0	74	935.0	122	835.0
28	808.0	76	808.0	124	822.0
30	845.0	78	808.0		
32	932.0	80	845.0		
34	1013.0	82	860.0		
36	1023.0	84	835.0		
38	817.0	86	817.0		
40	800.0	88	800.0		
42	820.0	90	820.0		
44	880.0	92	830.0		
46	980.0	94	835.0		
48	988.0	96	808.0		

Table 11: MODEL TEMPERATURES—HOT SIDE

TIME — 1.5 MINUTES					
NODE NUMBER	TEMP. (°RANKINE)	NODE NUMBER	TEMP. (°RANKINE)	NODE NUMBER	TEMP. (°RANKINE)
1	549.00	49	550.00	97	549.00
3	548.50	51	549.50	99	548.90
5	548.00	53	549.00	101	550.00
7	547.50	55	548.50	103	549.75
9	547.00	57	548.00	105	549.25
11	546.90	59	547.90	107	549.15
13	549.25	61	550.00	109	550.00
15	548.75	63	549.75	111	549.50
17	548.25	65	549.25	113	549.40
19	547.75	67	548.75	115	550.00
21	547.25	69	548.25	117	549.75
23	547.15	71	548.15	119	549.50
25	549.50	73	550.00	121	550.00
27	549.00	75	549.50	123	549.82
29	548.50	77	549.00		
31	548.00	79	548.50		
33	547.50	81	548.40		
35	547.40	83	550.00		
37	549.75	85	549.75		
39	549.25	87	549.25		
41	548.75	89	548.75		
43	548.65	91	548.65		
45	550.00	93	550.00		
47	549.50	95	549.50		

Table 12: MODEL TEMPERATURES—HOT SIDE

TIME—3.0 MINUTES					
NODE NUMBER	TEMP. (°RANKINE)	NODE NUMBER	TEMP. (°RANKINE)	NODE NUMBER	TEMP. (°RANKINE)
1	571.50	49	574.00	97	571.50
3	571.00	51	572.50	99	571.40
5	570.00	53	571.50	101	574.00
7	570.00	55	571.00	103	573.00
9	570.00	57	570.00	105	572.00
11	570.00	59	571.00	107	571.88
13	572.00	61	574.00	109	574.00
15	571.20	63	573.50	111	572.50
17	570.50	65	572.00	113	572.46
19	570.00	67	571.20	115	574.00
21	570.00	69	570.50	117	573.50
23	570.00	71	571.00	119	573.17
25	572.50	75	574.00	121	574.00
27	571.50	75	572.50	123	573.65
29	571.00	77	571.50		
31	570.00	79	571.00		
33	570.00	81	571.00		
35	570.00	83	574.00		
37	573.50	85	573.50		
39	572.00	87	572.00		
41	571.20	89	571.20		
43	570.50	91	571.00		
45	570.00	93	574.00		
47	570.00	95	572.50		

Table 13: MODEL TEMPERATURES—HOT SIDE

TIME—4.5 MINUTES					
NODE NUMBER	TEMP. (°RANKINE)	NODE NUMBER	TEMP. (°RANKINE)	NODE NUMBER	TEMP. (°RANKINE)
1	619.00	49	623.00	97	619.00
3	617.50	51	620.00	99	618.45
5	616.00	53	619.00	101	623.00
7	615.00	55	617.50	103	622.00
9	615.00	57	616.00	105	619.50
11	615.00	59	615.70	107	619.40
13	619.50	61	623.00	109	623.00
15	617.50	63	622.00	111	620.00
17	617.40	65	619.50	113	620.40
19	615.00	67	617.50	115	623.00
21	615.00	69	617.40	117	622.00
23	615.00	71	616.20	119	621.40
25	620.00	73	623.00	121	623.00
27	619.00	75	620.00	123	622.20
29	617.50	77	619.00		
31	616.00	79	617.50		
33	615.00	81	616.90		
35	615.00	83	623.00		
37	622.00	85	622.00		
39	619.50	87	619.50		
41	617.50	89	617.50		
43	617.40	91	617.60		
45	615.00	94	623.00		
47	615.30	95	620.00		

Table 14: MODEL TEMPERATURES—HOT SIDE

TIME—6.0 MINUTES					
NODE NUMBER	TEMP. (°RANKINE)	NODE NUMBER	TEMP. (°RANKINE)	NODE NUMBER	TEMP. (°RANKINE)
1	682.50	49	691.00	97	682.50
3	681.50	51	686.00	99	681.80
5	681.00	53	682.50	101	691.00
7	681.00	55	681.50	103	688.00
9	681.00	57	681.00	105	684.00
11	681.00	59	681.00	107	683.25
13	684.00	61	691.00	109	691.00
15	682.00	63	688.00	111	686.00
17	681.00	65	684.00	113	685.00
19	681.00	67	682.00	115	691.00
21	681.00	69	681.00	117	688.00
23	681.00	71	681.00	119	687.30
25	686.00	73	691.00	121	691.00
27	682.50	75	686.00	123	689.00
29	681.50	77	682.50		
31	681.00	79	681.50		
33	681.00	81	681.00		
35	681.00	83	691.00		
37	688.00	85	686.00		
39	684.00	87	684.00		
41	682.00	89	682.00		
43	681.00	91	681.10		
45	681.00	93	691.00		
47	681.00	95	686.00		

Table 15: MODEL TEMPERATURES—HOT SIDE

TIME—7.5 MINUTES					
NODE NUMBER	TEMP. (°RANKINE)	NODE NUMBER	TEMP. (°RANKINE)	NODE NUMBER	TEMP. (°RANKINE)
1	869.00	49	760.00	97	869.00
3	864.00	51	876.00	99	851.80
5	859.00	53	869.00	101	760.00
7	854.00	55	864.00	103	840.00
9	850.00	57	859.00	105	872.00
11	850.00	59	850.60	107	852.30
13	872.0	61	760.00	109	760.00
15	867.0	63	840.00	111	876.00
17	861.00	65	872.00	113	852.70
19	857.00	67	867.00	115	760.00
21	852.00	69	861.00	117	840.00
22	850.10	71	850.85	119	851.00
25	876.00	73	760.00	121	760.00
27	869.00	75	876.00	123	820.00
29	864.00	77	869.00		
31	859.00	79	864.00		
33	854.00	81	851.25		
35	850.25	83	760.00		
37	840.00	85	840.00		
39	872.00	87	872.00		
41	867.00	89	867.00		
43	861.00	91	851.50		
45	857.00	93	760.00		
47	850.45	95	876.00		

Table 16: MODEL TEMPERATURES—HOT SIDE

TIME—9.0 MINUTES					
NODE NUMBER	TEMP. (°RANKINE)	NODE NUMBER	TEMP. (°RANKINE)	NODE NUMBER	TEMP. (°RANKINE)
1	1037.0	49	1040.0	97	1037.0
3	1030.0	51	1050.0	99	1030.0
5	1025.0	53	1037.0	101	1040.0
7	1023.0	55	1030.0	103	868.0
9	1023.0	57	1025.0	105	1040.0
11	1023.0	59	1024.0	107	1037.0
13	1040.0	61	1040.0	109	1040.0
15	1030.0	63	868.0	111	1050.0
17	1026.0	65	1040.0	113	1049.0
19	1023.0	67	1030.0	115	1040.0
21	1023.0	69	1026.0	117	868.0
23	1023.0	71	1025.0	119	950.0
25	1050.0	75	1040.0	121	1040.0
27	1037.0	75	1050.0	123	880.0
29	1030.0	77	1037.0		
31	1025.0	79	1030.0		
33	1023.0	81	1027.0		
35	1023.0	83	1040.0		
37	868.0	85	868.0		
39	1040.0	87	1040.0		
41	1030.0	89	1030.0		
43	1026.0	91	1028.0		
45	1023.0	93	1040.0		
47	1023.0	95	1050.0		

Table 17: MODEL TEMPERATURES—HOT SIDE

TIME—10.5 MINUTES					
NODE NUMBER	TEMP. (°RANKINE)	NODE NUMBER	TEMP. (°RANKINE)	NODE NUMBER	TEMP. (°RANKINE)
1	1110.0	49	1070.0	97	1110.0
3	1100.0	51	795.0	99	1110.0
5	1092.0	53	1110.0	101	1070.0
7	1090.0	55	1100.0	103	875.0
9	1090.0	57	1092.0	105	1130.0
11	1090.0	59	1091.5	107	1130.0
13	1130.0	61	1070.0	109	1070.0
15	1105.0	63	875.0	111	795.0
17	1097.0	65	1130.0	113	990.0
19	1090.0	67	1105.0	115	1070.0
21	1090.0	69	1097.0	117	875.0
23	1090.0	71	1093.0	119	830.0
25	795.0	73	1070.0	121	1070.0
27	1110.0	75	795.0	123	913.0
29	1100.0	77	1110.0		
31	1092.0	79	1100.0		
33	1090.0	81	1095.0		
35	1090.0	83	1070.0		
37	875.0	85	875.0		
39	1130.0	87	1130.0		
41	1105.0	89	1105.0		
43	1097.0	91	1100.0		
45	1090.0	93	1070.0		
47	1090.0	95	795.0		

Table 18: MODEL TEMPERATURES—HOT SIDE

TIME—12.0 MINUTES					
NODE NUMBER	TEMP. (°RANKINE)	NODE NUMBER	TEMP. (°RANKINE)	NODE NUMBER	TEMP. (°RANKINE)
1	1050	49	1000	97	1050
3	1170	51	940	99	1085
5	1160	53	1050	101	1000
7	1150	55	1170	103	950
9	1150	57	1160	105	960
11	1150	59	1159	107	985
13	960	61	1000	109	1000
15	1135	63	950	111	940
17	1170	65	960	113	940
19	1155	67	1135	115	1000
21	1150	69	1170	117	950
23	1150	71	1167	119	942
25	940	73	1000	121	1000
27	1050	75	940	123	965
29	1170	77	1050		
31	1160	79	1170		
33	1152	81	1170		
35	1150	83	1000		
37	950	85	950		
39	960	87	960		
41	1135	89	1135		
43	1170	91	1155		
45	1159	93	1000		
47	1152	95	940		

Table 19: MODEL TEMPERATURES—HOT SIDE

TIME—13.5 MINUTES					
NODE NUMBER	TEMP. (°RANKINE)	NODE NUMBER	TEMP. (°RANKINE)	NODE NUMBER	TEMP. (°RANKINE)
1	935	49	1000	97	935
3	1140	51	935	99	955
5	1250	53	935	101	1000
7	1210	55	1140	103	970
9	1170	57	1250	105	920
11	1170	59	1248	107	920
13	920	61	1000	109	1000
15	1010	63	970	111	935
17	1215	65	920	113	925
19	1230	67	1010	115	1000
21	1190	69	1215	117	970
23	1180	71	1235	119	955
25	935	75	1000	121	1000
27	935	75	935	123	981
29	1140	77	935		
31	1250	79	1140		
33	1210	81	1172		
35	1198	83	1000		
37	970	85	970		
39	920	87	920		
41	1010	89	1010		
43	1215	91	1060		
45	1230	93	1000		
47	1220	95	935		

Table 20: MODEL TEMPERATURES—HOT SIDE

TIME—15.0 MINUTES					
NODE NUMBER	TEMP. (°RANKINE)	NODE NUMBER	TEMP. (°RANKINE)	NODE NUMBER	TEMP. (°RANKINE)
1	890	49	1000	97	890
3	910	51	930	99	890
5	1040	53	890	101	1000
7	1250	55	910	103	960
9	1260	57	1040	105	910
11	1255	59	1085	107	899
13	910	61	1000	109	1000
15	895	63	960	111	930
17	960	65	910	113	920
19	1170	67	895	115	1000
21	1265	691	960	117	960
23	1275	71	983	119	950
25	930	73	1000	121	1000
27	890	75	930	123	973
29	910	77	890		
31	1040	79	910		
33	1250	81	925		
35	1260	83	1000		
37	960	85	960		
39	910	85	960		
41	895	89	895		
43	960	91	896		
45	1170	93	1000		
47	1212	95	930		

Table 21: MEAN TEMPERATURES AND $\sqrt{E/E_{700°}}$

	Time	Mean Temp. °R		Avg. Mean °R	°F	E	$\frac{E}{E_{700°}}$	$\sqrt{\frac{E}{E_{700°}}}$
		Hot	Cold					
1st	0.0	530	530	530	70	30.8	1.1271	1.0617
2nd	1.5	549	533	541	81	30.766	1.1259	1.0611
3rd	3.0	572	547	560	100	30.707	1.1237	1.0601
4th	4.5	619	575	597	137	30.593	1.1196	1.0581
5th	6.0	685	624	655	195	30.415	1.1130	1.0550
6th	7.5	844	725	785	325	29.681	1.0862	1.0422
7th	9.0	1036	851	944	484	28.767	1.0527	1.0260
8th	10.5	1031	888	960	500	28.675	1.0494	1.0244
9th	12.0	1059	893	976	516	28.583	1.0460	1.0228
10th	13.5	1044	863	954	494	28.709	1.0506	1.0250
11th	15.0	973	853	913	453	28.945	1.0592	1.0292
					700	27.325		

Aeronautical Systems Division, Flight Dynamics Laboratory, Wright-Patterson AFB, Ohio. Rpt Nr ASD-TDR-62-156. NONLINEAR AND THERMAL EFFECTS ON ELASTIC VIBRATIONS. Final report, Jun 62, 143p. incl illus., tables, 12 refs.

Unclassified Report

This report presents a theory and the digital procedures for predicting the effects of nonlinear structural behavior on the stresses, deformations, and small amplitude oscillations of a structure subjected simultaneously to loading and heating.

The method is used to analyze a thin wing to

(over)

1. Swept wing
2. Structures
3. Vibration
I. AFSC Project 1370 Task 137006
II. Contract No. AF 33 (616)-7898
III. The Boeing Co., Seattle 24, Wash.
IV. Raymond C. Weikel, et al.
V. Aval fr OTS
VI. In ASTIA collection

determine the frequencies and mode shapes of the first six natural vibration modes of the wing subjected to simultaneous heating and loading.

Aeronautical Systems Division, Flight Dynamics Laboratory, Wright-Patterson AFB, Ohio. Rpt Nr ASD-TDR-62-156. NONLINEAR AND THERMAL EFFECTS ON ELASTIC VIBRATIONS. Final report, Jun 62, 143p. incl illus., tables, 12 refs.

Unclassified Report

This report presents a theory and the digital procedures for predicting the effects of nonlinear structural behavior on the stresses, deformations, and small amplitude oscillations of a structure subjected simultaneously to loading and heating.

The method is used to analyze a thin wing to

(over)

1. Swept wing
2. Structures
3. Vibration
I. AFSC Project 1370 Task 137006
II. Contract No. AF 33 (616)-7898
III. The Boeing Co., Seattle 24, Wash.
IV. Raymond C. Weikel, et al.
V. Aval fr OTS
VI. In ASTIA collection

determine the frequencies and mode shapes of the first six natural vibration modes of the wing subjected to simultaneous heating and loading.

Aeronautical Systems Division, Flight Dynamics Laboratory, Wright-Patterson AFB, Ohio. Rpt Nr ASD-TDR-62-156. NONLINEAR AND THERMAL EFFECTS ON ELASTIC VIBRATIONS. Final report, Jun 62, 143p. incl illus., tables, 12 refs.

Unclassified Report

This report presents a theory and the digital procedures for predicting the effects of nonlinear structural behavior on the stresses, deformations, and small amplitude oscillations of a structure subjected simultaneously to loading and heating.

The method is used to analyze a thin wing to

(over)

determine the frequencies and mode shapes of the first six natural vibration modes of the wing subjected to simultaneous heating and loading.

1. Swept wing
2. Structures
3. Vibration
- I. AFSC Project 1370 Task 137006
- II. Contract No. AF 33 (616)-7898
- III. The Boeing Co., Seattle 24, Wash.
- IV. Raymond C. Weikel, et al.
- V. Aval fr OTS
- VI. In ASTIA collection

Aeronautical Systems Division, Flight Dynamics Laboratory, Wright-Patterson AFB, Ohio. Rpt Nr ASD-TDR-62-156. NONLINEAR AND THERMAL EFFECTS ON ELASTIC VIBRATIONS. Final report, Jun 62, 143p. incl illus., tables, 12 refs.

Unclassified Report

This report presents a theory and the digital procedures for predicting the effects of nonlinear structural behavior on the stresses, deformations, and small amplitude oscillations of a structure subjected simultaneously to loading and heating.

The method is used to analyze a thin wing to

(over)

determine the frequencies and mode shapes of the first six natural vibration modes of the wing subjected to simultaneous heating and loading.

1. Swept wing
2. Structures
3. Vibration
- I. AFSC Project 1370 Task 137006
- II. Contract No. AF 33 (616)-7898
- III. The Boeing Co., Seattle 24, Wash.
- IV. Raymond C. Weikel, et al.
- V. Aval fr OTS
- VI. In ASTIA collection